PHOTOPRODUCTION OF NEGATIVE PIONS IN DEUTERIUM

BY

H. C. EVANS

PRESENTED TO THE UNIVERSITY OF GLASGOW AS A THESIS FOR THE DEGREE OF DOCTOR OF PHILOSOPHY, AUGUST, 1961.

ProQuest LLC.
789 East Eisenhower Parkway
P.O. Box 1346
Ann Arbor, MI 48106 – 1346

PREFACE

Deuterium provides the most suitable target for studying the basic process of negative pion photoproduction at a free neutron. For photon energies well above threshold the spectator model has been used to relate pion photoproduction in deuterium to photoproduction at a free neutron. In 1957 when the work described in this thesis was initiated no experimental test of the spectator model that clearly supported its validity for negative pion photoproduction in deuterium had been reported. An experiment done using the bremsstrahlung beam of the Glasgow electron synchrotron is described. A scintillation counter technique was used, and the energy spectrum and angular distribution of the recoil protons detected in coincidence with negative pions from deuterium were compared with the predictions of the spectator model. Reasonable agreement was obtained.

Charged pion photoproduction in hydrogen and deuterium is discussed in Chapter I. A detailed discussion of experimental tests of the spectator model and the impulse approximation is given.

The calibration of the response of commercially available plastic scintillator is described in Chapter II.

This work was largely my own.

The construction, testing, and calibration of the scintillation counter telescopes and the associated electronics is given in Chapter III. The proton telescope was constructed by myself. The pion telescope was adapted from an existing counter telescope. The author assisted in the construction of the display unit and was entirely responsible for the counter tests described.

In Chapter IV the measurement of the recoil proton energy and angular distributions is described and the results presented. None of the work included in the description of the synchrotron was done by the author. The liquid target was constructed and operated by Mr. D. Miller. I was assisted in the collection of data by Mr. B. Patrick. The analysis of the data was done by myself.

The recoil proton energy spectra and angular distributions for $\gamma + n \rightarrow p + \pi^-$ and for the spectator model description of $\gamma + d \rightarrow 2p + \pi^-$ are calculated in Chapter V. The computation of the spectator model kinematics using Deuce was done by Mr. I.Harbour. The remainder of the work was done by the author.

The discussion and the conclusions presented in Chapter VI are my own.

I wish to thank Professor P.I. Dee F.R.S. for the interest he has shown in this work and for extending to me the privilege of working in his laboratory. I am grateful to Professor E.H. Bellamy for supervision during the first 3 years of this work and to Dr. J. Rutherglen for his assistance and advice during the later stages. It is a pleasure to thank Dr. McFarlane and his synchrotron crew for their invaluable assistance. I am also indebted to Mr. D. Miller, Mr. B. Patrick and Mr. I. Barbour.

I wish to acknowledge the financial support given me by the National Research Council of Canada during my first 3 years, and to thank the University of Glasgow for a University Research Studentship awarded me during the fourth year.

CONTENTS

CHAPTER I

(a) Introduction

The existence of the pion was first postulated by Yukawa (1935) in his theory of nuclear forces. Their existence in cosmic radiation was confirmed by the Bristol group led by Powell in 1947 (Lattes et al., 1947) by observing the decay of the pion into μ-mesons in nuclear emulsions. As high energy particle accelerators became available the production of pions in the laboratory in nucleon-nucleon and photon-nucleon collisions made possible detailed investigation of their properties. Pions are zero spin particles. They form an isotopic spin triplet and have odd intrinsic parity with respect to the nucleon. The masses and principal decay modes of charged and neutral pions are given below.

Pion	Decay Mode	Life Time (sec.)	Mass (MeV.)
$\pi^{\pm}$	$\pi^{\pm} \rightarrow \mu^{\pm} + \nu$	2.54×10^{-8}	139.6
π^{o}	$\pi^{o} \rightarrow 2\gamma$	5×10^{-16}	135.0

The first observation of pions produced in photon-nucleon collisions (photoproduction) were made at Berkeley (McMillan, 1949) using a carbon target. The investigation of photoproduction of charged pions carried out since then has been largely directed towards

understanding the basic processes for photoproduction of a single charged pion at a nucleon.

$$\gamma + p \rightarrow \pi^+ + n \qquad (1.1)$$

$$\gamma + n \rightarrow \pi^- + p \qquad (1.2)$$

Only the first of these can be observed for free nucleons due to the lack of a condensed neutron target. The most suitable nucleus for investigating (1.2) is the deuteron. The low binding energy and loose structure of the deuteron lead one to expect that the nuclear binding has less effect on charged pion photoproduction from deuterium than from heavier nuclei. The reactions for charged pion photoproduction in deuterium are

$$\gamma + d \rightarrow \pi^+ + 2n \qquad (1.3)$$

$$\gamma + d \rightarrow \pi^- + 2p \qquad (1.4)$$

The interpretation of (1.3) and (1.4) in terms of the free nucleon reactions (1.1) and (1.2) is complicated by a number of effects.

The photon beams available for experiment are produced by allowing artificially accelerated electrons to strike a target. This produces a bremsstrahlung beam

which contains photons of all energies between zero and the maximum energy of the incident electrons. The energy of a photon involved in production of a pion at a nucleus is in general unknown. In the special case of (1.1) which is a two body reaction, measurement of the angle of production and the energy of one of the final state particles uniquely defines the incident photon energy. This is due to the requirement of simultaneous energy and momentum conservation.

In the simplest model for reactions (1.3) and (1.4), photoproduction is considered to take place at a free nucleon, which is given a momentum distribution appropriate to a nucleon in deuterium. This is the spectator model, so called because the other nucleon takes no part in the interaction. In this model the measurement of the angle of production and energy of a pion allows one to define a range of energy for the incident photon. The interaction of the 3 particles in the final state can be expected to introduce additional effects. In reaction (1.4) there are 3 charged particles in the final state and Coulomb-interaction, which is absent in (1.3) is important at low energy.

In most experiments involving pion photoproduction from deuterium, only the pion is detected and the results

are interpreted in terms of free nucleon kinematics. Experiments in which more than one final state particle are observed allow one to investigate the validity of the various models used to interpret observations of (1.3) and (1.4). The purpose of this thesis is to describe an experiment done using the bremsstrahlung beam of the Glasgow electron synchrotron, in which a recoil proton was detected in coincidence with negative pions from deuterium using a scintillation counter technique.

Before discussing the detailed investigation of reactions (1.3) and (1.4) a brief account of pion photoproduction in hydrogen is given for the energy region up to 350 MeV in which pions are produced singly.

(b) Positive Pion Photoproduction at Protons

Photoproduction of positive pions at protons has been thoroughly investigated and the main features of this reaction are well known. The total cross section rises as the photon energy increases above threshold and reaches a maximum value in the region of 290 to 300 MeV. At higher energies the cross section decreases rapidly. This behaviour is due to a strong resonance in the

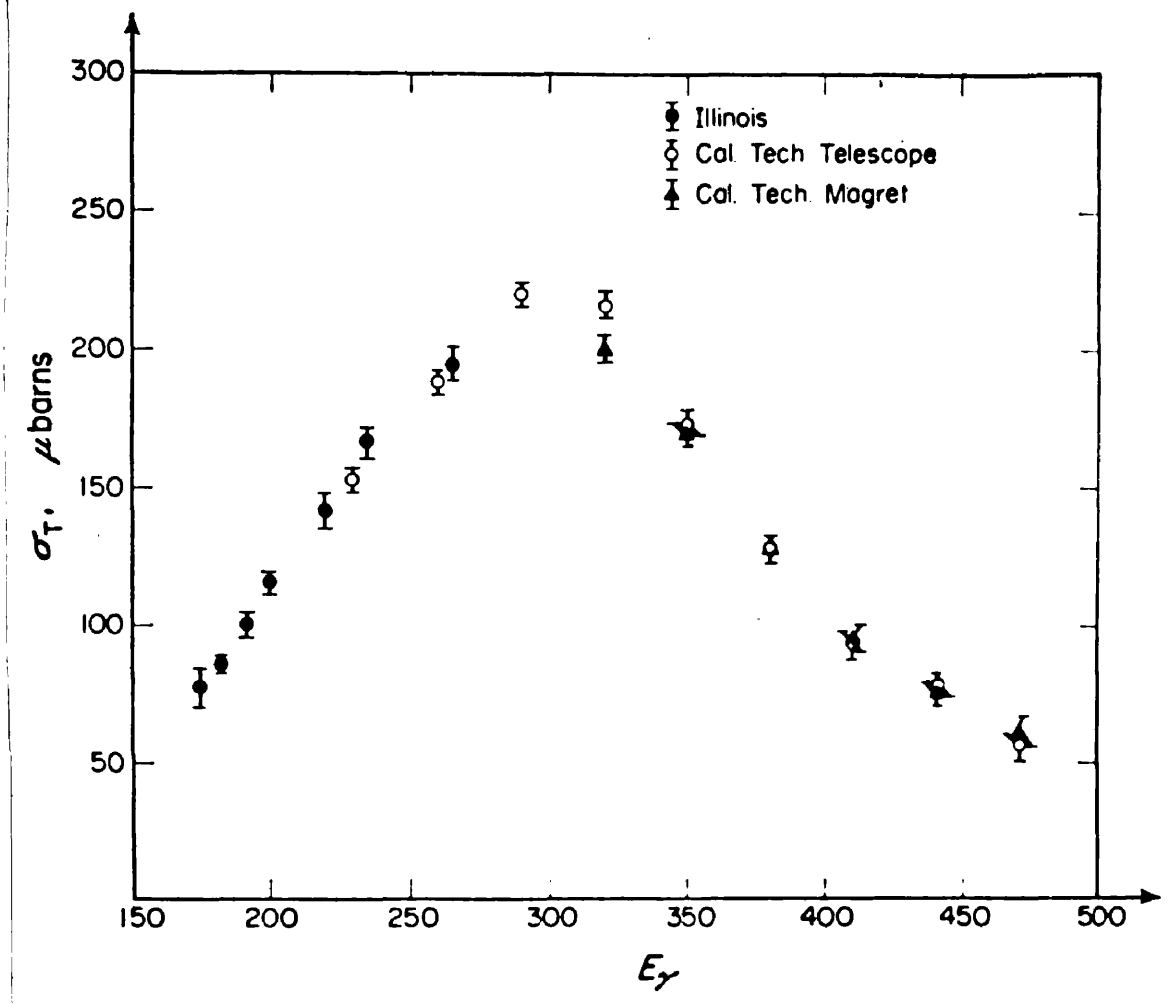

Total cross-section $\gamma + p \rightarrow \pi^+ + n$.

Figure 1.1.

$T = 3/2$, $J = 3/2$ pion nucleon state, where T and J are the isotopic spin and total angular momentum respectively. The total cross section is shown as a function of photon energy in figure 1.1, which has been taken from a review article by Bellamy (1960). The low energy data of Beneventano et al. (1956) obtained using nuclear emulsions at Illinois and that of the Cal. Tech. groups (Tollestrup et al.,1955 and Walker et al.,1955) are plotted together. The agreement between the three sets of data is good.

Measurements of the angular distribution show that pions are emitted almost isotropically in the centre of mass system near threshold. As the photon energy is increased an excess of production at backward angles becomes apparent. At 290 MeV a large maximum in the angular distribution is observed in the region between 90 and 120 degrees, the angle being measured with respect to the incident photon direction. This maximum decreases as the photon energy is increased further. At 380 MeV the angular distribution rises towards forward angles.

For photon energies below 350 MeV it is reasonable to assume that only S and P wave production are important. This assumption has led to an analysis of the angular distribution in the centre of mass system in terms of

a quadratic expression in cos θ,

$$\frac{d\sigma}{d\Omega} = A + B\cos\theta + C\cos^2\theta \qquad (1.5)$$

where θ is the angle of pion emission measured from the incident photon direction. Moravcsik (1956) pointed out that the direct interaction between the photon and the meson current introduces a term containing $(1 - \beta \cos\theta)^2$ in the denominator into the differential cross section. He has suggested that the analysis of the angular distribution be done using the fourth order polynomial in cos θ,

$$(1 - \beta\cos\theta)^2 \frac{d\sigma}{d\Omega} = A + B\cos\theta + C\cos^2\theta + D\cos^3\theta + E\cos^4\theta \qquad (1.6)$$

In the analysis the coefficients A to E are to be determined from the details of the theory and the resulting curve is compared with the measured angular distribution.

Recent angular distribution measurements (Halmberg et al., 1958, Uretsky et al., 1958, and Knapp et al., 1957, and 1959) have been compared with dispersion relation calculations of Chew et al. (1957) using this recipe. The angular distributions obtained by Uretsky et al. for

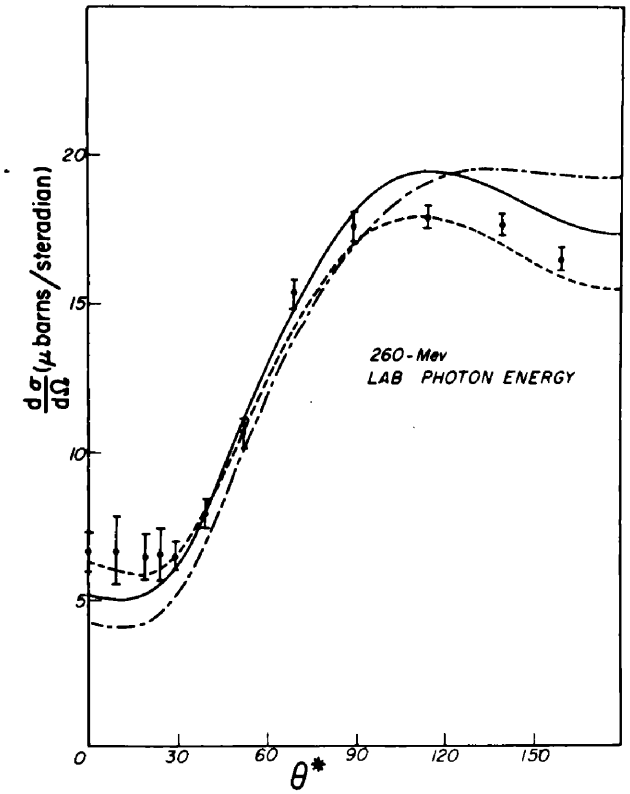

Angular distribution of positive photopions from hydrogen a: 260-Mev photon energy. For explanation of the curves see text.

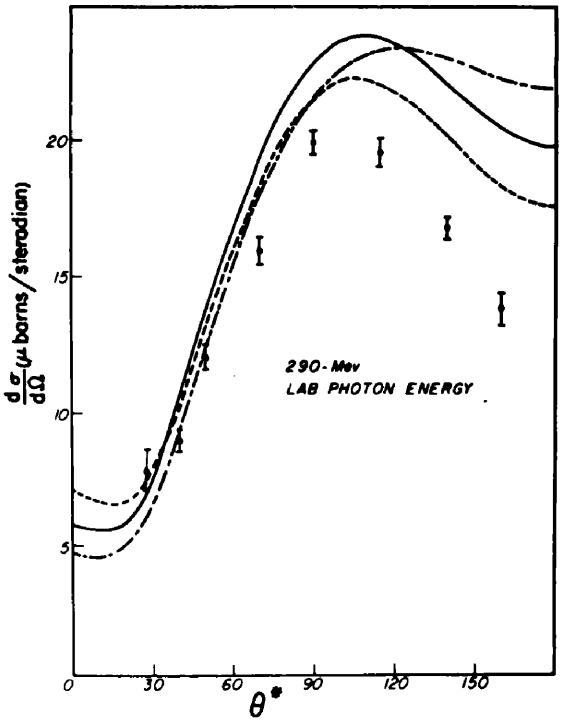

Angular distribution of positive photopions from hydrogen at 290-Mev photon energy. For explanation of the curves see text.

Figure 1.2.

260 and 290 MeV photon energies are shown in figure 1.2. The various curves are obtained for different assumed values of the small pion-nucleon phase shifts, δ_{11}, δ_{13} and δ_{31}. The subscript are twice the isotopic spin and total angular momentum respectively. The agreement shown between the experimental values and the theoretical predictions in figure 1.2 is reasonable. A precise knowledge of the values of the small phase shifts will be required before a detailed comparison with the theory can be made.

An interesting relationship exists between various threshold values in pion physics. It depends upon the well established principles of charge independence and detailed balance. The quantities involved in this relationship, that can be measured experimentally are;

1. the Panofsky ratio, $R = \frac{\omega(\pi^- + p \rightarrow \pi^0 + n)}{\omega(\pi^- + p \rightarrow \gamma + n)}$

2. the charge exchange scattering transition rate, $\omega(\pi^- + p \rightarrow \pi^0 + n)$

3. the threshold photoproduction transition rate $\omega(\gamma + p \rightarrow \pi^+ + n)$

4. the ratio, $r = \frac{\omega(\gamma + n \rightarrow \pi^- + p)}{\omega(\gamma + p \rightarrow \pi^+ + n)}$

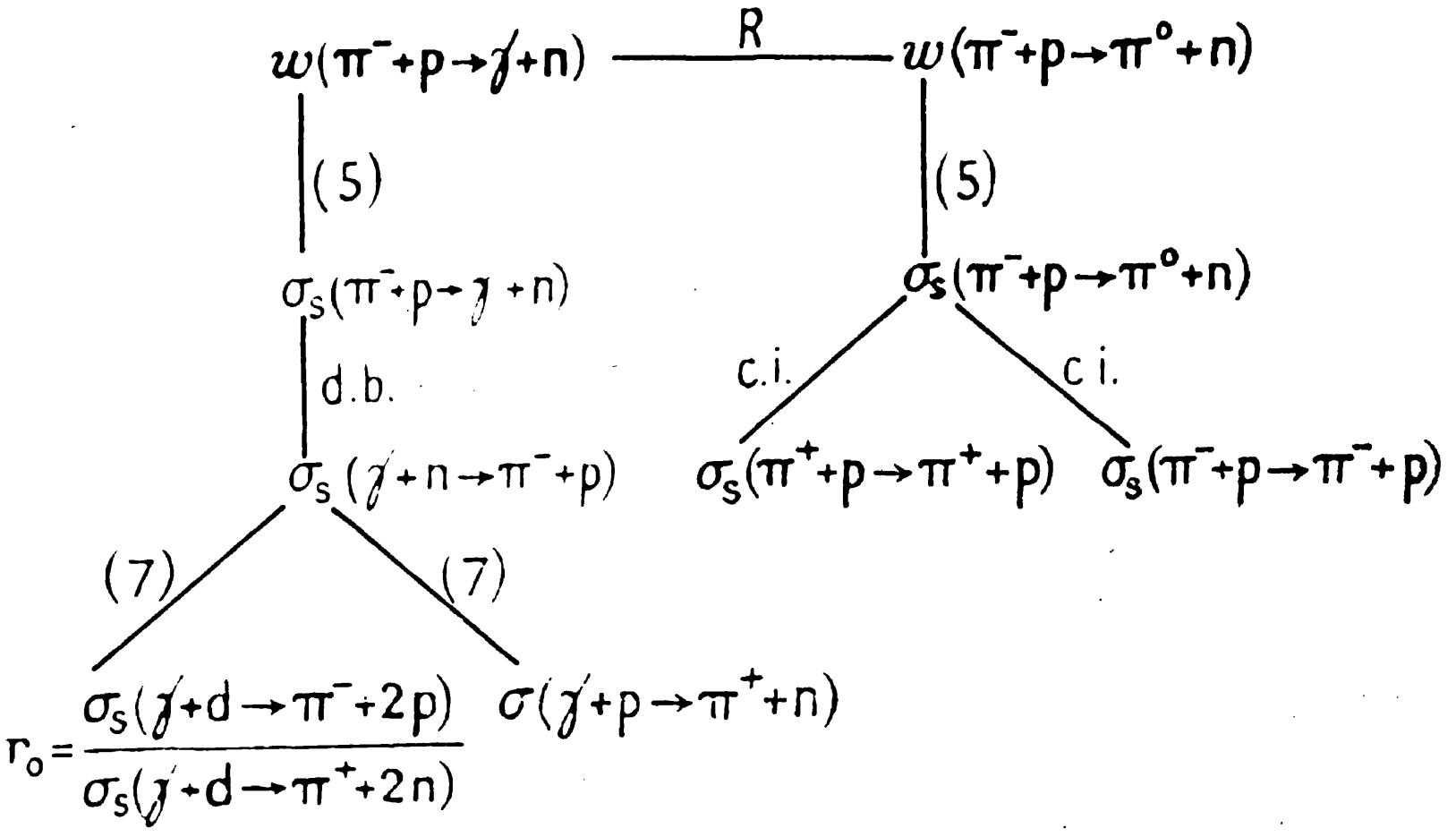

Figure 1.3. Phenomenological scheme of connection between negative pion capture, pion-proton scattering, and photoproduction. (Cassels 1957).

The relationship between these quantities is shown in figure 1.3. The Panofsky ratio is measured for zero energy pions. The experimental observation of 2, 3, and 4 are made at positive energy and must be extrapolated to threshold. Initially the measured values of 2, 3 and 4 led to a prediction of 2.5 for the Panofsky ratio as compared with 1.5 ± .1 for the experimentally observed ratio. Cini et al. (1958) showed that the discrepancy may be resolved, if the extrapolation to zero energy of pion photoproduction and charge exchange scattering are done in a manner consistent with the theoretical energy dependence for these processes.

The measurement of the 90 degree differential cross section as a function of photon energy provides an experimental test of the Cini extrapolation. The coefficient a_o is plotted in figure 1.4, where a_o is related to A in equation 1.5 by

$$a_o = A/W \qquad \text{where} \qquad W = \mu\,\mu_o(1 + V/M)^{-2} \tag{1.7}$$

where μ and μ_o are the pion momentum and energy respectively, V is the photon momentum and M is the nucleon mass. The experimental points are those of Rutherglen and

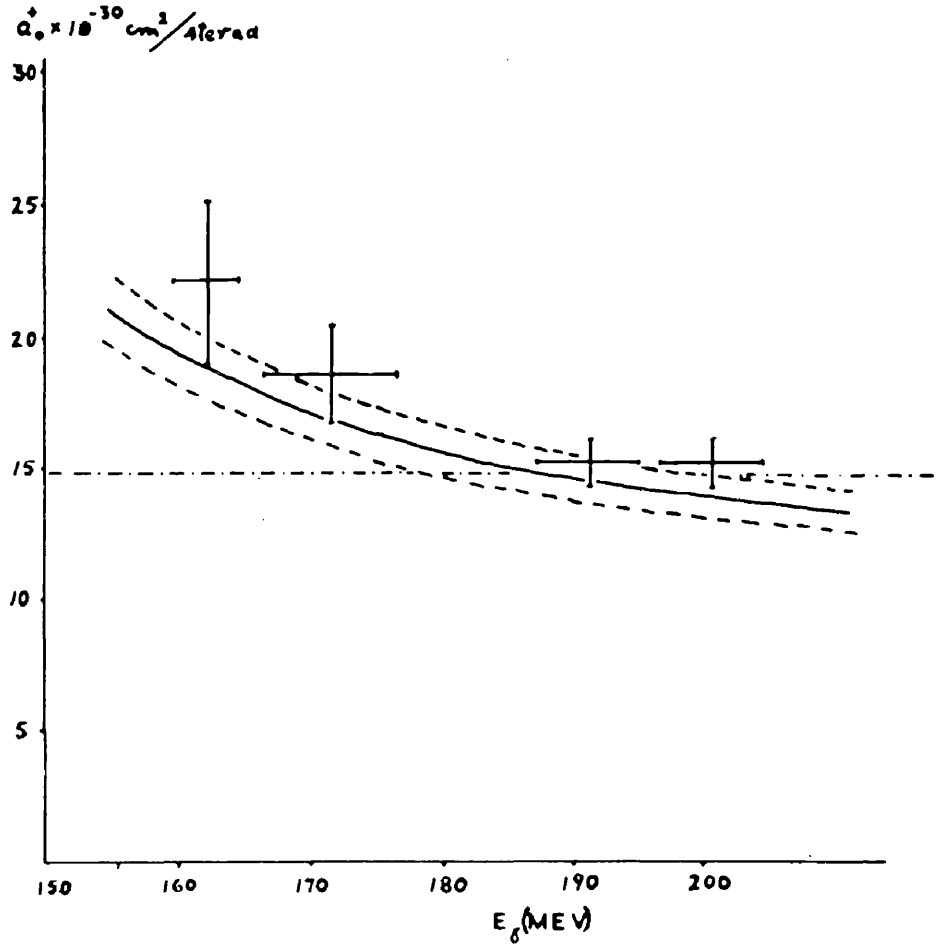

$|M^+(90^\circ \text{ c.m.s.})|^2$ from the measurements of Rutherglen et al [15].

Figure 1.4. The solid curve is the Cini extrapolation.

Walker reported at the Rochester Conference (1960). They provide experimental confirmation of the dispersion relation predictions.

The minus - plus ratio, Γ , for pion photoproduction that is measured experimentally is that for deuterium. It must be corrected for the effect of nuclear binding before it is introduced into the threshold relationship. A discussion of charged pion photoproduction in deuterium is given in the next section.

(c) Charged Pion Photoproduction in Deuterium.

It was pointed out above, that one of the main reasons for the interest in pion photoproduction in deuterium is that it is the most practical target for studying the basic interaction (1,2), for pion photoproduction at a neutron. The many measurements of the negative to positive ratio for pion production are the best example of this approach. The study of pion photoproduction in deuterium may also be directed towards understanding the effect of nuclear binding on the fundamental pion production reactions. An example of this approach is the measurement of the ratio of positive pion photo-

production cross sections in deuterium and hydrogen.

The investigations directed towards the understanding of 1.2 require a model to relate the measurements of pion photoproduction at the bound neutron to photoproduction at a free neutron at rest. The simplest model is the phenomenological spectator model in which the photoproduction takes place at one nucleon only. The other nucleon leaves the interaction with momentum equal to its initial internal momentum. Photoproduction in deuterium may then be reduced to production at a free nucleon. This nucleon is not at rest and must be given a momentum distribution appropriate to the bound nucleon. The effect of the binding energy may be included in this model. The measurement of the angle of emission and energy of the pion say, permit the complete solution of the two body kinematics involved in the spectator model for assumed values of the initial nucleon momentum. Thus the energy spectrum of photons that can produce a pion at a particular angle and energy may be evaluated for any assumed nucleon momentum distribution. In the interpretation of experimental results for pion photoproduction in deuterium the kinematics for production at

a free nucleon at rest have often been used to relate photon energy to pion energy and angle. This procedure implicitly assumes the validity of the spectator model and in addition that the spread in photon energies due to nucleon momentum is not large. Although the spectator model has generally been assumed to be valid in the energy region well above threshold ($E\gamma > 200$ MeV) no experimental work clearly supporting it had been published until a year ago.

At photon energies below 200 MeV the spectator model is not expected to give a good description of pion photoproduction in deuterium. This model ignores final state interactions which become increasingly important at low energies. In the energy region near threshold and up to 200 MeV the impulse approximation is useful. It was suggested by Chew (1950) and was first used by him to deduce free neutron-neutron scattering cross sections from neutron-deuteron inelastic scattering data. The application of the impulse approximation to pion photoproduction in deuterium has been discussed in detail in a series of papers by Chew and Lewis (1951), Chew and Wick (1952), and by Lax and Feshback (1951, 1952).

The fundamental assumption of the impulse approximation is that the pion production amplitudes from various nucleons are linearly superposable to form the production amplitude for the whole nucleus. The conditions required for the validity of the impulse approximation are threefold. They are stated below in the form given by Chew and Wick.

1. The incident particle never interacts strongly with more than one nucleon at the same time.
2. The amplitude of the incident wave falling on each nucleon is almost the same as it would be if the nucleon were alone.
3. The binding forces between the nucleons are negligible during the decisive phase of the interaction when the incident particle interacts strongly with the nucleus.

Conditions 1 and 3 must be satisfied if the many body features of the problem are to be avoided. The transparency condition 2, is not essential but permits a considerable simplification. The third condition is sometimes restated in an alternative form, namely that the collision time is short compared to the period

of the nucleon system.

The above conditions are expected to be well satisfied for pion photoproduction in deuterium. Condition 1 is certainly satisfied for the incident photon due to the smallness of the fine structure constant.

The transparency condition for the two nucleon system may be restated in terms of the probability of a meson produced at one nucleon being scattered at the second. Unless this probability is small the effect of multiple scattering will be important. A simple indication of the magnitude of the multiple scattering error may be obtained by considering the ratio of the pion-nucleon scattering cross section, to the size of the deuteron, i.e.

$$\sigma_s / \pi \bar{R}^2$$

where $\bar{R}$ is the mean nucleon separation. If we assume 20 millibarns for σ_s and use the value taken by Chew (1952) for $\bar{R} = 3.2 \times 10^{-13}$ cm., the above expression gives a multiple scattering error of 7 percent. This is in good agreement with the estimate of 5 percent obtained by MacDonald (1959) from detailed calculations.

The collision time is expected to be small compared

to the nuclear period since the energy conservation violation in the intermediate state is on the average equal to the pion rest mass.

The determination of the cross section in the impulse approximation is done by evaluating the transition matrix element for free nucleon photoproduction between initial and final nucleon states. The nucleon binding forces determine the initial and final states, and do not eneter the calculations directly. The procedure is illustrated by giving the calculation of Chew and Lewis (1951) in some detail.

They express the differential cross section for pion photoproduction in deuterium in the form

$$\frac{d\sigma_f}{d\mu\, dD} = (2\pi)^{-2} |Q|^2 \delta(\mu_0 + \epsilon + D^2/4M - \nu_0) \qquad 1.8$$

where μ and μ_0 are the pion momentum and energy,

ν and ν_0 are the photon momentum and energy,

D is the total momentum of the recoiling nucleon system,

and M is the nucleon mass.

$\epsilon = \epsilon_f - \epsilon_i$ where ϵ_f is the internal energy of

the final state nucleon system and $-\epsilon_i$ the deuteron binding energy.

Q is the matrix element which is to be evaluated in the impulse approximation. In 1.8, $\hbar = c = 1$ and the pion rest mass is set equal to 1.

The matrix is to be approximated by $T = T_1 + T_2$ where T_j is the part of the matrix element which describes photoproduction from the j^{th} nucleon acting alone.

$$T_j = (\sigma_j \cdot K + L) \exp[i(\nu - \mu) \cdot r_j] \tau_j^{\tau} \qquad (1.9)$$

where r_j , σ_j and τ_j are the nucleon position, spin, and isotopic spin respectively. The matrix element is written in two parts, $\sigma_j \cdot K$ represents the spin dependent production in which the spin of one nucleon is reversed, i.e. spin-flip occurs. L represents the spin independent part in which the nucleon spin state remains unchanged. The matrix element is evaluated between the initial deuteron state and the final symmetric and antisymmetric states. The matrix element is squared, summed over final nucleon states, and averaged over initial spin states and photon polarization

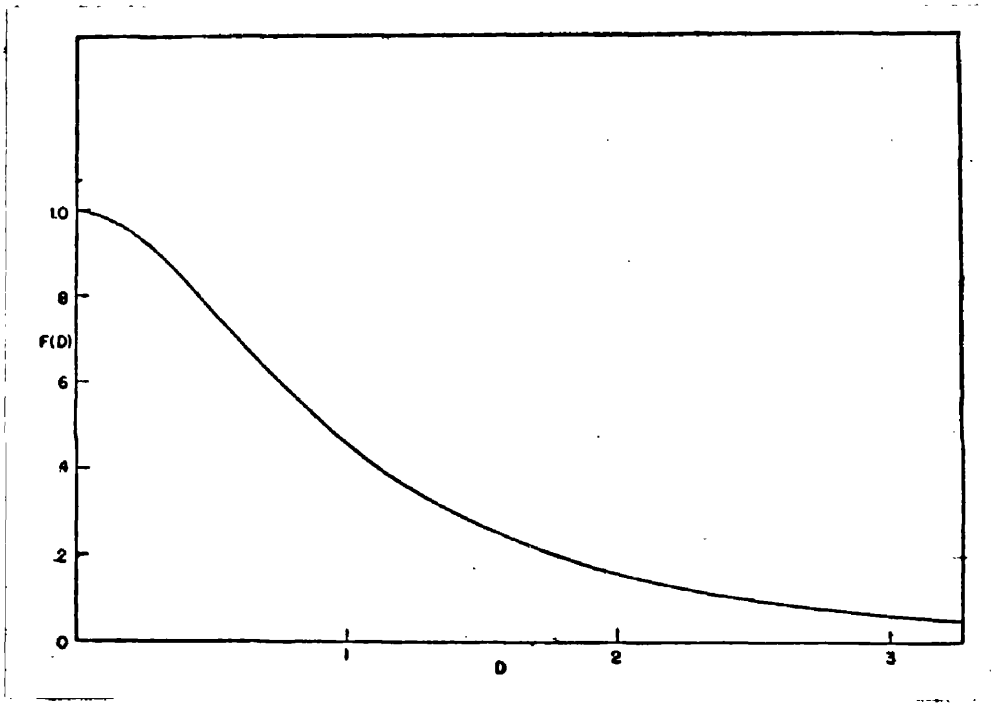

Figure 1.5. Exclusion principle function F(D) calculated by Chew and Lewis (1951).

giving,

$$|Q|^2 = \frac{2}{3}\langle|K^2|\rangle_{avg}\,|E_f|^2 + \left[\frac{4}{3}\langle|K^2|\rangle_{avg.} + 2|L|^2\right]\langle|O|^2\rangle_f \qquad (1.10)$$

where the K and L are the same as in (1.9) and E_f and O_f are defined by the integrals

$$E_f = \int u_{fe}^{*}(\rho)\exp(ik_0\rho)\,u_i(\rho)\,d\rho$$
$$O_f = \int u_{fo}^{*}(\rho)\exp(ik_0\rho)\,u_i(\rho)\,d\rho \qquad (1.11)$$

where u_{fe} and u_{fo} are the symmetrical and antisymmetrical final state wave functions and u_i is the deuteron wave function.

When the dependence on the pion momentum is eliminated, the cross section may be expressed as a function of D^2 in the form

$$d\sigma/dD^2 = \left[1 - \frac{1}{3}F(D)\right]\frac{d\sigma_K}{dD^2} + \left[1 - F(D)\right]\frac{d\sigma_L}{dD^2} \qquad (1.12)$$

in which the spin-flip part $d\sigma_K/dD^2$ and the non spin-flip part $d\sigma_L/dD^2$ are written separately. The function F(D) is shown in figure 1.5. The corresponding

expression for photoproduction at a free proton is

$$\frac{d\sigma}{dD^2} = \frac{d\sigma_K}{dD^2} + \frac{d\sigma_L}{dD^2} \qquad (1.13)$$

The effect of the Pauli exclusion principle is illustrated by 1.12. When D = 0 F(D) = 1 and the non spin-flip production is suppressed while 2/3 of the spin-flip production is allowed. This may also be seen from a simple consideration of the initial and final nucleon states involved. The initial state is the ground state of the deuteron which is a ^3S state. The Pauli principle allows transitions to ^1S, ^3P, ^1D states etc., but forbids transitions to ^3S, ^1P, ^3D states. Near threshold where the energy available is not sufficient for the nucleons to be in a P state the transition will be inhibited if spin-flip production does not occur. In the region near threshold D will always be small, and the dependence on D obtained by Chew and Lewis is expected.

Their analysis showed that small values of D correspond to emission of the pion at small angles to the incident photon direction. It follows that experiments designed to determine the nucleon spin dependence must be done at forward angles where the exclusion principle

effect is large. In principle a measurement of the ratio of positive pion photoproduction from deuterium to that from hydrogen at small angles will determine the spin dependence. Experiments at small forward angles are difficult to perform due to the high electron background and the results of experiments of this type are not conclusive.

The final state interaction of the particles in positive and negative pion photoproduction from deuterium (1.3 and 1.4) are considered in detail by Baldin (1958) for photon energies near threshold. He expresses the cross section in the form

$$\frac{d\sigma}{dp\,dq} = A(p,q)\,|K|^2 + B(p,q)\,|L|^2 \qquad (1.14)$$

where $p = \frac{1}{2}(p_1 - p_2)$,

$q = \frac{1}{2}(p_1 + p_2)$,

and p_1 and p_2 are the momentum of the two final state nucleons in the laboratory system. $|K|^2$ and $|L|^2$ are the squared spin-flip and non spin-flip matrix elements for pion photoproduction at free nucleons.

A and B are functions of p and q and express the dependence of the cross section measured for deuterium

on the initial and final nucleon states. For positive pion production they are the equivalent of the $1 - \frac{1}{3} F(D)$ and $1 - F(D)$ obtained by Chew and Lewis. Baldin has evaluated A and B in a detailed manner appropriate to the threshold region. The Coulomb interaction between the two protons is included in the evaluation of A and B for negative pion production. The Coulomb interaction between the negative pion and the protons is introduced separately. These calculations represent the most rigorous treatment of the final state interaction, that has yet been done for negative pion photoproduction in deuterium. The effect of the Coulomb correction near threshold is to increase σ^- measured for a deuterium target relative to the value for photoproduction from a free neutron. The Coulomb corrections in the threshold region are summarized in the table below.

Pion Energy	Positive Coulomb Correction p-π^- interaction	Negative Coulomb Correction p-p interaction
< 10 MeV	can be $> 10\%$	negligible
> 10 MeV	negligible	can be appreciable.

Baldin concludes that the final state Coulomb corrections

can not be neglected in the evaluation of σ^- for free neutrons from the deuterium data. The results of Baldin's calculations have been used to interpret the result of an experiment done by Adamovic et al. (1959) in which negative pion photoproduction was investigated near threshold. This experiment will be discussed in detail later.

Photodisintegration of the deuteron

$$\gamma + d \rightarrow n + p$$

will compete with pion photoproduction. Wilson (1956) has developed a theory in which the photodisintegration of the deuteron takes place through a process of pion emission and reabsorption. He assumed that the pion is reabsorbed and that photodisintegration is the result, if the nucleons are within a pion Compton wave length of each other. He obtained good agreement with the measured photodisintegration cross sections for deuterium above 100 MeV, when he used reasonable values for pion photoproduction cross sections. Even at high energies where the spectator model is expected to be valid the competition of photodisintegration may be expected to reduce the cross section for positive pion production from deuterium below that for hydrogen.

The preceding consideration of charged pion photoproduction in deuterium indicates that a careful consideration of the experimental conditions that obtain for any particular experiment is required if pion production in deuterium is to be related to reactions (1.1) and (1.2).

(d) Review of Published Experimental Work.

The experimental investigation of charged pion photoproduction in deuterium may be divided into two categories, experiments in which only one final state particle is detected, and those in which two or all three particles are detected. Experiments in the first category have the advantage of being suitable to the use of counter techniques and good statistics are in general possible. The interpretation of the results of these experiments requires a model to relate pion photoproduction in deuterium to that in hydrogen. Experiments in the second category suffer from poor statistical accuracy, whether the experiment employs a visual technique where the analysis is tedious, or a counter technique requiring the simultaneous detection of more than one particle where counting rates will be low. These experiments

allow an investigation of the validity of the various models for pion photoproduction in deuterium in addition to measuring pion photoproduction cross sections. Experiments in which one particle only is detected will be discussed first.

The negative to positive pion ratio from deuterium (hereafter called the -/+ ratio) was measured by Beneventano et al.(1954, 56, 58). A liquid deuterium target was irradiated by the 300 MeV bremsstrahlung beam of the Illinois betatron. The pions were detected in pellicles which were immersed in a large block of emulsion. This arrangement compensated for scattering losses, and the effective solid angle was defined by the pellicle size. The pellicles were underdeveloped to reduce the effect of the large electron background present near the photon beam. Identification of the negative and positive pions depended upon the track endings. A knowledge of the star-prong frequency of negative pion endings was required. This was obtained from ~~exposure of~~ plates exposed to a negative pion beam from the Chicago cyclotron. Several exposures were made in which the electron background was greatly reduced. This allowed normal development, and the positive pions could be identified by the $\mu - e$

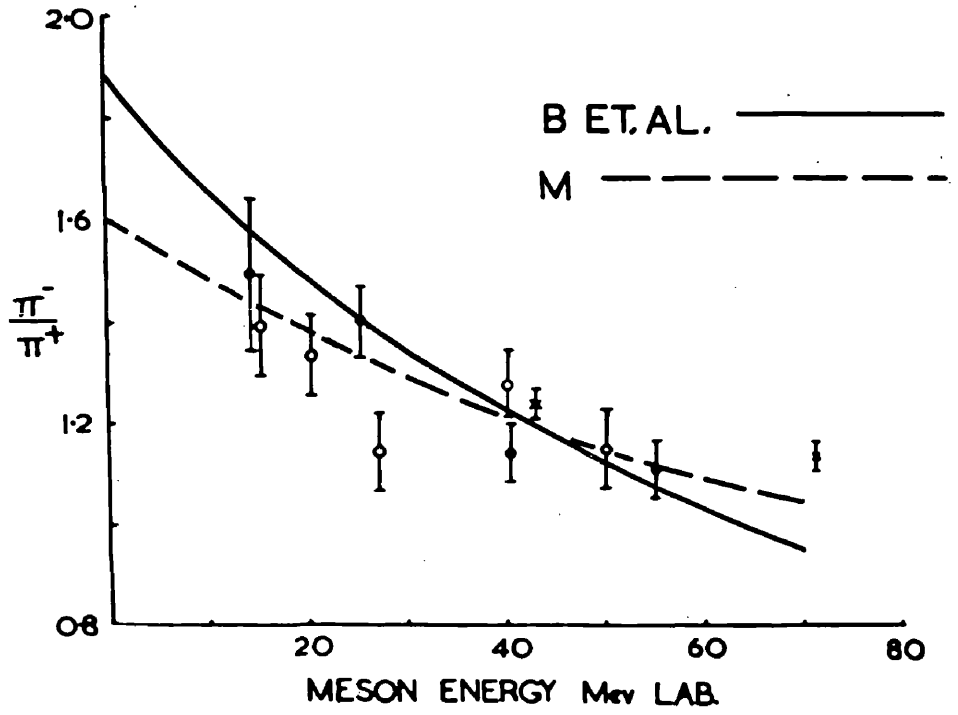

π^-/π^+ RATIO FROM DEUTERIUM AS A FUNCTION OF PION ENERGY, ANGLES MEASURED IN THE LAB. SYSTEM.

× 73° Sands et al, 1954.

● 75° Beneventano et al, 1956.

O 75° HOGG & BELLAMY

Figure 1.6.

decays. The prong-frequency for the negative pion endings obtained from these exposures agreed well with that obtained from the plates exposed to the cyclotron pion beam. The uncertainty in the negative to positive ratio due to pion identification was small. The -/+ ratio obtained by Beneventano et al. at 75 degrees in the laboratory system is shown in figure 1.6.

The -/+ ratio from deuterium has been measured by a number of groups using various types of counters as detectors and magnetic deflection to separate negative and positive pions. Sands et al. (1954) measured the -/+ ratio for pions produced in a cooled high pressure gas target at 3 angles in the laboratory system. Their measurement extended over pion kinetic energies from 30 to 200 MeV. Hogg and Bellamy (1958) detected 15 to 70 MeV pions produced in a liquid deuterium target at 75 degrees in the laboratory. The measurements of Sands et al. and Hogg and Bellamy are shown with those of Beneventano et al. in figure 1.6 The agreement between the three sets of data is good. The solid curve is the extrapolation to threshold used by Beneventano which gives a value of 1.87 for the -/+ ratio at threshold. The Coulomb corrections reduce the cross section at a free

neutron by about 10 percent. Moravcsik (1958) has shown that by applying small but reasonable corrections to the parameters used by Beneventano a significant difference in the extrapolation is obtained. The dashed curve is due to Moravcsik. His extrapolation implies a -/+ ratio from free nucleons of 1.4 in good agreement with the theoretically predicted threshold ratio of 1.3.

Adamovic et al. (1959) measured the negative pion production cross section in deuterium very near threshold. The same workers also measured positive pion cross sections from hydrogen (Adamovic, 1960). They obtain a threshold value for the -/+ ratio of 1.3 ± .15 for photoproduction at free nucleons. The agreement among the various sets of data is good, and the threshold -/+ ratio from free nucleons may be regarded as well established.

It is interesting to note that the three sets of data shown in figure 1.6 were obtained with very different peak photon energies namely, 235 MeV Hogg and Bellamy, 300 MeV Beneventano et al., and 500 MeV Sands et al. The agreement between these measurements indicates that the -/+ ratio is not strongly dependent upon peak photon energy at these energies. Near threshold however the measured -/+ ratio from deuterium may be strongly effected

by the maximum photon energy available due to the different threshold energies for negative and positive pion photoproduction (Khavlomov, 1959). The effect will be large if the maximun photon energy is close to the threshold.

Recently Land (1959) has measured the -/+ ratio from deuterium due to monoenergetic photons using a photon difference method. The M.I.T. synchrotron was operated with maximum energy E max at 307 and 292 MeV. The pion yields measured at these values of E_{max} are normalized and subtracted to give the yield due to monoenergetic photons at 292 ± 8 MeV. The pions were detected using magnetic deflection and a scintillation counter telescope. The -/+ ratios obtained for monoenergetic photons are, 0.90 ± .23 at 73 degrees for 98 MeV pions and 1.07 ± .16 at 120 degrees for 30 to 90 MeV pions. These values are below those obtained in this experiment, and below values obtained by other workers for the -/+ ratio measured using bremsstrahlung beams. Land suggests that for production due to a bremsstrahlung beam, pions will be counted due to photons outside the 292 ± 8 MeV interval. Since the ratio rises with decreasing energy and little contribution can be expected from higher energy

photons (E_{max} = 307) the contribution from lower photon energies will tend to increase the ratio measured using bremsstrahlung beams. This suggestion is surprising, considering the agreement between the various measurements shown in figure 1.6. The errors assigned to the monenergetic measurement need to be reduced before a definite disagrement can be said to exist.

A convenient summary of the experimental data from -/+ ratio measurement prior to 1957 is given by Moravcsik (1957). He compares the -/+ ratio calculated using various approximations with the measured ratio over a wide range of photon energy and pion production angles. The -/+ ratio is always greater than one. Except at backward angles it decreases with increasing photon energy. The -/+ ratio rises towards backward angles at all energies.

The ratio of positive pion photoproduction from deuterium and hydrogen (hereafter called the D/H ratio) has been measured in a number of experiments (Beneventano et al.,1958, Hagerman et al.,1957, White et al.,1952). The techniques used are similar to those employed in the -/+ ratio measurements. The measurement by Beneventano for photon energies up to 230 MeV shows that the D/H

ratio is less than unity and that it decreases towards forward angles and low energy. This behaviour is predicted by the Chew and Lewis calculations, since low photon energies and forward angles is the region of small D. Attempts to obtain spin dependence of pion production from measurement of the D/H ratio have led to inconclusive results.

Photoproduction of negative pions in deuterium near threshold has been investigated by Adamovic et al. (1959). This experiment is the most complete study of this reaction that has been reported. It will be described in detail.

Nuclear emulsions loaded with heavy water were exposed to 200 and 250 MeV bremsstrahlung beams from the Lebedev Physics Institute synchrotron. In this experiment the loaded emulsions acted as target and detector. Pions up to 30 MeV kinetic energy could be registered in the heavy water loaded emulsions allowing measurement of the cross section for photon energies up to 174 MeV. Just over 2000 cm^2 of emulsion were scanned and 720 events due to photons between 174 Mev. and threshold were found. A few more sensitive plates were used to measure the cross section for photons between 174 and 202

MeV.

The three final state charged particles were registered in the emulsion. The identification of particles that stopped in the emulsion presented no problem. Some tracks which left the emulsion were identified by multiple scattering and grain counting techniques. A small fraction of the events (8%) in which one or two particles left the emulsion were identified using the momentum and energy conservation conditions for reaction (1.4). All 3 prong stars were analysed using this condition and an error ΔP was obtained for each star. The star distribution was plotted as a function of ΔP for the heavy water loaded emulsion, and compared with the distribution in ΔP obtained from plates loaded with water. No events were found in the latter set of plates in the range of ΔP where events were ascribed to reaction (1.4). The identification of stars due to (1.4) was considered to be unambiguous.

For each event the photon energy, pion energy and angle of emission, $p = \frac{1}{2} p_1 - p_2$, and $q = \frac{1}{2} p_1 + p_2$ were determined. The impulse approximation calculation of Baldin gives the cross section for reaction (1.4) as a function of p and q. A detailed comparison between

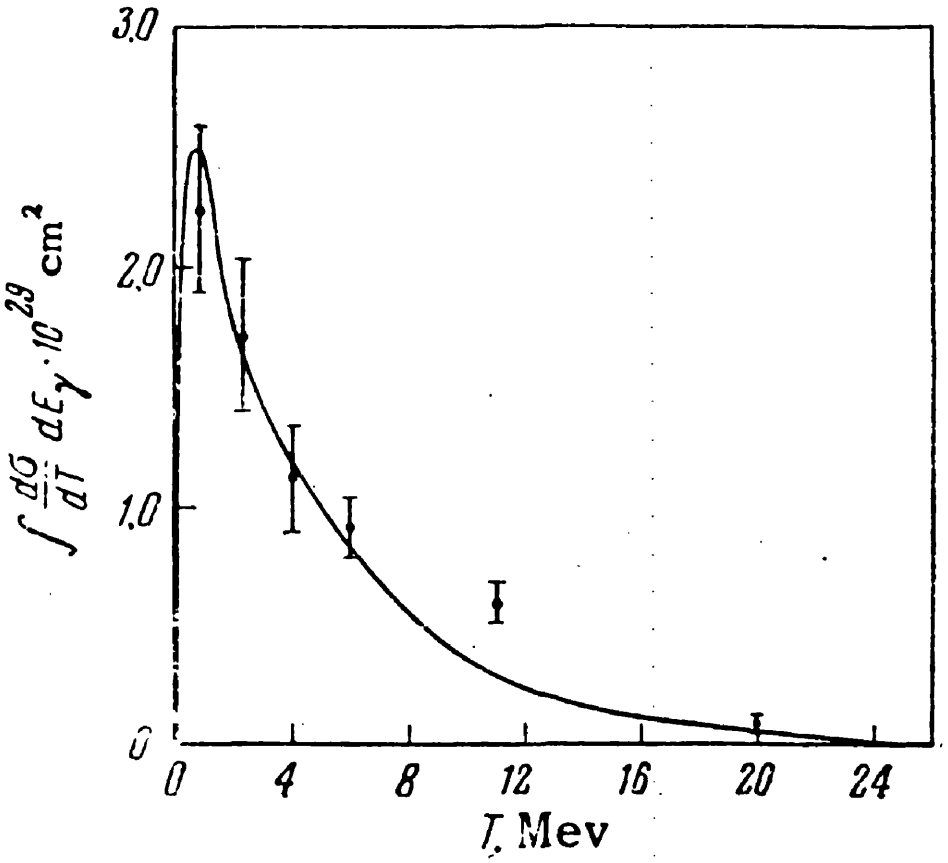

Figure 1.7 Energy spectrum of the relative motion of the two protons.

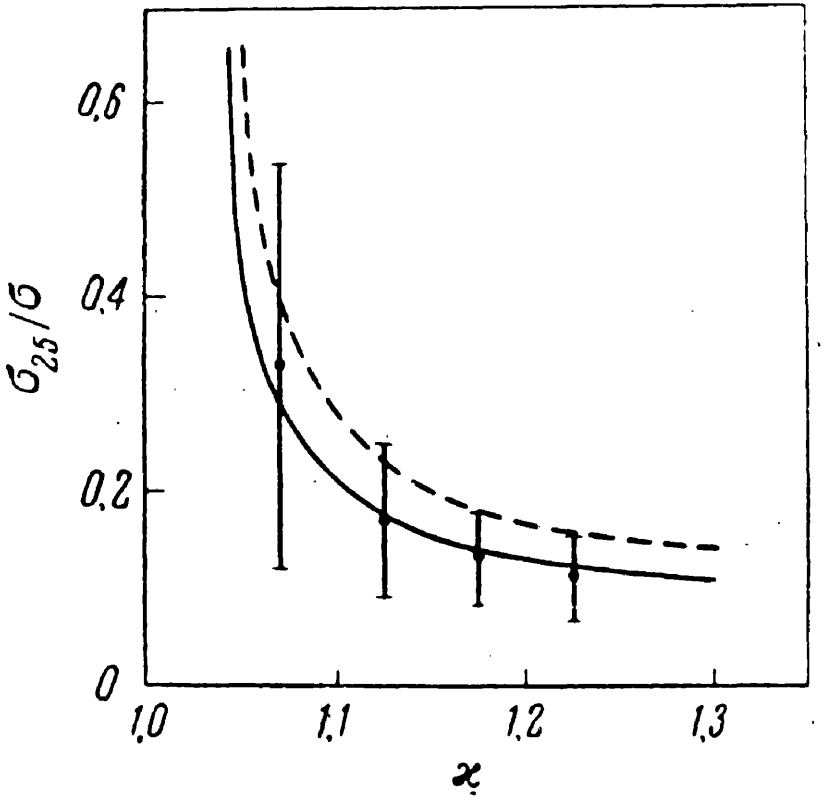

Figure 1.8 Dependence of the ratio $\sigma_{2.5}/\sigma$ on the photon energy $\varkappa$.

the predictions of Baldin's calculations and the experimental results was made. The energy spectrum of relative motion of the two protons is shown in figure 1.7. The theoretical spectrum is calculated for L = 0, and a value of $|K_n|^2$ obtained from the positive pion cross section from hydrogen and the theoretical value of 1.3 for the -/+ ratio. In figure 1.8 the ratio $\sigma_{2.5}/\sigma$ is shown as a function of photon energy. Here σ is the total cross section and $\sigma_{2.5}$ is the cross section for production of a pion when $q/p \geqslant 2.5$. The solid curve represents the theoretical ratio $\sigma_{2.5}/\sigma$ the dashed curve was calculated omitting the Coulomb interaction.

The observed cross section is isotropic in the centre of mass system, and shows an η^2_{max} dependence, where η_{max} is the maximum possible pion momentum. Adamovic (1959) compares these properties of the data with the dependence predicted for various transitions.

Finally the squared matrix element for pion photoproduction at a free nucleon $|K_n|^2$ is obtained from a careful consideration of the experimental and calculated cross sections for values of p and q where the calculations of Baldin are known to be accurate. In a subsequent experiment Adamovic et al. (1960) measured the cross

section for positive pion production near threshold. The statistical accuracy of the data is not sufficiently good to enable the choice to be made between $|K_p|^2$ and $|K_n|^2$ constant and the Cini extrapolation. $|K_p|^2$ and $|K_n|^2$ were extrapolated to threshold using the Cini method to obtain the threshold -/+ ratio. This ratio should be independent of systematic errors in beam monitoring.

The results of these experiments may be summarized as follows:

1. The impulse approximation is valid for this interaction provided the Coulomb interaction in the final state is included.
2. Near threshold the transition occurs through electric dipole absorption of the photon, the pion is emitted in an S state and the nucleons are left in a singlet S state, i.e. spin-flip production occurs.
3. The -/+ ratio at threshold is 1.3 ± .15 in good agreement with the predicted value of 1.3.

An experiment in which the bremsstrahlung beam of the Berkeley electron synchrotron was passed through a 4 inch deuterium bubble chamber is reported by Swanson

Table I. σ^-/σ^+ as a function of photon energy and meson angle.

Bins	Spectator photon energy (Mev)[a]	θ^* pion c.m. angle, (deg)	σ^-/σ^+ Before (R_d) Coulomb correction	σ^-/σ^+ After (R) Coulomb correction
I	152 - 158	0 - 90	1.22 ± 0.16	1.08 ± 0.14
II	158 - 165	90 - 140	1.36 ± 0.19	1.27 ± 0.18
III	165 - 175	135 - 180	1.54 ± 0.21	1.44 ± 0.20

[a]The spectator photon energy (lab) and pion angle θ^* (lab) are from $(\gamma + p \rightarrow \pi^+ + n)$ two-body kinematics.

Figure 1.9.

(1960). Negative and positive pion production in deuterium were observed. The former reaction was identified using energy and momentum conservation conditions, the latter by the characteristic range of the decay μ meson. The -/+ ratio for deuterium obtained by Swanson is shown in figure 1.9. The photon energy and centre of mass pion angle were assigned using the two-body kinematics for both reactions since the true photon energy was not determined for positive pion production. The negative pion yield was corrected for Coulomb effects to obtain the -/+ ratio for free nucleons. The ratio for the lowest energy "bin" is below the theoretical value. The average value for the -/+ ratio for deuterium and free nucleons are 1.38 ± .12 and 1.27 ± .11 respectively. The distribution of photon energies contributing to negative pion production for events in "bin" 2 is presented. The distribution is peaked about the two-body photon energy, but extended 10 MeV below and 20 MeV above that value. The width of this distribution indicates that considerable uncertainty may be introduced by use of two body kinematics to assign photon energies.

Although separate measurement of negative pion production in deuterium and positive pion production in hydrogen can introduce uncertainty in beam monitoring,

this procedure is to be preferred to that of Swanson et al. since the kinematics are then completely defined for both reactions.

Keck and Littauer (1952) have investigated the spectator model for pion photoproduction in deuterium using a scintillation counter technique. In this experiment D^2O and H^2O targets were irradiated by 310 MeV bremsstrahlung. A three counter telescope detected pions emitted at 90 ± 10 degrees with an energy of 56 ± 9 MeV. The pions were identified by their specific ionization and range, the first two counters were operated in coincidence and in anticoincidence with the third counter. The protons were detected in a NaI(Tl) crystal that could stop 69 MeV protons. The proton energy was measured using a pulse height analyser. The angular distribution and energy spectrum of the protons detected in coincidence with the pions are shown in figure 1.10. Curves A were calculated for pion production at a free neutron at rest. The angular resolution and energy acceptance of the counter system is included. Curves B represent the distributions expected if the spectator model is assumed. Once again the resolution of the counter system is included.

The agreement between the observed angular distribution

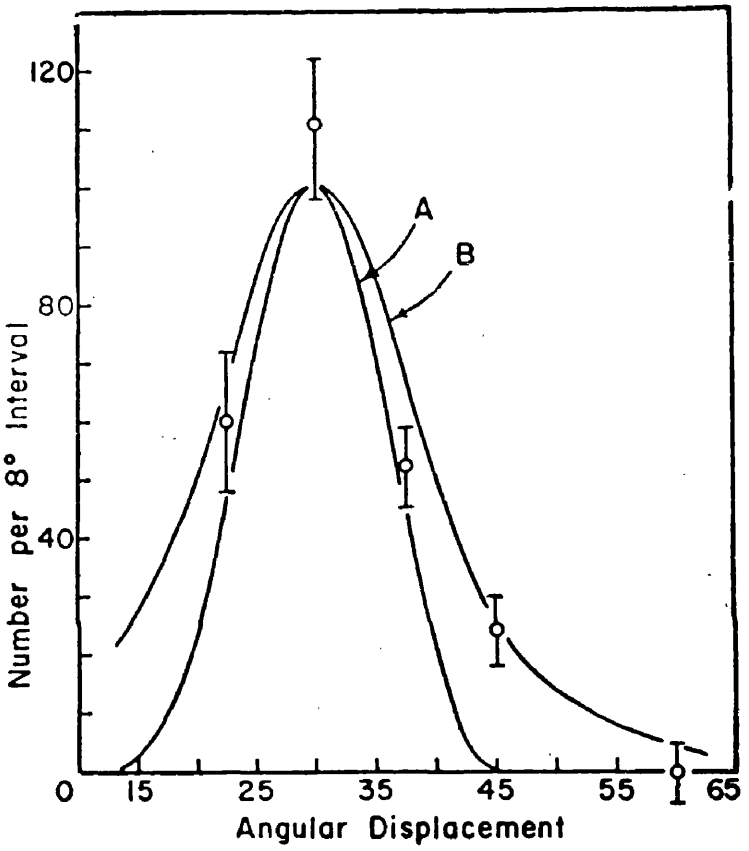

Angular distribution of recoils counted in coincidence with a 56-Mev meson at 90°. See text for explanation of curves.

Figure 1.10a.

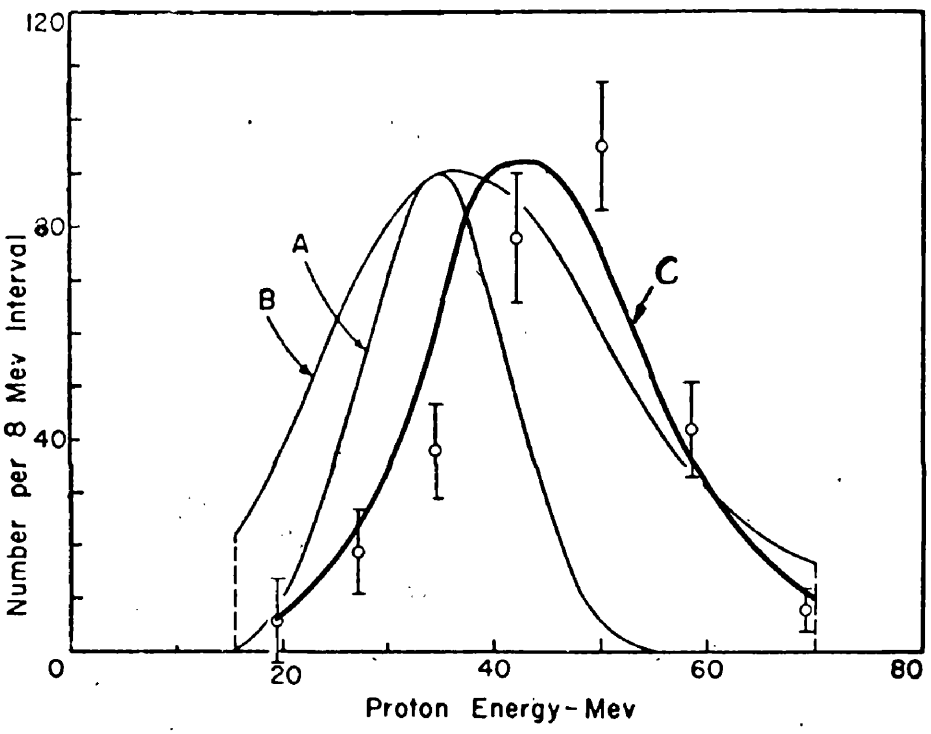

Energy distribution of recoils at 30° counted in coincidence with a 56-Mev meson at 90°. See text for explanation of curves.

Figure 1.10b.

and that predicted by the spectator model is satisfactory. The experimental points for the proton energy spectrum do not agree with either curve A or B. They appear to be shifted towards higher energy by 12 to 15 MeV. This discrepancy was not resolved. The energy calibration of the proton counter was done using three different methods. The pulse height in the proton counter was measured for the Cs 137 photopeak at .67 MeV. The pulse height produced by cosmic-ray mesons at 9.5 MeV was measured. The number-bias curve obtained using a beam of inhomogeneous protons was extrapolated to high energy cut off at 69 MeV. These methods agreed to within ±5 percent. Other sources of error were considered. The effect of pions scattering around the third counter in the pion telescope was shown to be negligible. Multiple scattering of the protons in the targets, and possible variations in the pion cross section were shown to be small effects.

The differential cross section for negative pion photoproduction accompanied by a correlated recoil proton was calculated using curve B for the angular distribution. This gave $10.8 \pm 1 \times 10^{-30}$ cm.^{2} per steradian in good agreement with the value $11.8 \pm 1.2 \times 10^{-30}$ cm.^{2} per steradian obtained from the total pion counting rate and the -/+ ratio for

deuterium measured by Littauer and Walker (1952).

The impulse approximation theory of Chew and Lewis was used by Thie (1952) to derive an expression for the cross section for detection of a pion and recoil proton in coincidence. The expression is

$$\frac{d\sigma}{d\Omega_\mu\, dE_p\, d\Omega_p} = \frac{M P \mu \mu_0 \left[\mu(\mu_0+2M) - \mu_0 v_0 \cos\theta_\mu\right]}{32\pi^2 \left|\mu(\mu_0+M) + \mu_0 P\cos(\theta_p+\theta_\mu) - \mu_0 v_0 \cos\theta_\mu\right|} \mathcal{F} \qquad (1.16)$$

where P is the nucleon momentum,

$$E_p = P^2/2M,$$

$$\mathcal{F} = \left[\frac{1}{3}|E_f|^2 + \frac{2}{3}|O_f|^2\right] K^2 + |O_f|^2 L^2,$$

$\theta\mu$ and θ_p are the pion and proton angles respectively, $d\Omega_\mu$ and $d\Omega_p$ are the solid angle for the pion and proton respectively, and the remaining symbols have been defined. Curve C in figure 1.10 was obtained from the above expression by a numerical integration. Although the maximum occurs at higher energy than for curves A and B it does not agree with the experimental points.

Reaction (1.4) was studied by White et al. (1960) for photon energies between 200 and 1000 MeV. They used a large diffusion cloud chamber filled with deuterium gas at 14 atmospheres and operated in a magnetic field of 6 kilogauss. The 1040MeV bremsstrahlung beam from the

Cornell synchrotron was hardened using lithium hydride to reduce the relative number of low energy photons and passed through the chamber. Reaction (1.4) was distinguished from other three prong events, multiple pion production for example, by a detailed kinematical analysis of each event.

The spectral shape of the hardened beam was known so that the cross section for negative pion production in deuterium was obtained. The cross section for photoproduction at a free neutron at rest was derived from the measured cross section, by first transforming each event into the centre of mass system to obtain the cross section for a bound neutron at rest and then by dividing this quantity by the D/H ratio. The cross section derived in this way agrees well with that obtained by the more conventional method of multiplying the positive pion cross section at a proton by the -/+ ratio.

A direct comparison is made between the observed momentum distribution of the spectator proton and the momentum distribution of the nucleon bound in the deuteron. Figure 1.11 shows a histogram of the laboratory distribution of the spectator momenta. The observed distribution has been corrected for a cross section bias

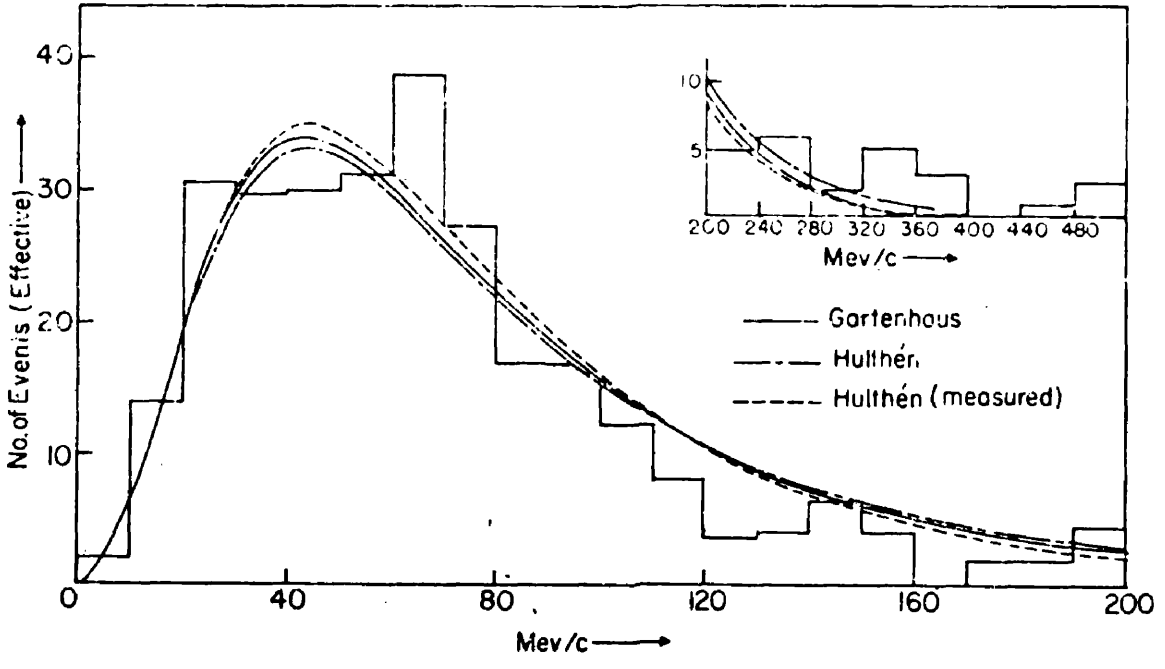

Figure 1.11 Histogram of the laboratory distribution of spectator momenta, corrected for cross-section bias. Curves represent internal deuteron momentum distributions as calculated by the Hulthén and Gartenhaus wave function, as well as the Hulthén momentum spectrum with the spectator identity ambiguity and inaccessibility folded in (see text). One event is above 500 Mev/c, and is not shown.

due to the nucleon momentum. The curves are the momentum distributions calculated from the Gartenhaus and Hulthén wave functions. The spectator model has an inherent ambiguity in identifying the lower momentum proton as the spectator. This effect will be greatest for large spectator momenta. The "measured" curve includes the effect of this ambiguity on the shape of the momentum distribution. The agreement shown in figure 1.11 is good. A few protons of high momentum were observed and must be considered to have interacted in the final state. White attributes the deficiency in the 100 to 200 MeV/C region to the competing photodisintegration process. The number of events did not permit a detailed analysis of the angular distribution. A definite excess of spectator protons was observed in the forward direction for photon energies above 250 MeV. This could be interpreted by assuming an average momentum transfer to the spectator proton of 10 MeV/C.

The work of White et al. gives strong support to the validity of the spectator model description of pion photoproduction in deuterium in the region from 200 to 500 MeV. At higher energy the data is scarce. On the other hand the discrepancy observed by Keck and Littauer

in the recoil proton energy compared to the spectator model predictions would indicate that the spectator model is suspect. The experimental study of negative pion photoproduction in deuterium described in this thesis was directed towards investigating this discrepancy from the experimental side.

(e) The Present Experiment.

The experimental method consisted of simultaneous detection and measurement by scintillation counter telescopes of the proton and negative pion produced in the reaction $\gamma + d \rightarrow p + p + \pi^-$ (1.4). A thin liquid deuterium target was irradiated by the 307 MeV bremsstrahlung beam of the Glasgow electron synchrotron. Pions were detected at 90 ± 3.7 degrees in the laboratory and in an energy range from 46 to 60 MeV using a scintillation counter telescope. The coincident protons were detected in a second scintillation counter telescope. The angular distribution and energy spectrum of the coincident protons were measured.

The pion telescope consisted of 4 scintillation counters operated in a 1 + 2 + 3 - 4 coincidence-anticoincidence sequence. The pions were identified

by their specific ionization in counters 1 and 2 and by their range. The two counter determination of specific ionization permitted much better separation of pions from other charged particles than is possible with a single counter.

The proton telescope had three scintillation counters. The front scintillator was thin, the second had a range equal to that of 81 MeV protons. This counter telescope identified protons in the energy range from 12 to 81 MeV, by means of their specific ionization and energy.

The detection of a pion by the first counter telescope triggered the sweep of an oscilloscope. The pulses from counters 1 and 2 in the proton telescope were displayed on the oscilloscope trace which was photographed. The position of the pulses on the oscilloscope trace were used to eliminate the background events. The energy spectrum of the protons was obtained from the pulse height distribution of the pulses from counter 2. The ability to identify both the pion and the proton greatly reduced the possibility of including events due to interactions other than (1,4). The use of the liquid deuterium target marks a definite improvement over the $D^2O - H^2O$ subtraction technique.

CHAPTER II

The Response of Plastic Scintillator.

In many experiments in nuclear physics the pulse height produced by charged particles in scintillation counters is used to measure the energy loss in the scintillator. The present investigation is an example of such an experiment. Scintillators having a linear response to particle energy are to be preferred in such applications. The inorganic scintillators, sodium iodide and caesium iodide, are often used for this reason. When intense pulsed sources of radiation are used the long scintillation decay time common to inorganic scintillators (of the order of a μ second) makes their use difficult. Organic scintillators have decay times of a few nanoseconds, and may be used where very high instantaneous counting rates are expected (e.g. 10^7 per sec.). The response of organic scintillators to heavily ionizing particles is known to be non-linear. The response to a particular particle, protons or pions say, must be determined before calibration at one or two energies only will permit accurate measurement of particle energies. The commercially available plastic scintillator is the most convenient scintillator for use in counter experiments in

which large area counters are required. Since the response of plastic scintillator to protons had not been measured a direct calibration was done (Evans and Bellamy, 1959).

Birks (1953) has developed a theory describing the scintillation process in organic scintillators. He interprets the scintillation phenomena in terms of emission of primary photons by molecules that are ionized or excited by the incident particle. These photons are in the ultraviolet region and are reabsorbed. The reabsorption may be accompanied by fluorescence in the visible or near ultraviolet region. Non-radiative capture is a competing process, and the relative importance of the two processes will largely determine the scintillation efficiency of a particular material. The saturation observed in the response of organic scintillators to heavily ionizing particles is explained by molecular damage in the ionization column. Let A dE/dx represent the number of ionized or excited molecules per unit path length capable of primary photon emission, where dE/dx is the specific ionization. The number of damaged molecules is also proportional to dE/dx, i.e. B dE dx. If the probability for capture by a damaged

molecule for the primary photon is k times that for capture and fluorescence by an undamaged one then the specific fluorescence is

$$\frac{dS}{dx} = \frac{A\ dE/dx}{1 + kB\ dE/dx} \qquad (2.1)$$

For small values of dE/dx, kBdE/dx $\ll$ 1 and (2.1) reduces to

$$dS/dx = AdE/dx \qquad (2.2)$$

in agreement with the linear response observed for electrons in organic scintillator. For very heavily ionizing particles, kBdE/dx $\gg$ 1 and (2.1) becomes

$$dS/dx = A/kB \qquad (2.3)$$

indicating that the specific fluorescence approaches a limiting value for heavily ionizing particles.

In organic solution phosphors or phosphor-plastic mixtures, the primary emission is by the solvent or base, and the values of A and kB would be expected to depend upon the nature of the base and the fluorescent material and its concentration.

The response of a plastic scintillator has been investigated by Borelli and Grimeland (1955). They

assumed equation (2.1) to be true and measured dS/dx for electrons and polonium 210 alpha particles. Using (2.2) and (2.3) they obtained a value of kB = 10.5 cm air equivalent per MeV. The scintillator they used was of a different manufacture than those currently available. The calibration of plastic scintillator described below does not depend upon the assumption that (2.1) correctly described the specific ionization and is the first direct calibration of plastic scintillator response to protons reported.

Protons of an initial energy of 14.8 MeV were obtained from the reaction $d + He^3 \rightarrow p + He^4$ using deuterons accelerated in a Cockroft-Walton high voltage machine. The He^3 was present as a decay product in a tritium target so that the reaction $d + H^3 \rightarrow n + He^4$ also occurred producing 14 MeV neutrons. The yield of protons relative to neutrons increases as the energy of the incident deuterons is reaised above 120 KeV where a resonance in the neutron production occurs. The high voltage machine was operated at 400 kilovolts near the resonance for proton production. To further reduce the background due to knock on protons from the high neutron flux the protons were detected using a coincidence

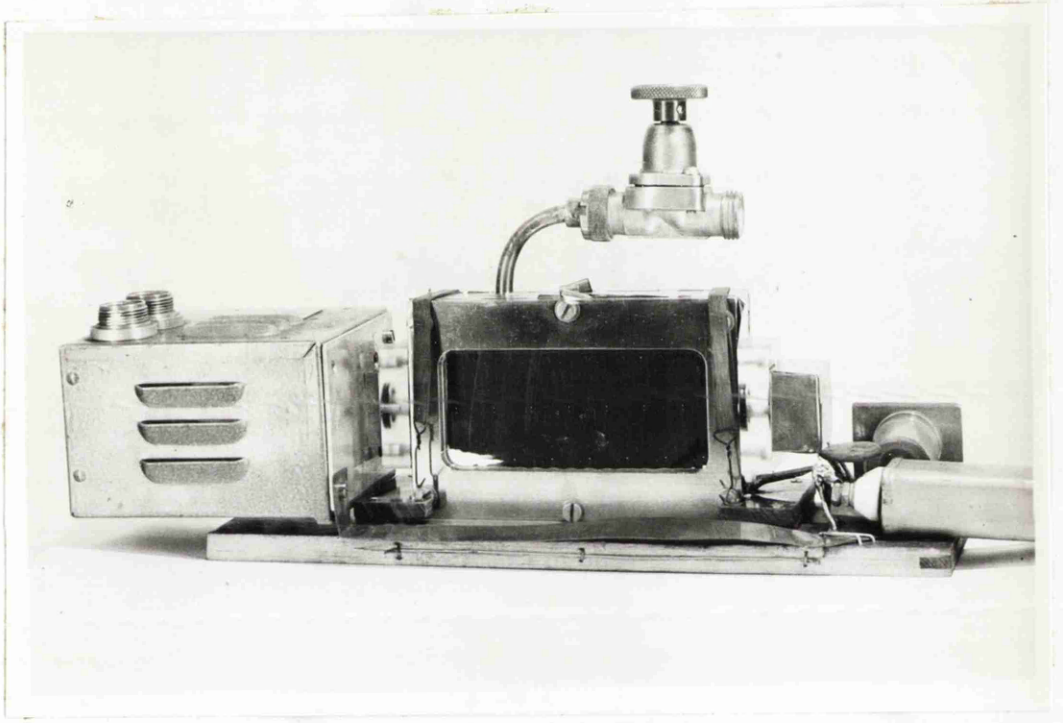

Figure 2.1. Thin proportional counter and head amplifier.

counter telescope.

The front counter was a thin gas filled counter operated in the proportional region shown in figure 2.1. It was constructed by milling a $4\frac{1}{2}$ by 2 inch hole out of a 1 inch thick piece of brass. The central wire was 3 thou tungsten. Since only the central portion of the counter was used no special precautions were taken to eliminate end effects. Celophane aluminized on the inside was used for the windows. The celophane sheets were sealed against "O" rings by means of clamping plates. The counter was filled with a 93 percent argon 7 percent methane mixture at a pressure of one atmosphere. The response of this counter was tested using protons and polonium α-particles and shown to be approximately proportional to the particle energy lost in the counter. The use of the counter to discriminate against neutrons however did not depend upon this property.

In the second counter the scintillator under test was viewed by an R.C.A. 6810 photomultiplier. A short length of lucite was interposed between the scintillator and the photomultiplier to reduce effects due to uneven response over the area of the photocathode. The photomultiplier output was integrated at the collector

so that the counter pulses corresponded to the total scintillation response.

The proportional counter was used to gate the output from the scintillation counter. The latter was amplified and displayed on a 100 channel kicksorter. A delay was introduced between the scintillation counter and the kicksorter to allow the kicksorter gate time to operate. The amplitude of the input pulse to the kicksorter was adjusted so that the peak in the pulse height distribution occurred near the middle of the kicksorter range. This was done using an attenuator in the amplifier, which was adjustable in 2 db steps. The accuracy of the attenuator settings was checked and found to be correct to within 2 percent. No correction was made for this error. The pulse height at the collector of the photomultiplier was never greater than .3 volts so that saturation in the photomultiplier was avoided. A block diagram of the circuit is shown in figure 2.2.

The experimental arrangement is shown in figure 2.2. A 1 thou mylar window allowed the protons to leave the vacuum system of the high voltage machine with minimum loss of energy. The scintillator was 11 cm, from the exit window and the maximum proton energy entering the

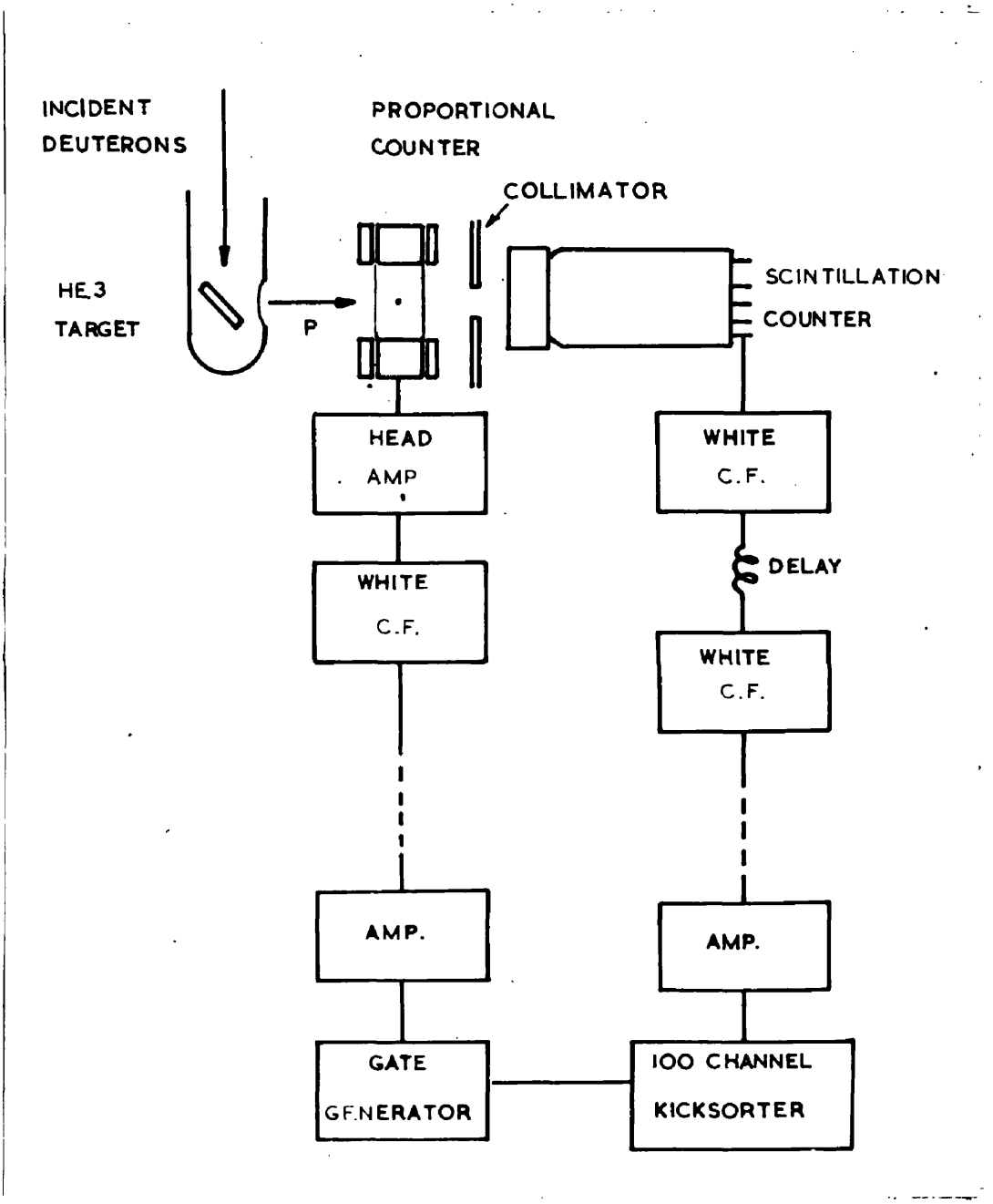

Figure 2.2. Experimental arrangement and block diagram of circuit used in calibration of plastic scintillator.

scintillator at that position was 14.0 MeV. The energy of protons entering the scintillator was varied by interposing aluminium absorbers between the two counters. The pulse height distributions for protons at nine energies between 14.0 ± .05 MeV and 3.08 ± .18 MeV were determined. The protons entering the scintillator were collimated by a 1½ inch hole in a 1/16 inch sheet of aluminium to reduce the spread in energy due to protons traversing the absorber at large angles. The pulse height distribution for protons of energy 1.2 ± .1 MeV was obtained using protons from the reaction $C^{12} + d \rightarrow C^{13} + p$.

The response of the scintillator to protons was normalized to the electron response using the Compton edges for 2.62 MeV thorium gamma rays and the 1.28 MeV sodium 22 gamma rays.

The pulse height distributions obtained for 14.0 ± .05 MeV protons is shown in figure 2.3. The two curves A and B are the distributions obtained with and without the gate. The pulse height distributions for protons that have traversed 245 milligrams/cm.^{2} of aluminium is also shown. Considerable deterioration in pulse height resolution is evident.

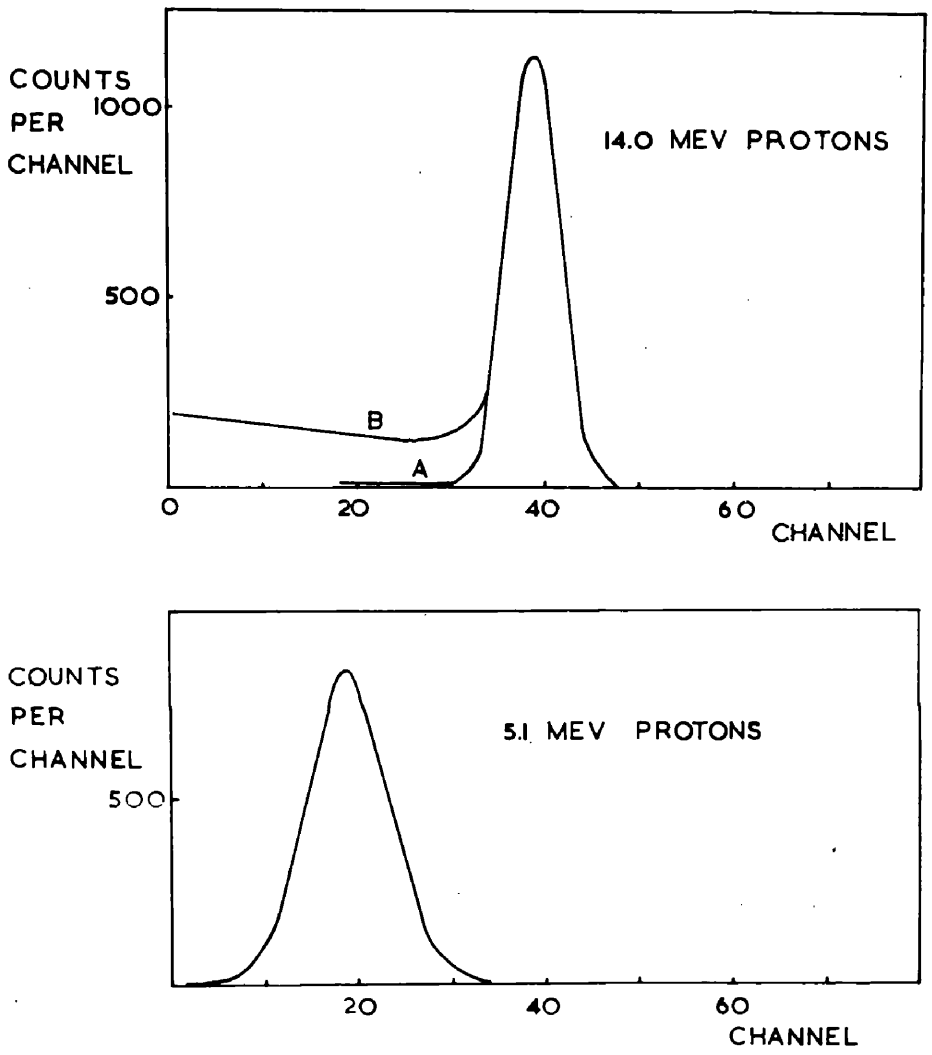

Figure 2.3. Pulse height distributions obtained for protons in scintillator calibration.

The response of two commercially available plastic scintillators was measured. A 2 inch diameter ½ inch thick sample of NE 102 produced by Nuclear Enterprises G.B. Ltd., and a 3 inch diameter 2 inch thick sample manufactured by Messrs. Nash and Thompson Ltd. were used. Both scintillators have a polyvinyltoluene base.

The results of the measurements are given in table 2.1. The thickness of the aluminium absorber is given in the first column. The range energy tables of Atkinson and Willis (1957) were used to determine the residual energy of the proton entering the scintillator. The proton energy is given in the second column. The errors include uncertainty in absorber thickness and in initial proton energy. In the third column the pulse height relative to that for a 1 MeV electron is given. The half width at half maximum of the pulse height distribution obtained at each energy is also given.

The response of plastic scintillator NE 102 is shown in figure 2.4. The experimental points are taken from table 2.1. The calibration points obtained from the Compton edges for thorium and sodium 22 gamma rays are shown. The indicated errors are the spread in pulse height from ¾ to ¼ height on the Compton edge.

Table 2.1a.

Response of Plastic Scintillator NE 102 to Protons.

Absorber Thickness (gms/cm^2) $\times 10^{-3}$	Proton Energy (MeV)	Pulse Height Relative to 1 MeV Electrons.
0	14.0 ± .05	8.08 ± .55
27.0 ± .1	13.2 ± .05	7.46 ± .6
74.5 ± .2	11.8 ± .05	6.30 ± .5
147.3 ± .4	9.4 ± .08	4.73 ± .4
172.6 ± .5	8.4 ± .10	4.07 ± .5
219.2 ± .6	6.4 ± .12	2.84 ± .4
244.5 ± .7	5.1 ± .14	1.80 ± .4
259.5 ± .7	4.2 ± .15	1.37 ± .4
274.5 ± .8	3.08 ± .18	.82 ± .4
$C^{12}(d,p)C^{13}$	1.2 ± .13	.25 ± .1

Table 2.1b.

Response of Nash and Thompson Plastic Scintillator to Protons.

Absorber Thickness (gms/cm.^{2}) x 10^{-3}	Proton Energy (MeV)	Pulse Height Relative to 1 MeV Electrons.
0	13.8 ± .05	7.33 ± .7
25.3 ± .1	13.1 ± .05	6.83 ± .6
72.8 ± .2	11.7 ± .05	5.89 ± .6
98.1 ± .3	10.9 ± .05	5.26 ± .5
144.7 ± .4	9.3 ± .08	4.37 ± .5
170.0 ± .5	8.3 ± .08	3.52 ± .5
219.0 ± .6	6.15 ± 1.1	2.31 ± .4
244 ± .7	4.8 ± 1.2	1.39 ± .4

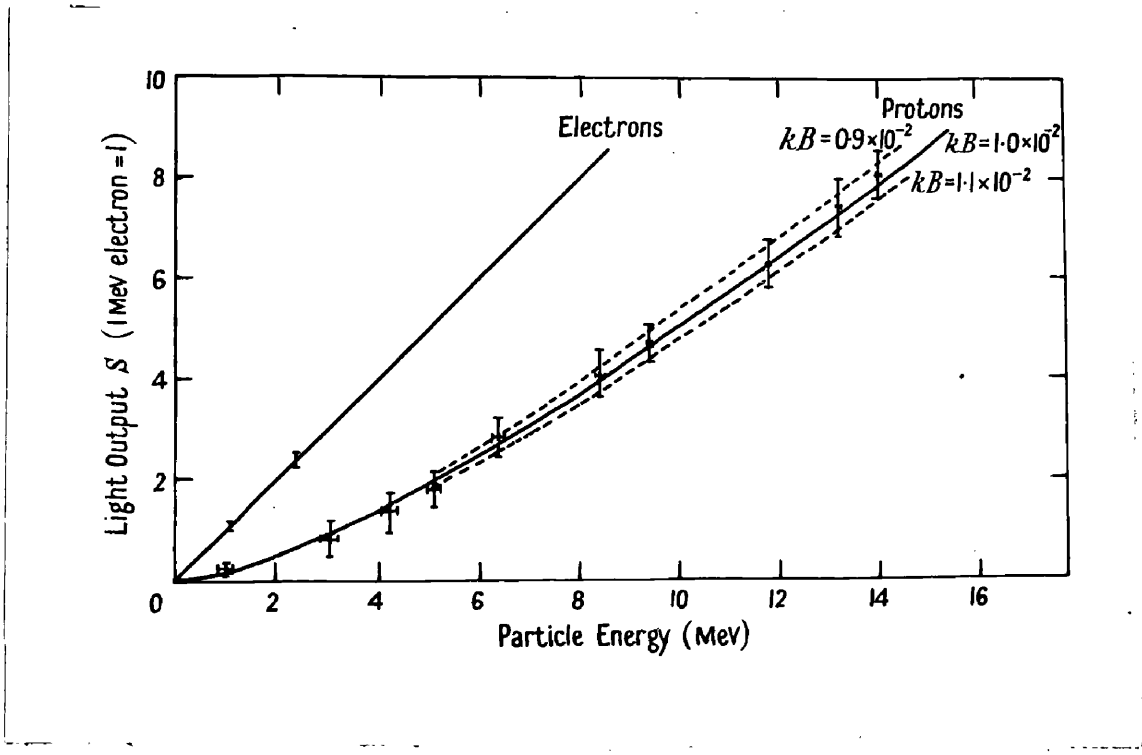

Figure 2.4. Response of plastic scintillator to protons. The curves were calculated using Birks' expression for specific fluorescence in organic scintillator for the values of kB shown.

The response of the scintillator predicted by Birks' expression, (2.1), may be obtained by integrating the specific fluorescence over the particle range.

$$S(E) = \int_0^R \frac{dS}{dx}\,dx = \int_0^R \frac{dE/dx}{1 + kB\,dE/dx}\,dx$$

$$\approx \sum_0^E \frac{\Delta E_i}{1 + kB(dE/dx)_i} \qquad (2.4)$$

where A = 1 corresponding to normalizing the pulse height to 1 MeV electrons, $(dE/dx)_i$ is the specific ionization appropriate to a proton of energy E_i, and R is the particle range. The last expression in (2.4) was used to calculate the curves in figure 2.4 for various assumed values of kB. The range energy relationship in plastic was taken as that for CH given by the tables of Rich and Madey (1954). The composition of plastic scintillator is given by the manufacturers as $CH_{1.105}$. Since the difference between the range energy relationship for CH and CH_2 is small, the error in assuming CH for plastic is negligible.

It is evident that a 10 percent variation in kB does not introduce a large change in the calculated response. The experimental points for NE 102 are best fitted when kB = 1.0×10^{-2} gms.cm^{-2} MeV^{-1}. A value of

1.1×10^{-2} gms. $cm.^{-2}$ MeV^{-7} was adopted for the Nash and Thompson sample.

These values agree well with that obtained by Borelli and Grimeland which was equivalent to 1.1×10^{-2} gms. $cm.^{-2}$ MeV^{-1} if the air equivalent range is defined at 15°C and 760 mm Hg.

Recently Gooding and Pugh (1960, and private communication) have measured the response of plastic scintillator NE 102 to protons up to 160 MeV and to deuterons up to 120 MeV. They compared their measurements to the response calculated for these particles by integrating the formula

$$dS/dr = \log (1 + a\, dE/dr) \qquad (2.5)$$

for the specific fluorescence due to Wright (1953). The measurements described above imply a value of 25 ± 2 mg. $cm.^{-2}$ MeV^{-1} for a. Gooding and Pugh obtain a best fit to their measured response for a = 28 ± 5 mg. $cm.^{-2}$ MeV^{-1}.

There is good agreement among the various measurements. Since the concentration of fluorescent material used by the manufacturers is generally chosen to optimize the light output, and since samples using both polystyrene and polyvinyltoluene bases behave similarly it is plausible

that similar values of kB would apply to all such plastic scintillators. Uncertainties in the value of kB of about 10 percent lead to small inaccuracies in proton energy measurement using electron calibration. This can be seen from the table below.

Electron Equivalent Pulse Height from Protons

Proton Energy	1	10	50	100
$S(kB = 1.1 \times 10^{-2})$	.19	4.82	37.26	82.70
$S(kB = 1.0 \times 10^{-2})$	.20	5.03	39.96	83.70

The results of the calibration of plastic scintillator are summarized below.

1. Birks' expression (2.1) for specific fluorescence of organic scintillator accurately predicts the response of plastic scintillator to protons.
2. The value of the coefficient kB is close to $1.0 \pm .1 \times 10^{-2}$ gms. $cm.^{-2}$ MeV^{-1} for commercially available plastic scintillators.

It is reasonable to assume that (2.1) may be used to obtain the response for plastic to other heavily ionizing particles.

CHAPTER III

The Detection System

(a) Introduction.

Many experiments in nuclear physics require the detection and identification of charged particles. An experiment in which a beam of particles are incident on a target is a typical example. The identification of particles of a particular mass among a flux of different particles emitted by the target is an essential requirement in most experiments of this type. In general the particle identification will require simultaneous measurement of two properties of the particle which have different dependence on particle mass. The specific ionization and range, or specific ionization and energy are often used. (Wolfe et al.,1955, Keck,1955, Rutherglen and Walker,1960).

The dependence of specific ionization on energy for non relativistic particles may be expressed as

$$dE/dx \propto \frac{M^{.8} Z^2}{E^{.8}} \qquad (3.1)$$

where M, Z, and E are the particle mass, charge and energy. The specific ionization for single charged

particles is nearly proportional to particle mass. The specific ionization for pions, protons, and deuterons of the same energy are in the ratio .22: 1: 1.7.

Wolfe showed that the specific ionization and residual range, R of a particle are related by

$$dE/dx \propto \frac{M^{.45} Z^{1.1}}{R^{.45}} \qquad (3.2)$$

The relative specific ionization for pions, protons, and deuterons having the same residual range is .4: 1: 1.3 respectively.

Scintillation counter telescopes are suitable for identifying charged particles by either of the above methods. The specific ionization and energy can be measured using a thin front scintillator and a thick scintillator in which the particles stop. Particle range may be defined by pulse height selection in the second counter or by introducing a third counter operated in anticoincidence with the other two. The separation of charged particles obtainable in practice is not as good as indicated by (3.1) and (3.2). The need to have reasonable pulse height resolution in the dE/dx measurement means that the energy loss must not be

too small. The pulse height is then not strictly proportional to dE/dx. When organic scintillators are used the saturation of specific fluorescence for heavily ionizing particles makes particle identification more difficult. A comparison of (3.1) and (3.2) indicates that the method of specific ionization and energy is to be preferred.

Two scintillation counter telescopes have been constructed to identify and measure the energy of protons and pions. They are described in the following sections.

(b) The Proton Telescope.

The scintillation counter telescope used to detect the protons (here after called the proton telescope) consists of 3 counters in which plastic scintillators are viewed by R.C.A. 6810 photomultipliers. The front scintillator was 26 thou. thick and 3 by 2 3/8 inches in area. The second and third scintillators were cylindrical in shape being 3 and 4½ inches in diameter and 2 and ½ inch thick respectively. Plastic scintillator NE 102 was used in counters 1 and 3. The second scintillator was the sample, manufactured by Nash and Thompson Ltd., used in the Scintillation calibration.

Good optical coupling between the scintillators and perspex light guides and between the light guides and photomultipliers was obtained using silicone fluid.

This counter telescope identified protons by means of dE/dx and E. The development of a thin dE/dx scintillation counter was crucial to the experimental technique used. This counter will be described in detail.

The thin plastic scintillator was made by heating and pressing a piece of plastic. It was carefully cleaned and placed on a clean piece of plate glass. A second piece of plate glass was supported above the scintillator. The glass plates and scintillator were heated in an oven to 150°C. After about an hour the supports for the top glass plate were removed and lead blocks loaded on to press the scintillator. The thickness of the pressed scintillator was determined by spacers placed between the glass plates. When the top glass plate appeared to be resting on the spacers the oven was switched off and allowed to cool slowly with the door closed. The slow cooling annealed the scintillator. The scintillator was removed from the glass plates by placing them under water and waiting for

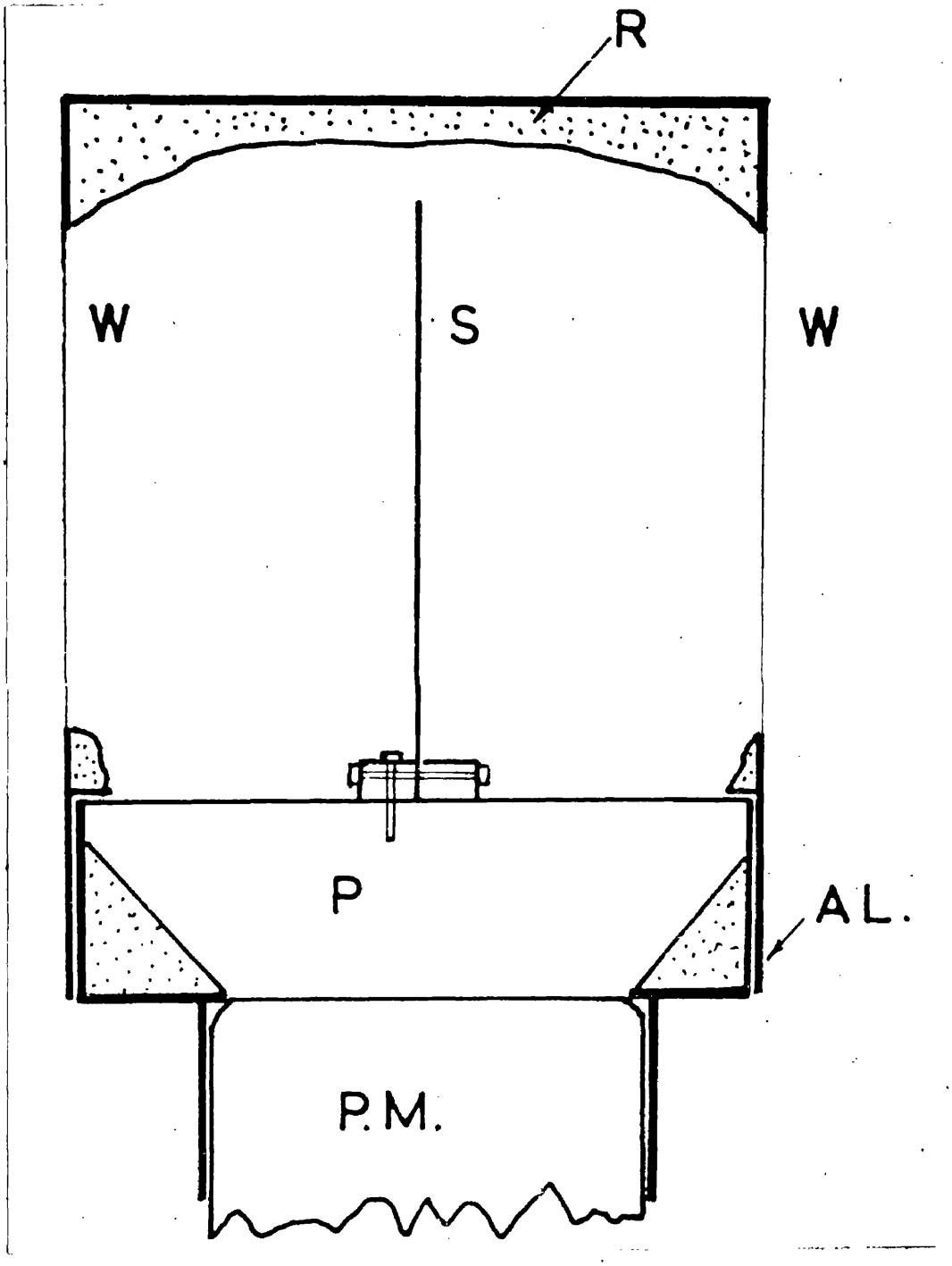

Figure 3.1. Thin Scintillator Mounting

S scintillator
W window
p perspex
Al aluminium
PM photomultiplier
R magnesium oxide reflector

them to separate. In order to obtain high quality scintillator it was necessary to produce a large sheet and to cut the required scintillator from the best part.

The scintillator mounting is shown in figure 3.1. The scintillator was clamped by the perspex strips. The aluminium enclosure surrounding the scintillator has two windows covered with $\frac{1}{2}$ thou aluminized mylar and a double layer of 0.2 thou aluminium foil: The interior shape of the enclosure was moulded using plaster of Paris, and coated with magnesium oxide by burning magnesium ribbon inside the enclosure. The photomultiplier used in this counter was selected for low noise level. The pulse height and resolution obtained with this counter were satisfactory.

The pulse height calibration was obtained using 160 KeV internal conversion electrons from an indium 114 source. The source was collimated and placed close to the counter window. The electron energy incident on the scintillator was 96 KeV. The pulse height distribution due to the indium electrons was obtained using a 100 channel kicksorter. A typical pulse height distribution is shown in figure 3.2. The background, which was mainly due to photomultiplier noise, is also shown. The spectra shown in figure 3.2 were obtained by counting for one

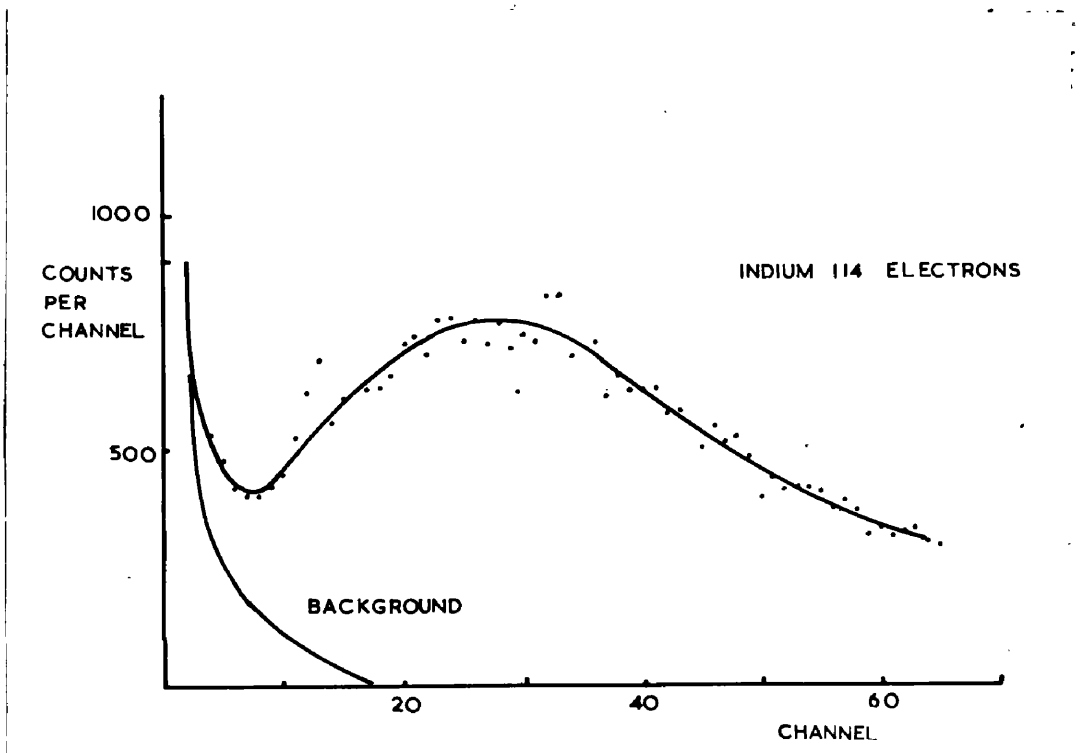

Figure 3.2. Pulse height distribution obtained with the thin scintillation counter for indium 114 internal conversion electrons. The upper curve includes the background.

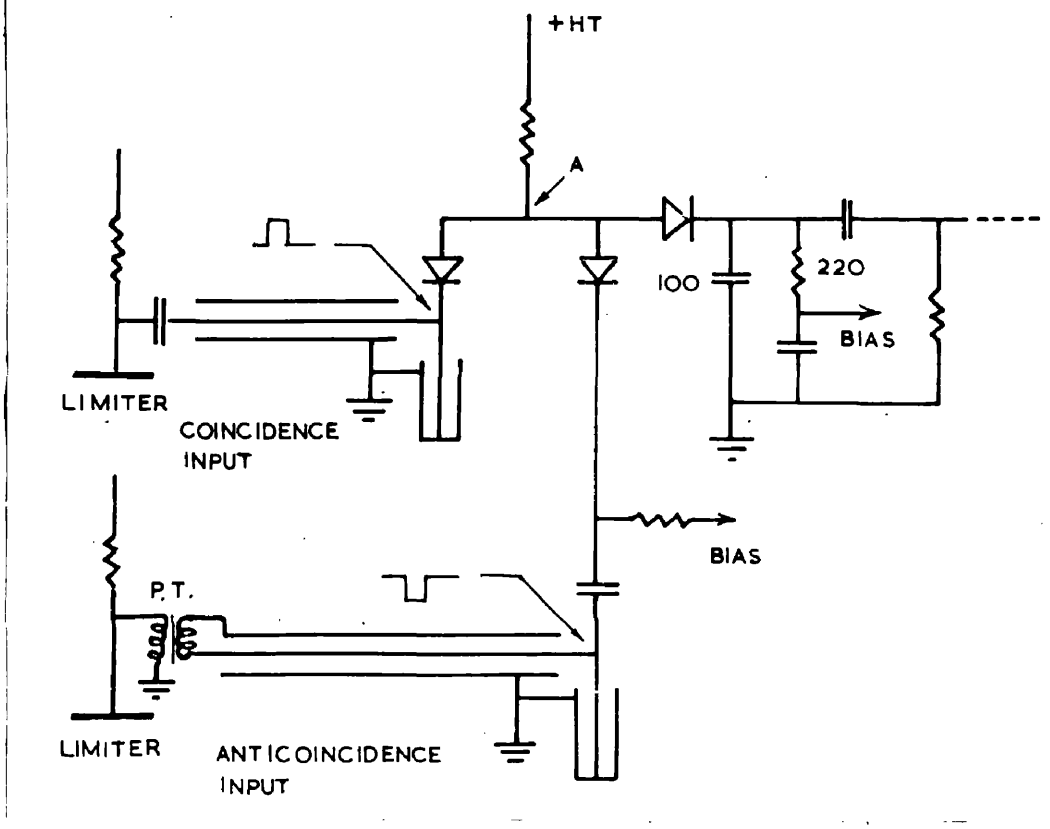

Figure 3.3. Coincidence circuit used with proton telescope. One coincidence and one anticoincidence input are shown.

minute. When the kicksorter bias is allowed for an the background subtracted the resolution of the peak is 60 percent half width at half height.

The proton telescope was operated in a 1 + 2 - 3 coincidence - anticoincidence sequence. The modified form of the Bell coincidence circuit shown in figure 3.3 was used. Each input is terminated in a shorted 100 ohm line, and is connected to the common point A through a germanium diode. For coincidence inputs the diode is normally conducting. When the coincidence bias is properly adjusted a coincidence to singles ratio of 20 to 1 is possible with this circuit. The diode at the anticoincidence input is normally biased off. A negative pulse causes the diode to conduct and prevents a large coincidence pulse from being formed at A. The negative input is obtained by inverting the limited pulses using a pulse transformer. Conventional limiter circuits using E 180 F valves are employed. When 1.5 metre shorted lines were used the coincidence resolving time was 5×10^{-9} seconds. A non inverting output from the limiter valve of counter 3 was used to determine the correct delay relative to the other counters. The principal advantage of this circuit lies in the separate

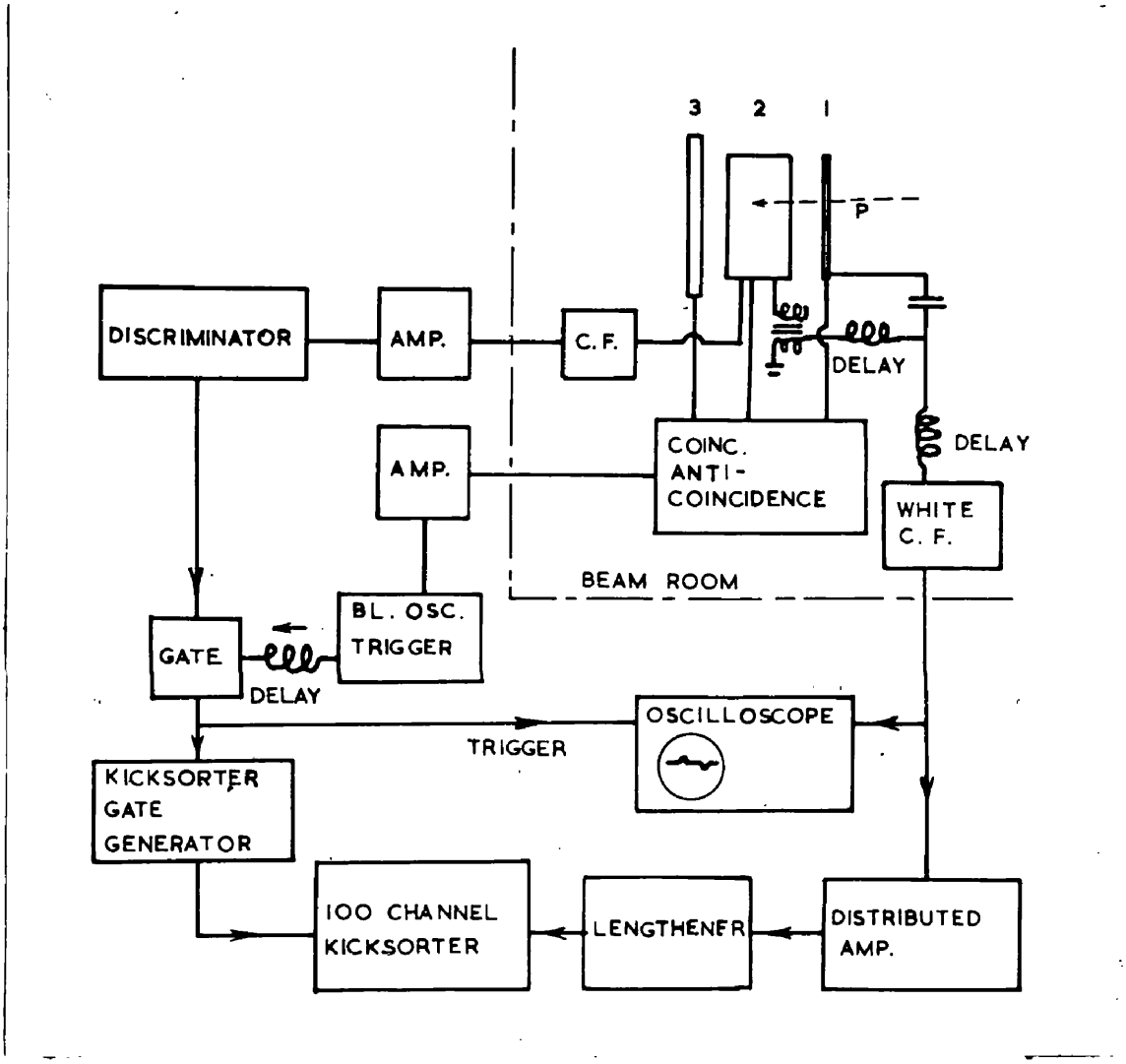

Figure 3.4. Block diagram of circuit used for testing and calibration of the proton telescope.

minute. When the kicksorter bias is allowed for an the background subtracted the resolution of the peak is 60 percent half width at half height.

The proton telescope was operated in a 1 + 2 - 3 coincidence - anticoincidence sequence. The modified form of the Bell coincidence circuit shown in figure 3.3 was used. Each input is terminated in a shorted 100 ohm line, and is connected to the common point A through a germanium diode. For coincidence inputs the diode is normally conducting. When the coincidence bias is properly adjusted a coincidence to singles ratio of 20 to 1 is possible with this circuit. The diode at the anticoincidence input is normally biased off. A negative pulse causes the diode to conduct and prevents a large coincidence pulse from being formed at A. The negative input is obtained by inverting the limited pulses using a pulse transformer. Conventional limiter circuits using E 180 F valves are employed. When 1.5 metre shorted lines were used the coincidence resolving time was 5×10^{-9} seconds. A non inverting output from the limiter valve of counter 3 was used to determine the correct delay relative to the other counters. The principal advantage of this circuit lies in the separate

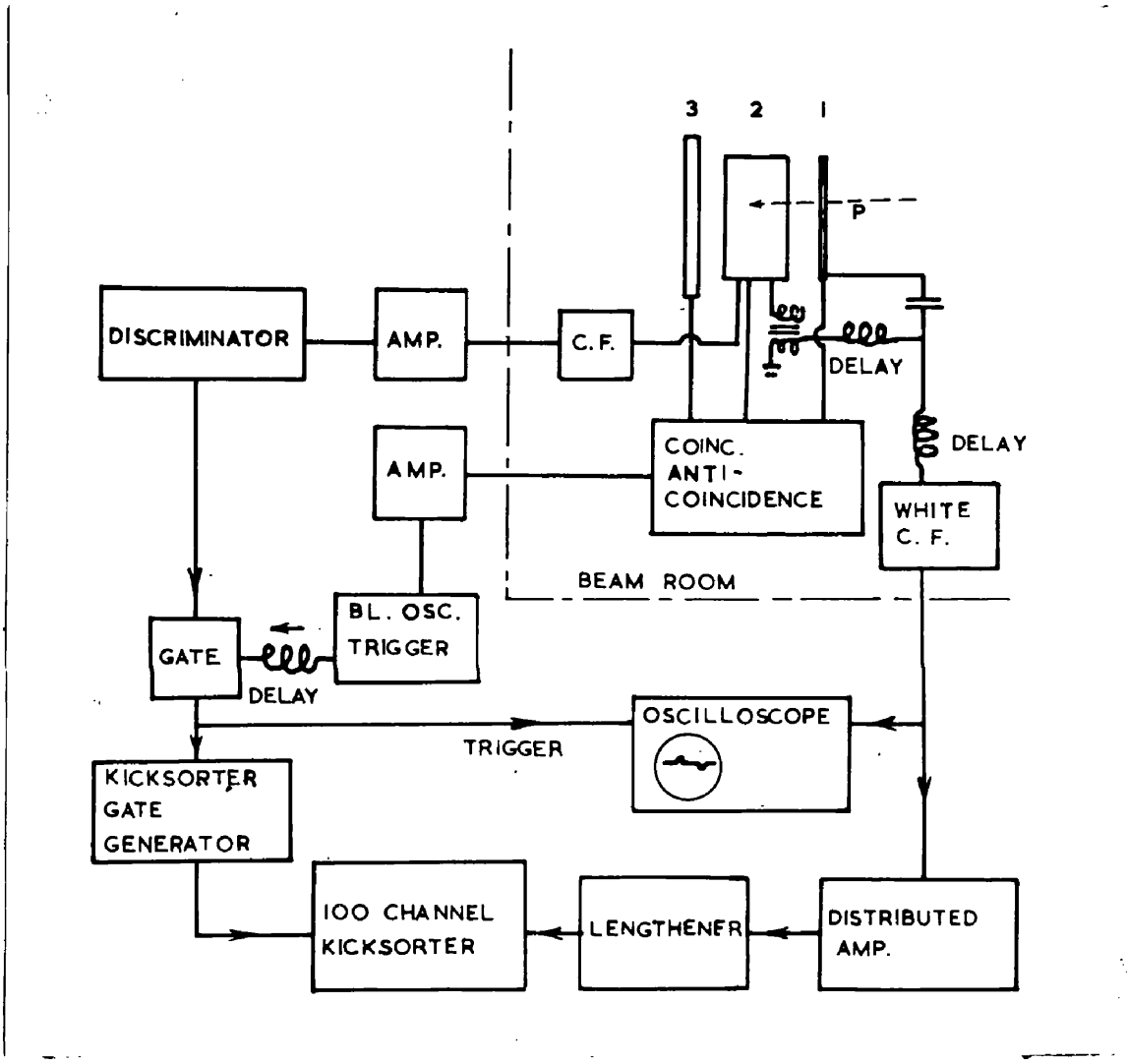

Figure 3.4. Block diagram of circuit used for testing and calibration of the proton telescope.

termination at each input. The addition of an extra coincidence or anticoincidence input does not involve complicated impedance matching.

The circuit used in the testing and calibration of the proton telescope is shown in figure 3.4. The pulses used to measure specific ionization and energy were taken from the 12th and 11th photomultiplier dynodes of counters 1 and 2 respectively. The pulse from counter 2 was inverted using a pulse transformer. A 2.2 μ sec delay was inserted between counter 2 and the White cathode follower. Counter 1 was connected directly into the delay line at a point separated from counter 2 by 0.4 μ seconds. When a 1 + 2 - 3 coincidence occurred a 541 Tektronix oscilloscope was triggered and the signals from counters 1 and 2 displayed. The oscilloscope sweep speed was .2 μ sec per cm. The inversion of one pulse greatly facilitated the identification of pulses due to 1 + 2 coincidences from random background. The pulse height discriminator was used to prevent low energy particles, mainly electrons, from triggering the oscilloscope.

Counter 2 was calibrated using pulse height distributions for thorium C'' and sodium 22 gamma rays. These sources

produce Compton edges at 2.39 and 1.07 MeV respectively. Counter 1 was calibrated using indium 114 internal conversion electrons. The counter pulses were amplified, lengthened, and the pulse height distribution was displayed on a 100 channel kicksorter.

The pulse height measured using the kicksorter was related to the observed deflection on the oscilloscope trace. A thorium source was placed between counters 1 and 2 and a slow coincidence counting rate was obtained (a few counts a minute) by setting the blocking oscillator trigger level to trigger only on the largest coincidence pulses. The kicksorter was gated to accept pulses when the blocking oscillator was triggered. The oscilloscope traces were photographed and the kicksorter channel in which each count occurred was recorded. A dozen pulses sufficed to obtain the correlation between the pulse height displayed on the oscilloscope and on the kicksorter. The above procedure was used each time the counters were calibrated so that the calibration did not depend on the long term stability of the distributed amplifiers.

The performance of the proton telescope was tested using the 310 MeV bremsstrahlung beam of the Glasgow

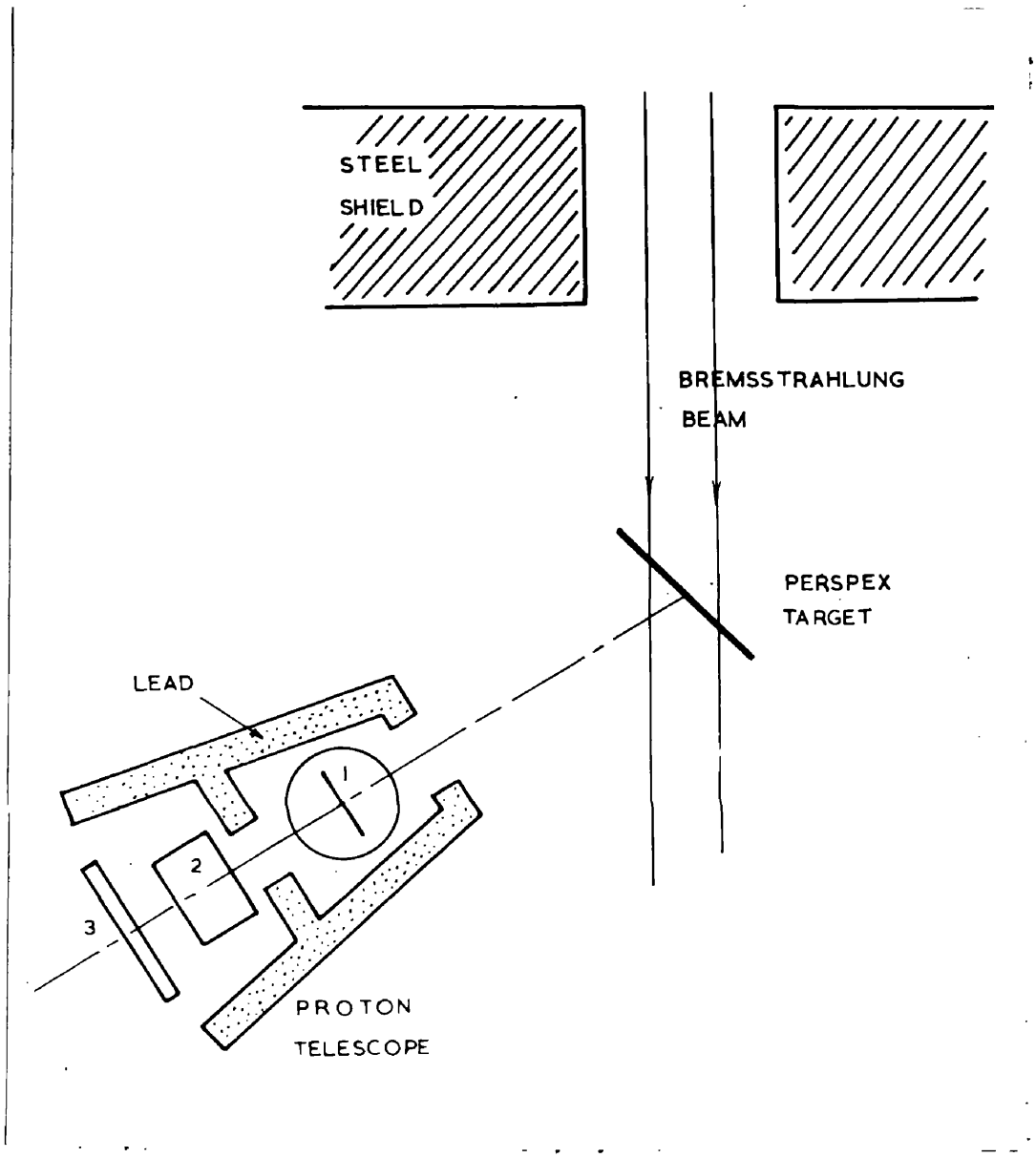

Figure 3.5. Plan of experimental arrangement used in proton telescope tests.

electron synchrotron. The various properties of the synchrotron and the photon beam are discussed in Chapter IV. A $^{1}/_{16}$ inch perspex sheet was placed in the beam 10 metres from the synchrotron target. Placing the perspex target in this position allowed the counter tests to be done at the same time as the beam was being used for another experiment. A six inch thick steel shield was positioned just in front of the target to shield the counters from the large flux of charged particles produced at small angles to the beam. The experimental arrangement is shown in figure 3.5. The counter telescope was positioned with its axis at 65 degrees to the incident beam direction. The lead shielding which was 1 inch thick was provided to reduce the random background in the counters. The aperture of the counter telescope was defined by a $2\frac{1}{8}$ inch hole in the lead block between counters 1 and 2. For the geometry used the aperture was .015 steradians. The average beam intensity and width during this test were 3×10^{8} equivalent quanta per minute and 400 μ seconds respectively. 1 + 2 - 3 coincidences were used to trigger the oscilloscope. The oscilloscope traces were photographed with a camera having an f 1.0 lens using Ilford HPS film. The

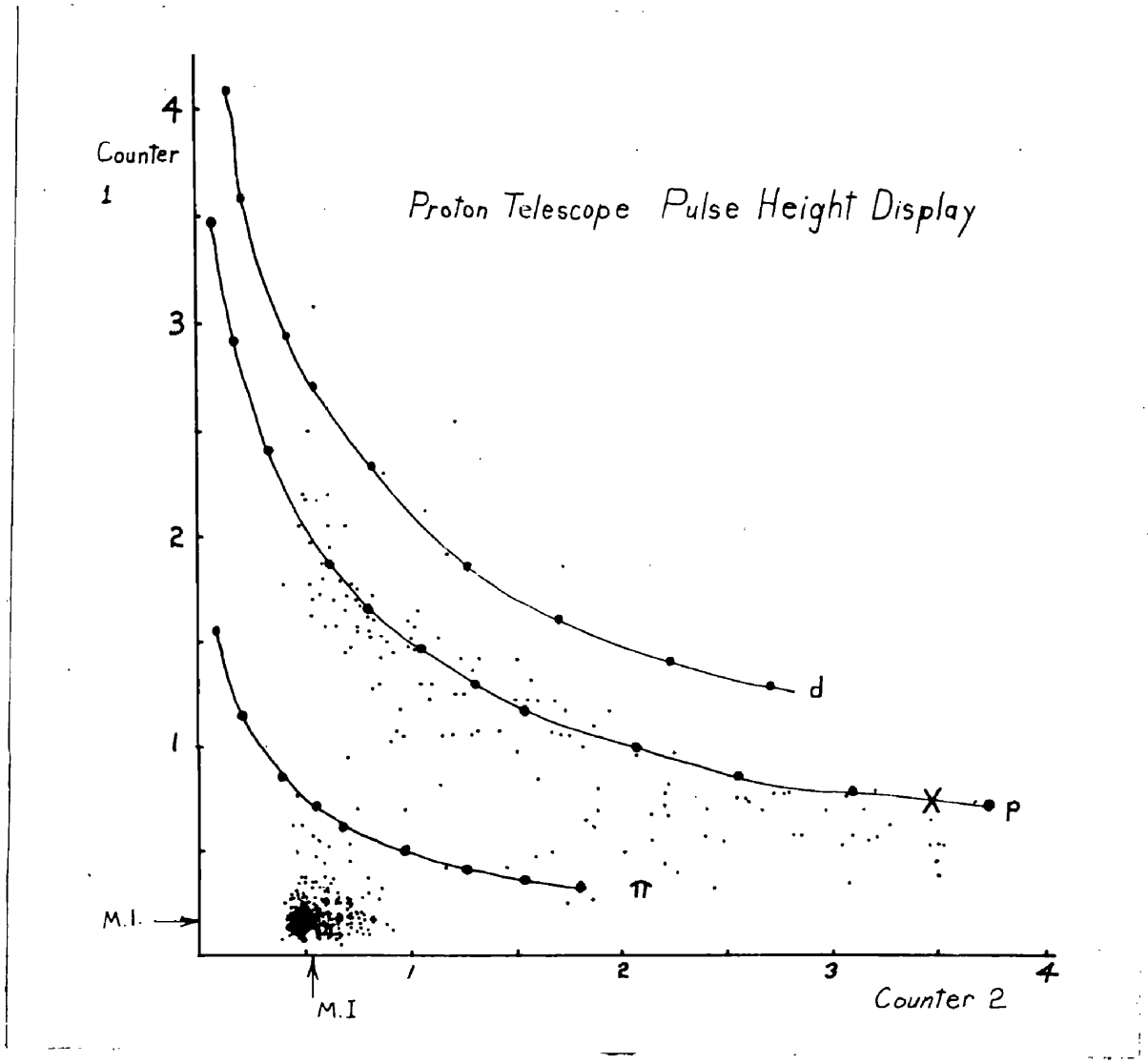

Figure 3.6. Plot of deflection in counter 1 against deflection in counter 2 showing the separation of pions, protons, and deuterons obtained by the method of dE/dx and E.

recorded traces were projected in a microfilm reader and the position, separation, and height of the two pulses measured. Events for which the separation or position of the pulses differed by more than 20 or 50 nanoseconds respectively from the mean were rejected. The absence of any traces in which the pulses occurring in the reverse order satisfied the position and separation requirements indicated that the probability of random pulses simulating a true 1 + 2 - 3 event is negligible.

The measured deflection of the pulse from counter 1 was plotted against that from 2 for all traces that satisfied the above conditions. The spots shown in figure 3.6 were obtained in a 15 minute run. The curves were calculated using the counter calibration obtained with the sources and the response of plastic scintillator for different charged particles. A reasonable separation between the various charged particles is obtained. The shape and position of the band of protons agrees well with the calculated curve. The X indicates the expected endpoint of the proton band at 81 MeV corresponding to the range of counter 2. The points lying between the proton and pion curves may be attributed to negative pions stopping in the second scintillator. Nuclear

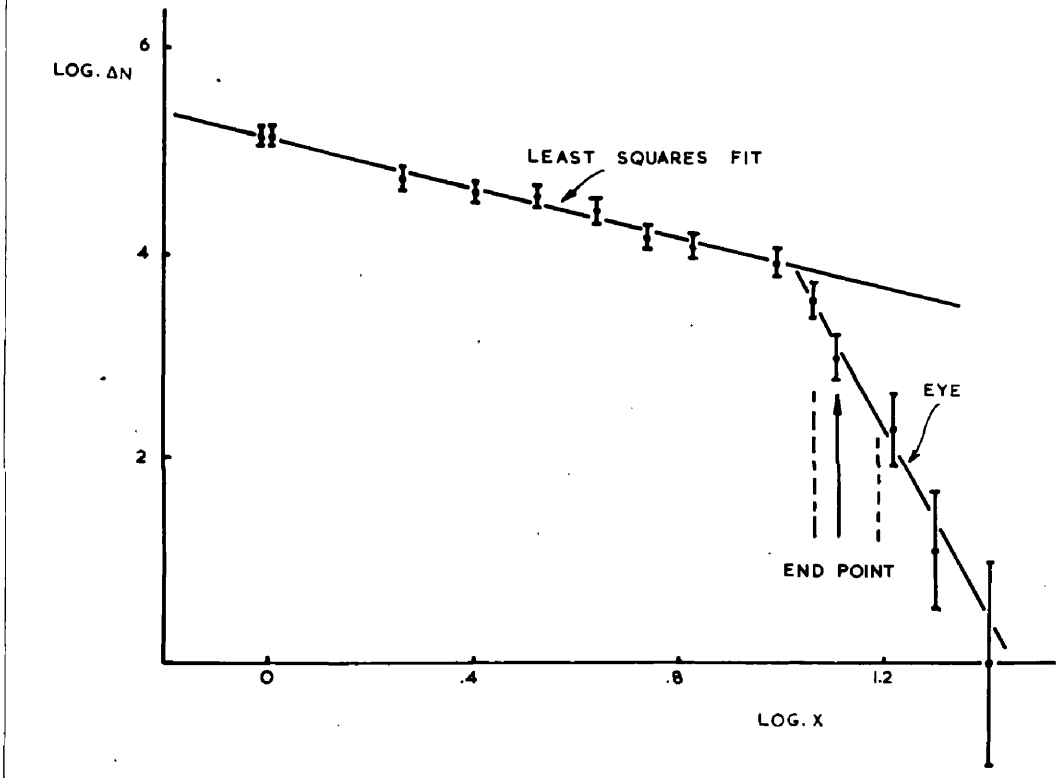

Figure 3.7. Graph of log ΔN vs log X used to obtain end point calibration of the proton telescope. The arrow indicates the end point adopted and the dashed lines, the estimated limit of error.

disintegration resulting from the capture of the negative pions produces a varying number of charged particles. Since this process happens very quickly the pulse height due to the charged nuclear particles will be added to that due to the pion kinetic energy. The arrows indicate the deflection expected for minimum ionizing particles traversing the scintillators.

The endpoint of the proton spectrum may be used to obtain a calibration of the counter telescope at high energy. In the test run described above a total of 740 protons were identified. The uncertainty in this number was of the order of $\pm$ 20 due to the difficulty of separating protons from pions and deuterons. A graph of log ΔN vs log x was plotted where ΔN is the number of spots in the proton band in an interval Δx about the deflection x. Figure 3.7 shows a typical log ΔN vs. log x plot. A straight line least squares fit was made to the points for log $x < 1$. The straight line through the points above log $x = 1$ was drawn by eye. The end point was defined as the deflection where the ordinate on the second line equals log $(\Delta N/2)$ as defined by the first line. The energy calibrations, determined using sources and the end point of the proton spectrum, agreed to within

5 percent.

The procedure outlined above may be justified by considering the known energy spectrum of protons produced in photodisintegration. Keck (1952) measured the energy spectrum of protons from carbon and cadmium produced by 300 MeV bremsstrahlung. He found that

$$d\sigma/dE \propto E^{-\gamma} \qquad (3.3)$$

where E is the proton energy in MeV and γ depends on the nucleus and the angle at which the protons are detected. For carbon he found $\gamma = 1.7$ up to 130 MeV at 67 degrees.

Since a perspex target (composition $C_5H_8O_2$) was mistakenly used in the proton counter tests a direct comparison with Keck's measurement is not possible. However the proton spectrum from perspex may be expected to show an approximate exponential energy dependence. The pulse height in counter 2 is proportional to the proton energy to a first approximation so that the log ΔN may reasonably be expected to show a linear dependence on log x. To check this assumption the energy spectrum of protons from perspex was obtained from the pulse height distribution using the average of the two calibrations. After correcting for energy loss in the target, the energy

spectrum was best fitted by $\alpha n E^{-\gamma}$ dependence with $\gamma = 1.5$.

The test of the proton counter telescope indicated that the separation of protons from the other charged particles is adequate to allow their identification by the method of simultaneous measurement of specific ionization and energy. The close agreement between the energy calibrations done at 2.4 and 81 MeV indicates that the pulse height in counter 2 may be used to measure proton energies between 15 and 81 MeV. The ability to register protons over the entire energy range that is of interest is very important in an experiment where low counting rates are expected.

(c) The Pion Telescope

The method of simultaneous measurement of specific ionization and energy is unsuitable for the detection of negative pions. The difficulty due to production of charged particles in negative pion capture by nuclei is avoided when specific ionization and range are used to identify pions. The energy lost by a charged particle traversing a counter which is thin with respect to the particle range may deviate substantially from the most probable energy loss. In particular large deviations

towards higher energy loss are observed. The distribution of energy loss has been described by Landau (1944) (see also Cranshaw, 1952). The loss in resolution in the measurement of specific ionization due to this effect may be largely avoided by measuring the specific ionization in two or more counters. The gain in the counters is adjusted so that the most probable pulse heights are equal and the smallest pulse selected. The counter telescope described below makes use of this method.

A scintillation counter telescope (herafter called the pion telescope) consisting of four counters was used to detect pions by the specific ionization and range method. Plastic scintillator NE 101 was used in counters 1 and 2, and NE 102 in counters 3 and 4. The scintillators 1, 2, 3, and 4 were 3, 3, 2 5/8, and 5 inches in diameter and $\frac{3}{4}$, $\frac{1}{2}$, $\frac{1}{4}$, and $\frac{1}{2}$ inch thick respectively. The aperture of the counter telescope was defined by counter 3. Particles which stopped in counter 3 produced a 1 + 2 + 3 - 4 coincidence - anticoincidence in a Bell type coincidence circuit having a resolving time of 20 nanoseconds. This circuit has been described by Rutherglen and Walker (Rutherglen, 1960, Walker, 1960).

The pulse height at the collector of counters 1 and 2 was measured using a display system described later.

Absorbers were introduced into the counter telescope (see fig. 3.8). Absorber A_3 served to increase the width of the particle range defined by the telescope. A_2 prevented charged particles produced by negative pion capture stars in counter 3 and A_3 from entering counter 2. A_1 was chosen so that the counter telescope detected pions in the required energy range. When A_1, A_2, and A_3 were 1, $\frac{1}{2}$, and $1\frac{1}{4}$ inch thick perspex sheets respectively, the telescope detected pions in the range 45.8 to 60.0 MeV and protons in the range 102 to 132 MeV.

The effect of negative pion star particles may be shown to be small. When A_2 is $\frac{1}{2}$ inch thick only protons with energy 35 MeV can enter counter 2. It is known that 10 percent of all negative pion captures in carbon produce protons of energy 30 MeV (Ammiraju and Lederman, 1956). From a consideration of the counter telescope geometry it was estimated that less than one percent of the negative pions produced star particles that enter counter 2. Counter 4 was placed as far behind counter 3 and A_3 as was consistent with efficient anticoincidence operation to reduce the number of particles from negative pion stars that enter counter 4. When this happens the event will not be registered.

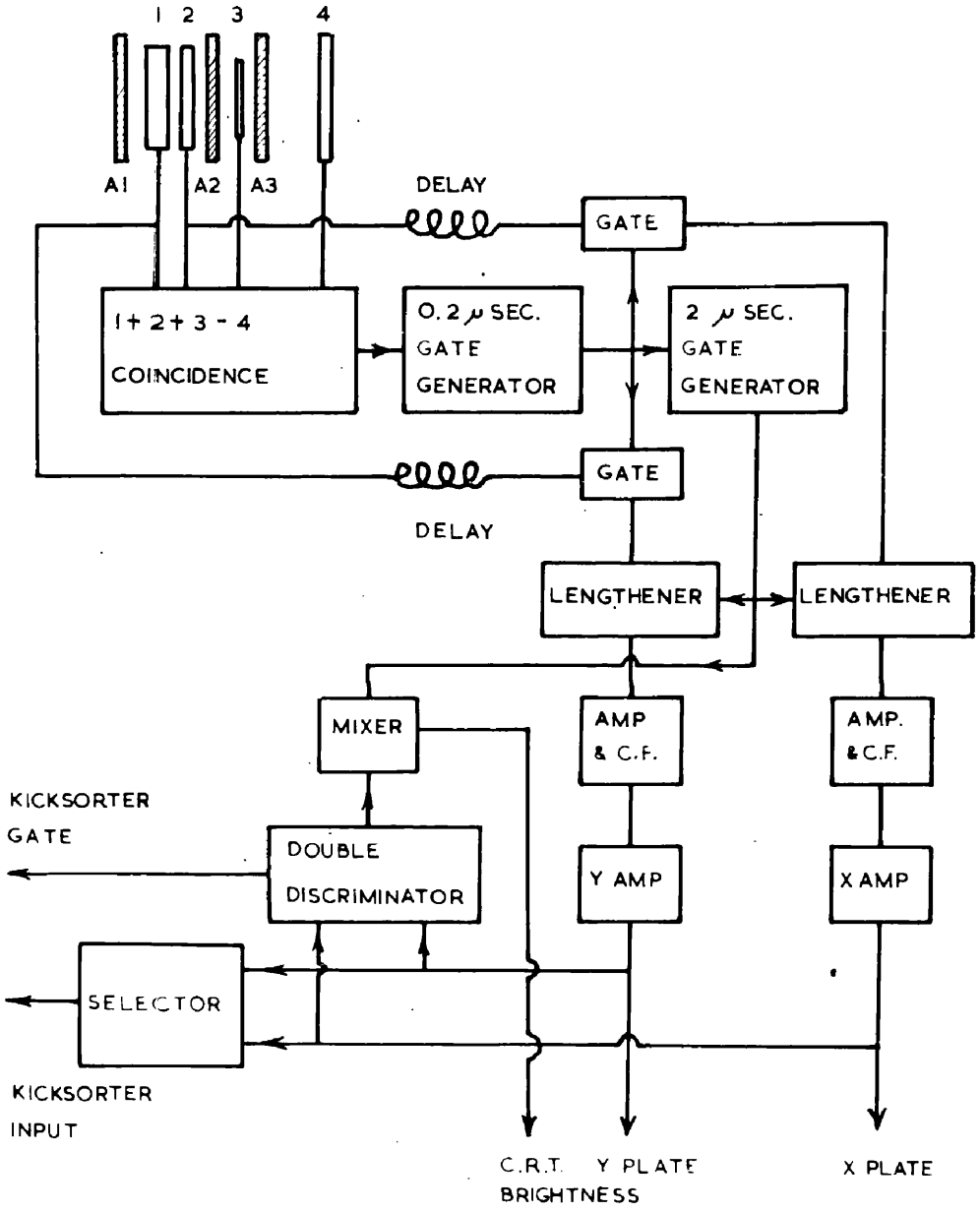

Figure 3.8. Block diagram of the circuit used with the pion telescope.

The pulses from the collector of counters 1 and 2 and a pulse signifying a 1 + 2 + 3 - 4 coincidence - anticoincidence were fed through 70 ohm cables to the display system. A block diagram of the display system facilities used in this experiment is shown in figure 3.8. The complete display system has been described by Rutherglen and Walker (1960) and by Walker (1960). The coincidence pulse triggers a blocking oscillator trigger circuit which produces a 20 volt pulse . 2 μ seconds long. This pulse was used to operate a linear gate which allowed the collector pulses from counters 1 and 2 to pass through to the lengthener circuit. The lengthened pulses are rectangular, 2 μ seconds long and proportional in height to the input pulses. They are amplified by two paraphase amplifiers and fed to the X and Y deflection plates of a cathode ray tube. A negative 40 volt pulse is simultaneously fed to the cathode of the C.R.T. This system produces a spot on the C.R.T. face which has X and Y deflections proportional to the pulse height in counters 1 and 2. The double discriminator is used to prevent the "bright up" occurring for X or Y deflections less than a minimum deflection. This eliminates a large number of spots due to low energy electrons. The

information is recorded by photographing the C.R.T. display. The selector is a conventional diode coincidence circuit which was designed to give an output proportional in height to the smaller of the two input pulses. The selector output was displayed on a 100 chennel kicksorter. The kicksorter was gated by the double discriminator to prevent a large number of electrons from introducing large dead time losses. The kicksorter display was used as a continuous check that the system was operating satisfactorily.

The performance of the pion telescope was tested using the 307 MeV bremsstrahlung beam of the Glasgow electron synchrotron. A $^{1}/_{16}$ inch perspex target was placed in the beam 6 metres from the synchrotron target. The pion telescope was 12 inches from the target. The telescope aperture subtended an angle of .019 steradians in this position. The beam passed through a hole in a steel screen which shielded the counters from charged particles produced by the beam in air. Signals from the counter telescope were fed to the display system located in the beam research room.

The E.H.T. supply voltages to the counters were adjusted so that collector pulses produced by 2.6 MeV

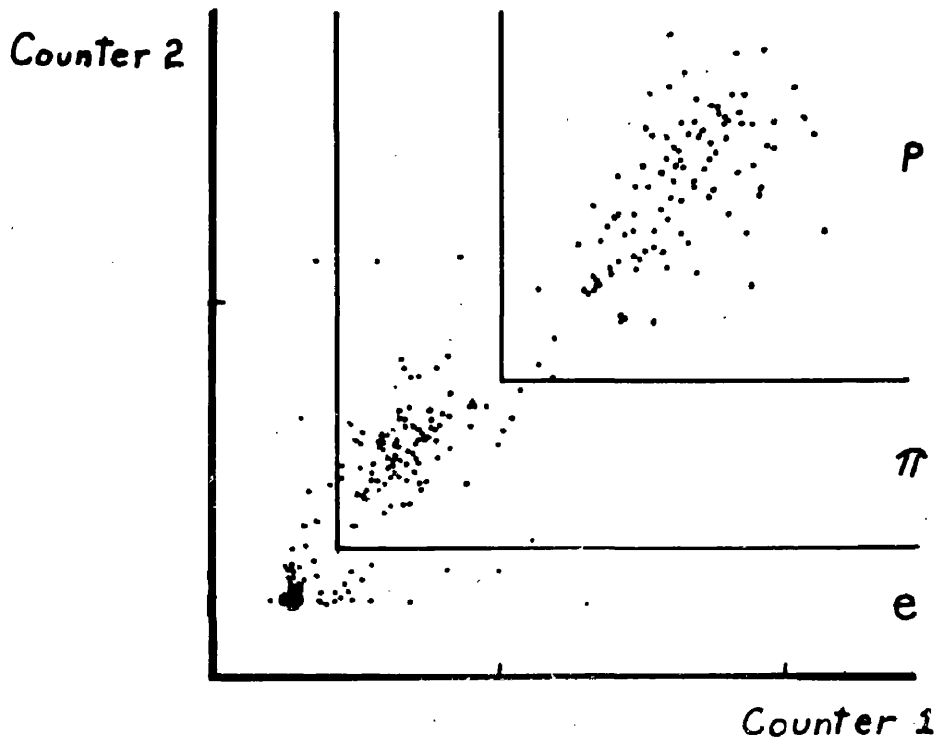

MESON TELESCOPE PULSE HEIGHT DISPLAY

Figure 3.9. Cathode ray tube display of pulse height from counters 1 and 2 of the pion telescope.

thorium C^{11} gamma rays fully cut off the limiter valves of the coincidence circuit. The E.H.T. supplies to counters 1 and 2 were then set so that the pulse height due to particles produced in the perspex target and stopping in counter 3 produced equal pulse height at the X and Y deflection plates of the display unit cathode ray tube. The C.R.T. display of pulses from counters 1 and 2 was photographed.

A typical spot picture is shown in figure 3.9. Most of the spots lie close to a line bisecting the angle between the X and Y axes. Spots that appear well of this line are produced when the energy loss in one counter is large with respect to the mean energy loss for the particle. The spots are seen to lie in 3 groups corresponding to electrons, pions, and protons. A thorium source was placed behind counter 2 so that energetic beta particles could penetrate counter 2 and enter counter 1. In the resulting C.R.T. display the spots coincided with the part of the electron group in figure 3.9 closest to the origin. It was concluded that the spot groups have been properly attributed to electrons, pions, and protons.

A typical pulse height distribution obtained using

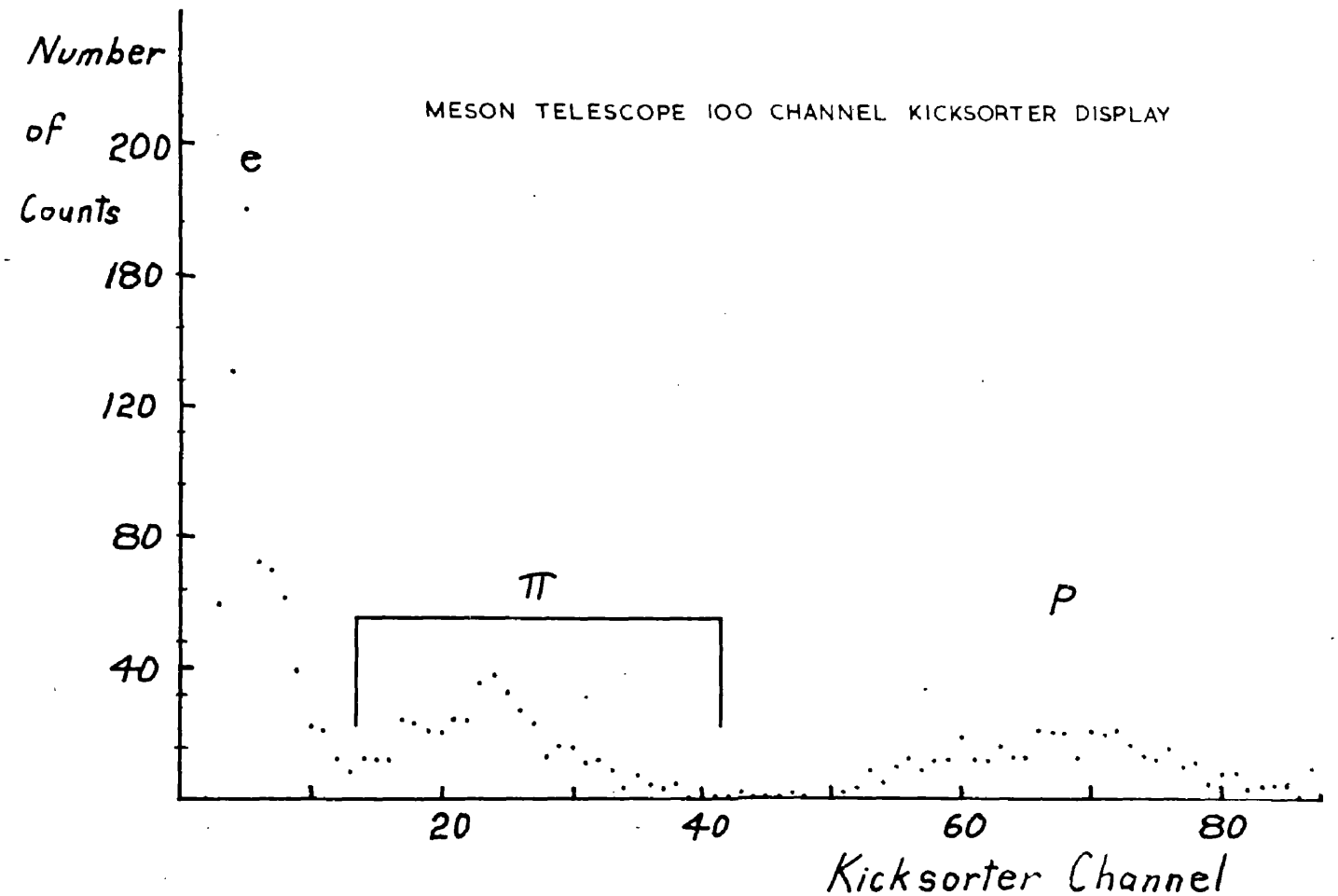
MESON TELESCOPE 100 CHANNEL KICKSORTER DISPLAY
Number of Counts
200
180
120
80
40
e
π
p
20
40
60
80
Kicksorter Channel

Figure 3.10.

the 100 channel kicksorter is shown in figure 3.10. A distinct separation into three groups is observed. The C.R.T. and kicksorter displays were correlated using a pulse generator. The height of pulses fed to the two signal inputs of the display unit were varied independently. The loci of C.R.T. deflections corresponding to a given kicksorter channel was obtained. They were found to be "L" shaped. Typical loci are the lines separating the electron, pion, and proton regions in figure 3.9. The bracket in figure 3.10 corresponds to the pion region in figure 3.9. It was concluded that the three groups shown in the kicksorter display corresponded to electrons, pions, and protons as indicated.

The work described above indicated that the pion telescope was capable of detecting and identifying pions by the method of specific ionization and range..

(d) Detection of Protons in Coincidence with Negative Pions.

The simultaneous detection of negative pions and protons from deuterium was accomplished using the counter telescopes described in the preceding sections. A block diagram of the complete electronic system is shown

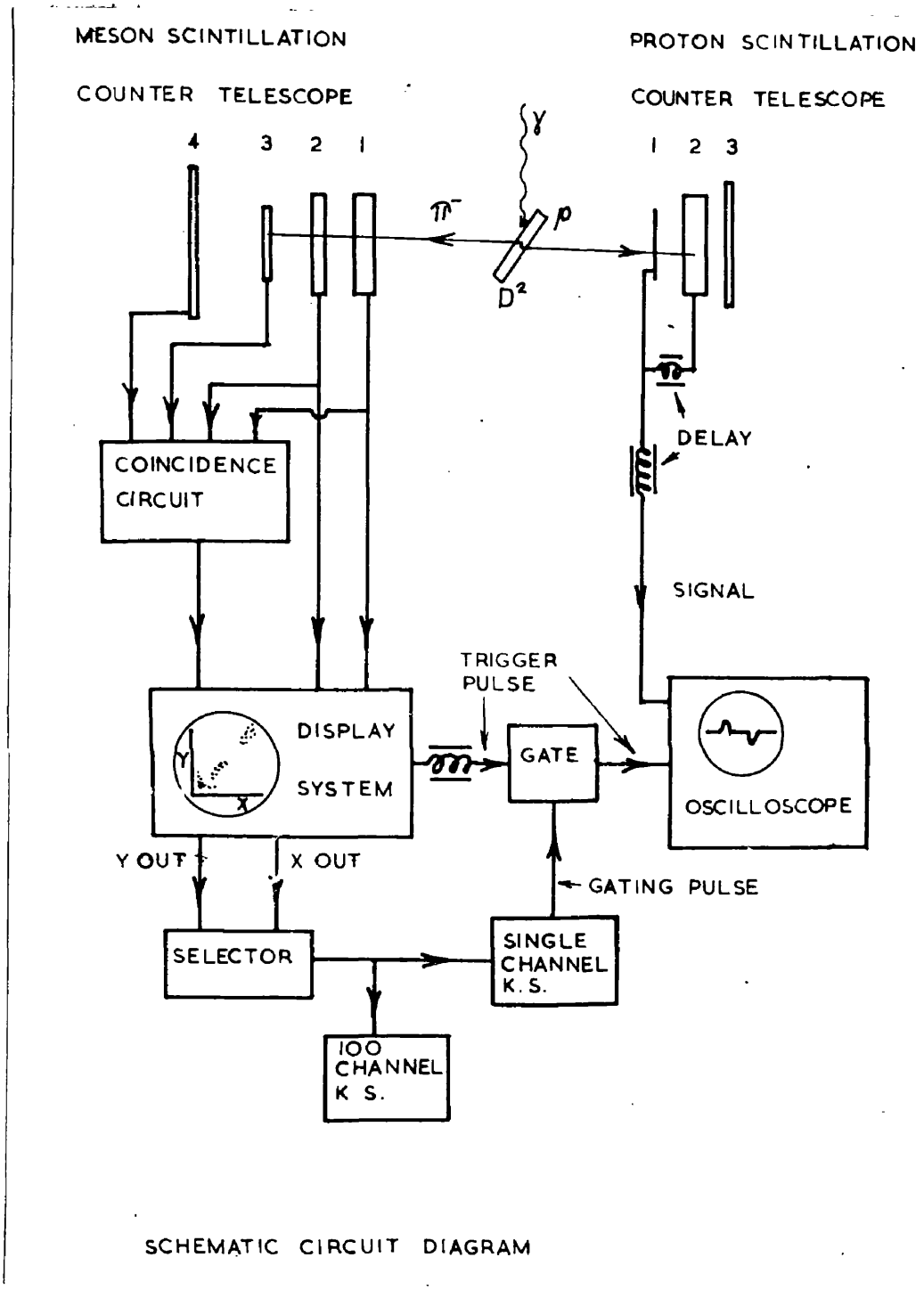

Figure 3.11. Block diagram of circuit used to detect protons in coincidence with negative pions from deuterium.

in figure 3.11. A 1 + 2 + 3 - 4 coincidence - anticoincidence is formed in the coincidence circuit. The pulse heights from counters 1 and 2 are displayed on the cathode ray tube display system and a pulse proportional in height to the smaller of 1 or 2 is fed to the 100 channel kicksorter. A single channel kicksorter is set to select pulses in the pion group. When a pulse occurs in the pion group the single channel kicksorter opens the gate and a trigger pulse from the display system blocking oscillator is fed to the trigger input of a 541 Tektronix oscilloscope. The signal pulses from counters 1 and 2 of the proton telescope are displayed on the oscilloscope trace. The signal delays are adjusted so that the signal pulses appear in the middle of the oscilloscope trace. The trigger pulse is delayed to allow the gate to open fully. No difficulty in distinguishing negative and positive pions arises since protons will only be produced in coincidence with the former.

The operation of a coincidence counter telescope at small angles to the bremsstrahlung beam is difficult. The large number of charged particles (mainly electrons) produced at forward angles produces high counting rates.

Large dead time losses and high random coincidence rates may then be encountered. The negative pion-proton detection system avoids these difficulties by demanding coincidences from the pion telescope only. It was situated at 90 degrees to the beam.

A preliminary test of the entire detection system was made using a heavy water target. An envelope was constructed by folding and welding 2 thou mylar sheet and was filled with 10 gms of heavy water. The heavy water target was suspended in the 307 MeV bremsstrahlung beam of the Glasgow electron synchrotron with the normal to the target at 45 degrees to the beam. The average thickness of heavy water in the beam was $\frac{1}{4}$ inch. The pion telescope was placed at 90 degrees to the beam with counter 3, which defined the counter/aperture, 17 inches from the target. The proton telescope was placed at 30 degrees to the incident beam. A 2 inch diameter hole in a $\frac{1}{2}$ inch thick lead block, placed between counters 1 and 2 and 16 inches from the target, defined the proton telescope aperture. Lead blocks 1 inch thick were placed either side of the proton telescope to shield the counters from the general room background. The photon beam passed through a hole in a 6 inch thick steel screen

which shielded the counters from charged particles produced in the air. The arrangement was identical to that shown in figure 4.6 except for the target. The total photon flux was monitored using a Cornell thick-walled copper ionization chamber.

The oscilloscope was triggered when a pion was detected in the pion telescope and the oscilloscope traces were photographed. A single channel kicksorter was set to accept pulses which were registered between channels 11 and 45 of the 100 channel kicksorter. The upper end of the electron group was included (see figure 3.10). This was done to ensure that pions were not missed. It was not expected that protons would be observed in coincidence with the extra electron triggers.

A total of 556 traces were recorded on film corresponding to a total beam flux of 8.0×10^{10} equivalent quanta. The film was analysed as described above. Seventeen traces were found which satisfied the criteria of pulse separation and position. The pulse heights from counters 1 and 2 were measured for these traces and a diagram similar to figure 3.6 was plotted. Comparison with the calculated response curve for protons indicated that 12 of the plotted points were consistent

with the particles being protons. The remaining 5 points lay well below the proton curve. The background of random pulses that occurred on these traces was not large and there was no ambiguity in the identification of the 17 coincidence particles.

The number of pion-proton coincidence events expected in this run was calculated. Free nucleon kinematics were assumed and the -/+ ratio and differential cross section for positive pion production at a proton were obtained from Moravcsik's paper (1957). This gave 70 negative pions. It was assumed that $^1/_5$ of the recoil protons would enter the proton telescope (detailed calculations later showed $^1/_{10}$ to be the correct fraction) indicating that 14 pion-proton coincidence events were expected.

The detection system has been shown to operate satisfactorily under more serious background conditions than are expected when a liquid deuterium target is used. An unambiguous identification of pion-proton coincidence events was obtained. The cathode ray tube and kicksorter displays provide a useful check that the system was functioning properly. The number of pion-proton coincidence events observed in this short run was of the order of magnitude expected. The detection system may

be expected to provide a satisfactory measurement of the energy distribution of protons observed in coincidence with negative pions.

CHAPTER IV

Photoproduction of Negative Pions in Deuterium.

(a) The Synchrotron.

The scintillation counter teloscopes described in Chapter III were used to determine the angular distribution and energy spectrum of protons detected in coincidence with negative pions from deuterium. The bremsstrahlung beam of the Glasgow electron synchrotron (McFarlane et al., 1955) provided the source of photons. In the Glasgow synchrotron the electrons are accelerated in a circular orbit 125 cm in radius. The guide field is provided by 20 C section magnets which are pulsed by discharging a condenser bank through the magnet coils. Electrons are injected at 70 to 80 KeV by a diode gun and are accelerated to relativistic velocity by betatron action. Synchrotron acceleration is obtained using two quarter wave resonators. The maximum energy of the circulating electron beam depends on the guide field and energies up to 340 MeV are obtained by varying the voltage on the condenser bank. The recent addition of D.C. bias to the magnet allows the maximum energy to be extended to 440 MeV. The bremsstrahlung beam is produced by allowing the maximum energy electrons to

spiral in and strike a .06 inch tungsten wire. The photons produced in the synchrotron target pass into an adjacent experimental beam room. The nature of the photon beam and the experimental conditions that obtain necessarily play a large part in the design of experiments using the synchrotron beam.

The bremsstrahlung beam contains photons of all energies between E_{max} and zero, where E_{max} is the maximum energy of the circulating electron beam. Over a considerable range of energy the number of photons is inversely proportional to their energy. There is a sharp cut off at E_{max}. The energy spectrum has been calculated by Schiff (1946) for an infinitely thin target. For targets available in practice, multiple scattering of the electrons is an important effect. In circular accelerators multiple traversals of the target also occurs. The bremsstrahlung spectrum of the collimated beam from the Glasgow synchrotron operated at a maximum energy of 314 MeV has been measured by Rutherglen and Walker (Walker, 1960) using a magnetic pair spectrometer. This instrument used 30 degree deflection. The electron-positron pairs were detected in coincidence using scintillation counters. The results

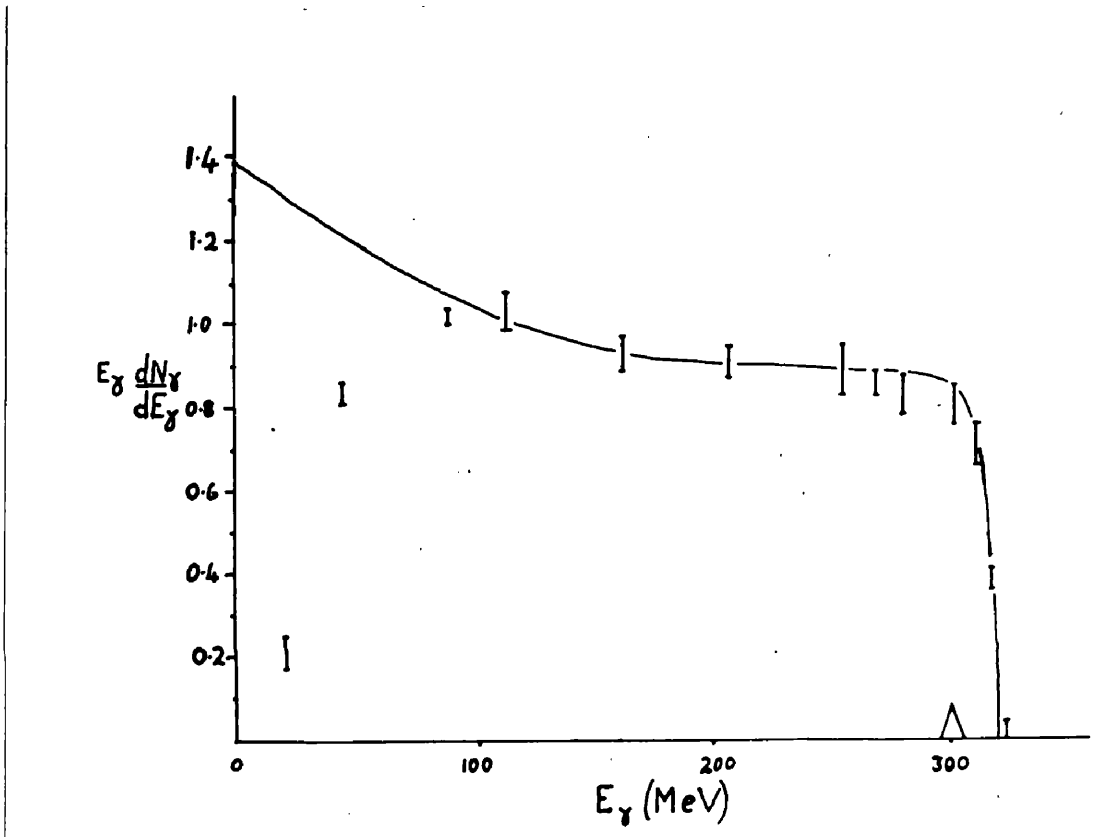

Figure 4.1. Bremsstrahlung spectrum. The curve is the Schiff thin target spectrum. The experimental points are due to Rutherglen and Walker (Walker 1960).

of this measurement are shown in figure 4.1. The energy resolution is shown at 300 MeV. The curve is the Schiff thin target spectrum, and the experimental points are in good agreement with it above 100 MeV. At lower energy multiple scattering of electrons introduced large errors.

Photons produced in the bremsstrahlung process are emitted in the direction of the incident electron with an angular spread $\sim mc^2/E_{max}$ where mc^2 is the electron rest mass and E_{max} is the incident electron energy. For 300 MeV electrons the angular spread is $\sim 1/10$ degrees. The angular width of the beam is increased by multiple scattering of the electrons in the target and by variation of the initial direction of the electrons due to multiple traversals of the target. The intensity distribution of the bremsstrahlung beam from the Glasgow synchrotron is bell shaped and has an angular full width at half maximum of .46 degrees (Atkinson et al., 1957). The width of the beam is thus mainly determined by multiple scattering. To improve the geometry of the beam a collimation system was developed and is described by Atkinson et al. The primary collimator is a $\frac{1}{4}$ inch hole in a 9 inch long lead cylinder placed 125 cm. from

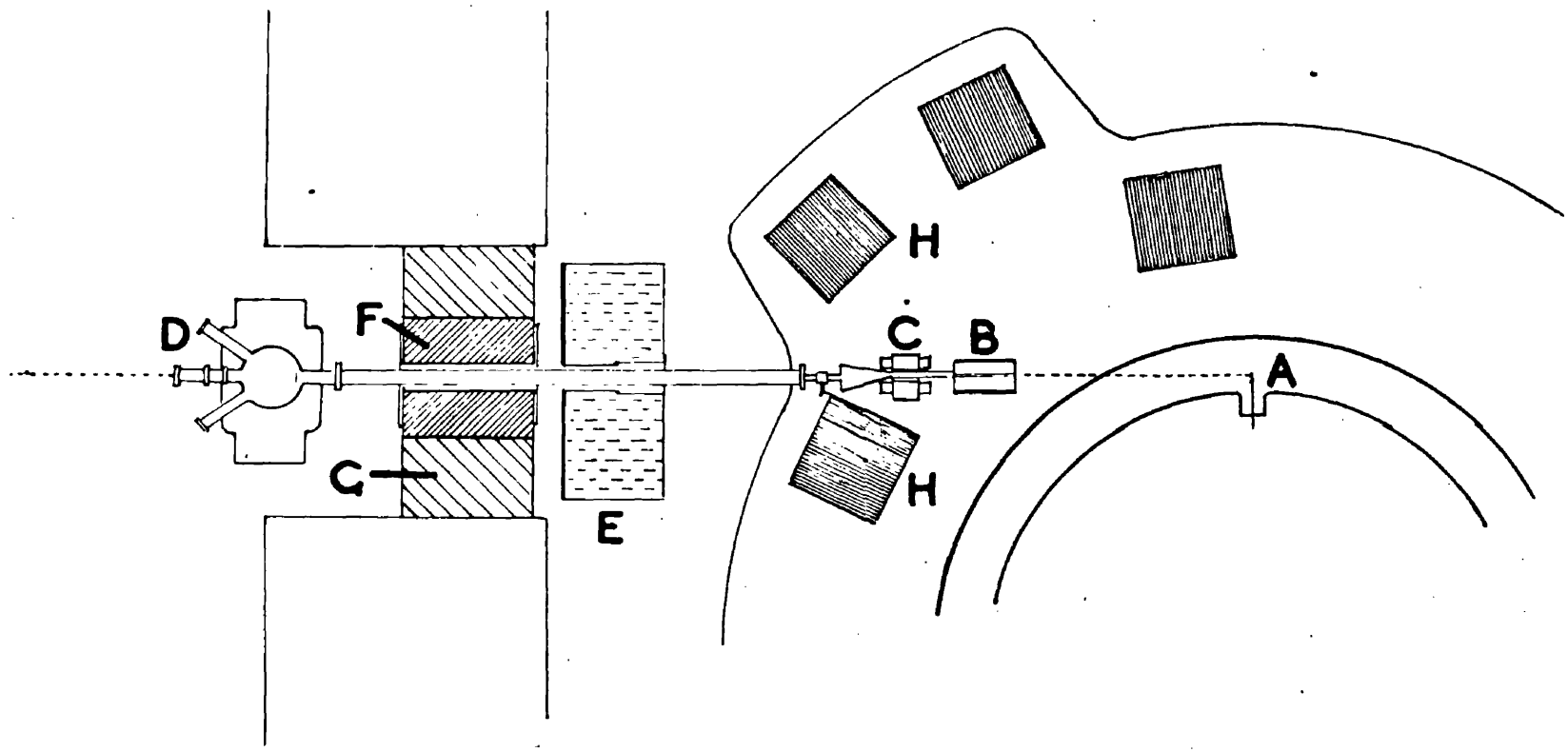

Median Plane Section of Collimator System.

A Synchrotron Target
B Collimator
C Scrubbing Magnet
D Pair Spectrometer
E Water Tank
F Lead Shielding
G Barytes loaded Concrete
H Part of Magnet Yoke

Figure 4.2.

the synchrotron target. The median plane section of the collimation system is shown in figure 4.2. The contamination of charged particles produced at the collimator is removed by a scrubber magnet, C. A secondary lead collimator serves to remove photons and electrons scattered in the primary collimator. The pair spectrometer magnet, D, may be used as a secondary scrubber. The beam tube is evacuated. The full width of the collimated beam is 0.20 degrees. An X-ray photograph of the collimated beam at 6.5 metres from the target is shown to scale in figure 4.5.

A bremsstrahlung beam is usually described by its maximum energy E_{max} and the number of equivalent quanta, Q, per unit time where,

$$Q = U/E_{max} = \int_0^{E_{max}} E/E_{max}\, N(E)\, dE \qquad (4.1)$$

where U is the total energy in the beam, and N(E)dE is the number of photons between E and E + dE per unit time. When Q, E_{max} and the spectral shape are known N(E) is defined.

The bremsstrahlung beam of the Glasgow synchrotron is monitored using a Cornell thick-walled copper ionization chamber (Corson et al., 1953). The thickness of the

copper walls is chosen so that the charge developed is largely due to ionization by electrons of a shower near the shower maximum. The number of electrons at the shower maximum is nearly proportional to the photon energy. The total charge collected is then roughly proportional to the total energy in the beam. The sensitivity of the chamber is expressed in MeV per coulomb and is dependent on E_{max}. The Cornell chamber is open to the atmosphere and the calibration is referred to normal temperature and pressure. Several of these chambers have been calibrated at Cornell, the agreement between the different chambers is good. The Cornell calibration is assumed for the Glasgow chamber. An ionization chamber constructed from the quantameter design of Wilson (1957) is also available but was not used in the work described here.

The maximum energy of the Glasgow synchrotron is determined by measuring the maximum magnet current, the guide field being known as a function of magnet current. Measurement of E_{max} made using the pair spectrometer showed good agreement with E_{max} obtained from magnet current measurements (McFarlane, private communication).

When the bremsstrahlung beam is used in counter

experiments it is desirable that the ratio of instantaneous intensity to the average intensity be as low as possible. The random coincidence rate, pile up, and dead time losses depend on the instantaneous intensity. The width of the beam from the Glasgow synchrotron may be extended to 2 milliseconds by suitable modulation of the radio frequency power supplied to the resonators. The beam shape is monitored by a thin scintillator placed directly in the beam.

(b) The Target

The thin liquid deuterium target used in this experiment was constructed by D. Miller and has been described by Bellamy et al. (1960). A section through the cryostat is shown in figure 4.3. The target chamber is in good thermal contact with a 1 litre reservoir containing liquid hydrogen refrigerant at atmospheric pressure. The target and liquid hydrogen reservoir are surrounded by a radiation shield at liquid nitrogen temperature ($77^{\circ}K$). The vacuum in the cryostat was maintained at less than 10^{-6} mm.Hg by an oil diffusion pump.

The target chamber is shown in figure 4.4. The

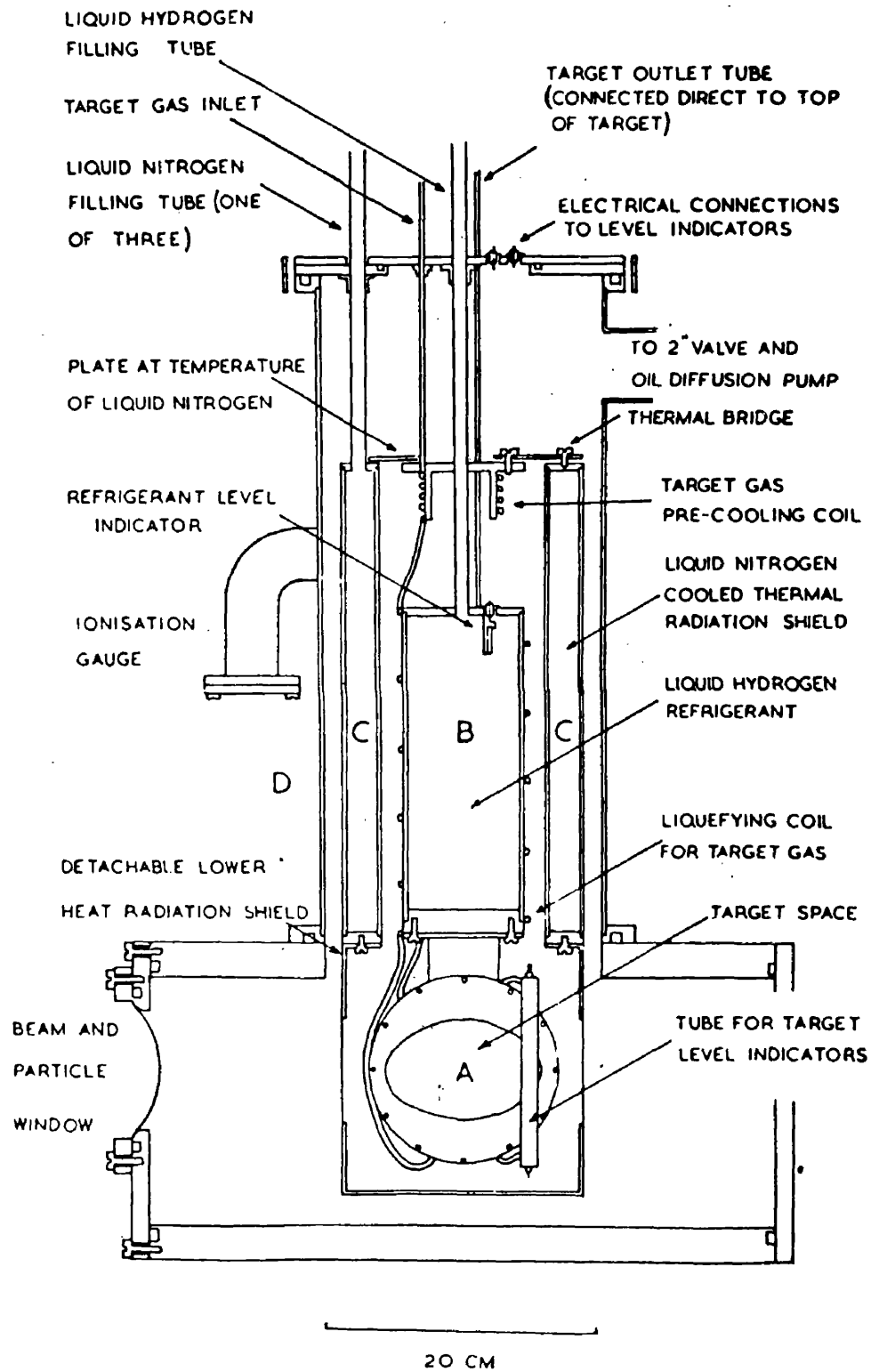

Figure 4.3 Vertical section through cryostat.

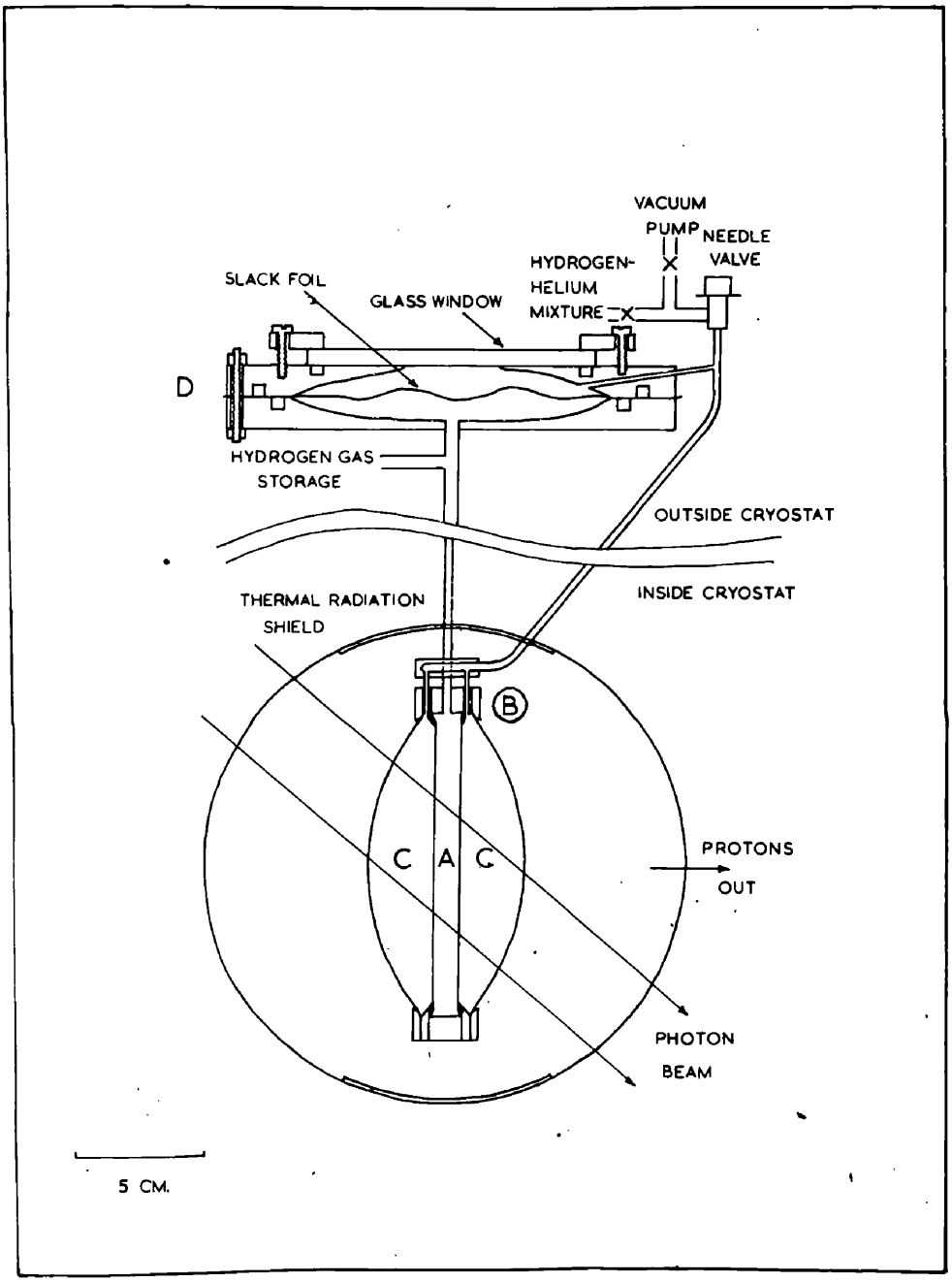

Figure 4.4. Liquid target.

A liquid deuterium
B level indicator
C hydrogen gas
D pressure compensating device

thin target walls are .001 inch mylar. The central section, A, contains the liquid deuterium. The outer sections, C, are connected together and filled with hydrogen gas. A zero pressure difference is maintained across the inner target walls so that the liquid target is flat and of uniform thickness. Slow changes in deuterium vapour pressure are compensated for by the slack foil device D. The target thickness was measured at room temperature using a microscope and found to be $1 \pm .003$ cm. Resistance type level indicators are used to show whether the target was empty or full.

The thickness of material traversed by the incident photon beam and by particles emitted from the target was small. The total target wall thickness was .004 inches. Ports cut in the radiation shield were covered with .0002 inch aluminium foil. Mylar windows .004 inch thick were provided in the outer vacuum jacket. Two of these windows were large ($4\frac{1}{2}$ x 16 inches) to allow the detection of emitted particles over a large angular range.

A wooden ring was attached to the top of the rectangular part of the outer vacuum jacket (see figure 4.3). The centre of this ring was located above the centre of the target to within 2 mm.by a complicated

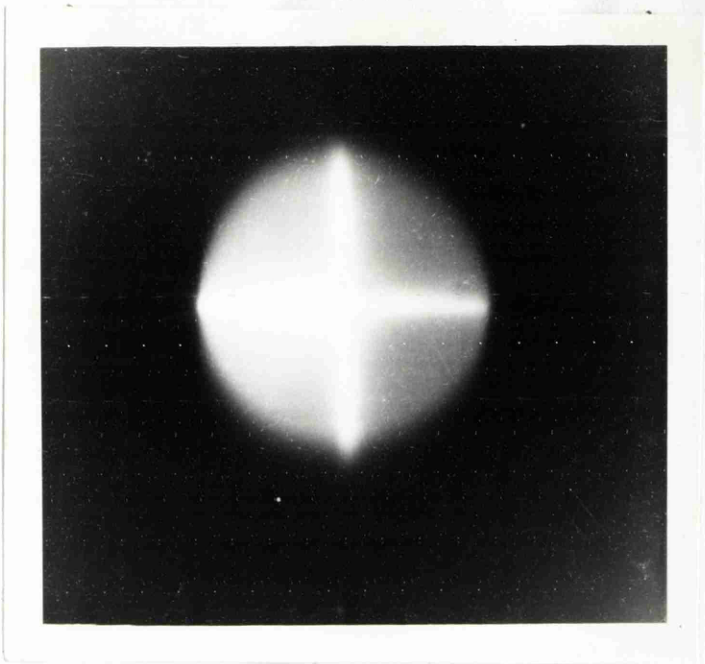

Figure 4.5. X-ray photograph of bremsstrahlung beam showing one of the crosses used to line up the target.

procedure using, marks on the target viewed through small holes in the radiation shield, and plumb lines suspended from the wooden ring. Since it was necessary to move the proton telescope to different angles during the experimental run a system was devised to aid the lining up of this telescope. A bracket attached to the proton telescope trolley fitted loosely around the cylindrical part of the target vacuum jacket. It was located by 4 screws so that the axis of the counter telescope passed through, and was constrained to rotate about the centre of the target.

The deuterium used to fill the target was produced by electrolysis of heavy water and was stored in a 160 litre tank at 80 cm.Hg.

(c) Experimental Procedure.

The deuterium target was placed in the 307 MeV bremsstrahlung beam 6 metres from the synchrotron target with the normal to the target surfaces at 40 degrees to the beam. The target was located in the beam using crosses suspended from the wooden ring. The alignment was checked by obtaining X-ray photographs. The final alignment is shown in figure 4.5

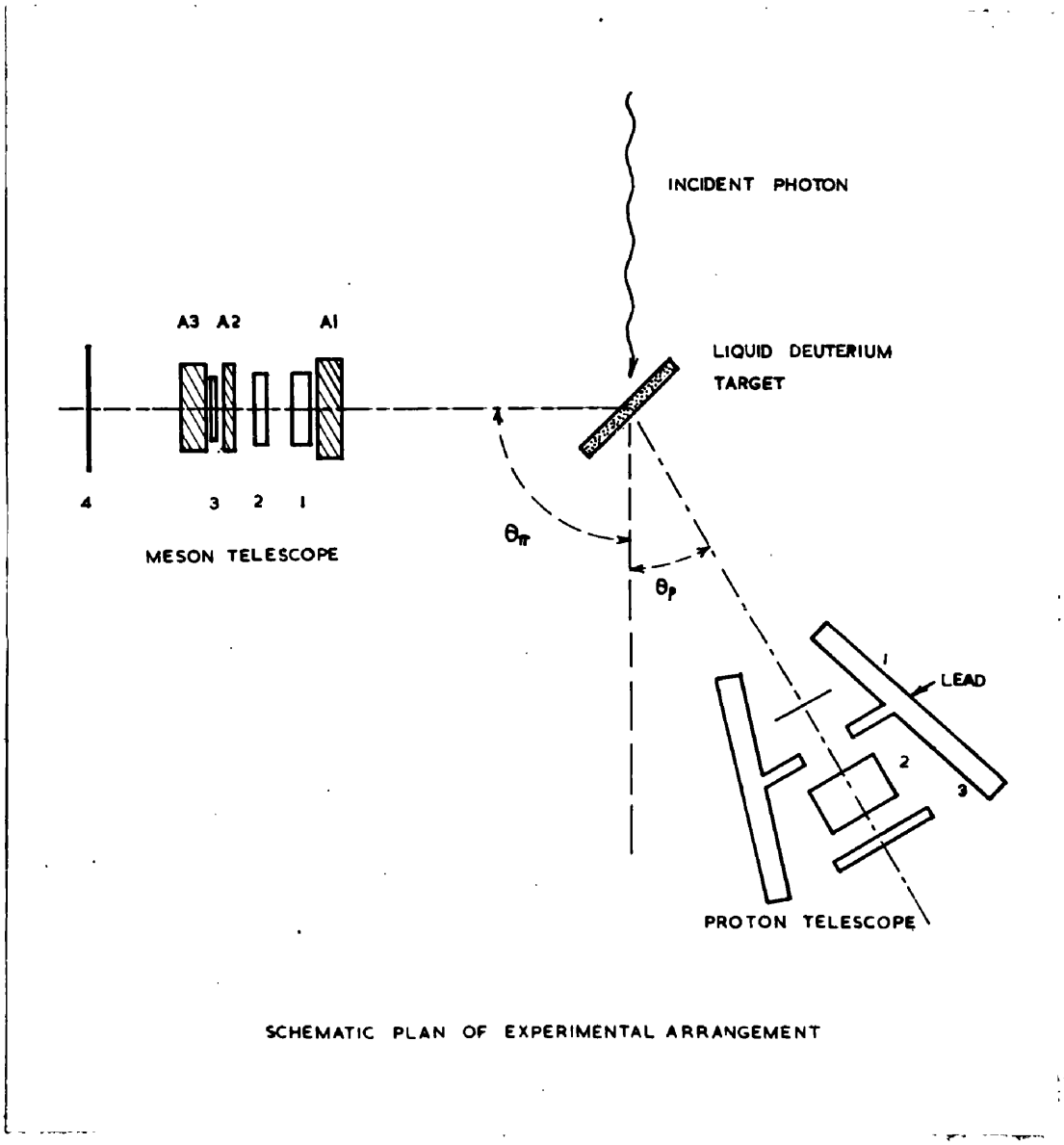

SCHEMATIC PLAN OF EXPERIMENTAL ARRANGEMENT

Figure 4.6.

The beam passed through vacuum between the primary collimator and the target except for 1 inch of air between the beam tube and the target vacuum. The experimental arrangement is shown in figure 4.6. A general view of the apparatus in the beam room is shown in figure 4.7. The beam tube passed through a 6 inch steel screen placed between the target and pair spectrometer. This provided extra shielding against charged particles swept out of the beam by the pair spectrometer magnet. The scrubber and pair spectrometer magnets were always on when data was being recorded.

The pion telescope was placed with its axis at 90 ± 1 degrees to the incident beam direction with counter 3, which defined the telescope aperature 17 ± .2 inches from the target. In this position it subtended an angle of .0187 ± .0005 steradians at the centre of the target. The angular acceptance was ±3.7 degrees. The pion telescope was operated in a 1 + 2 + 3 - 4 coincidence-anticoincidence sequence and detected pions incident on it, between 45.8 and 60.0 MeV.

The energy distribution of protons detected in coincidence with the pions was obtained. The proton telescope was positioned with its axis at 30 ± 1 degrees

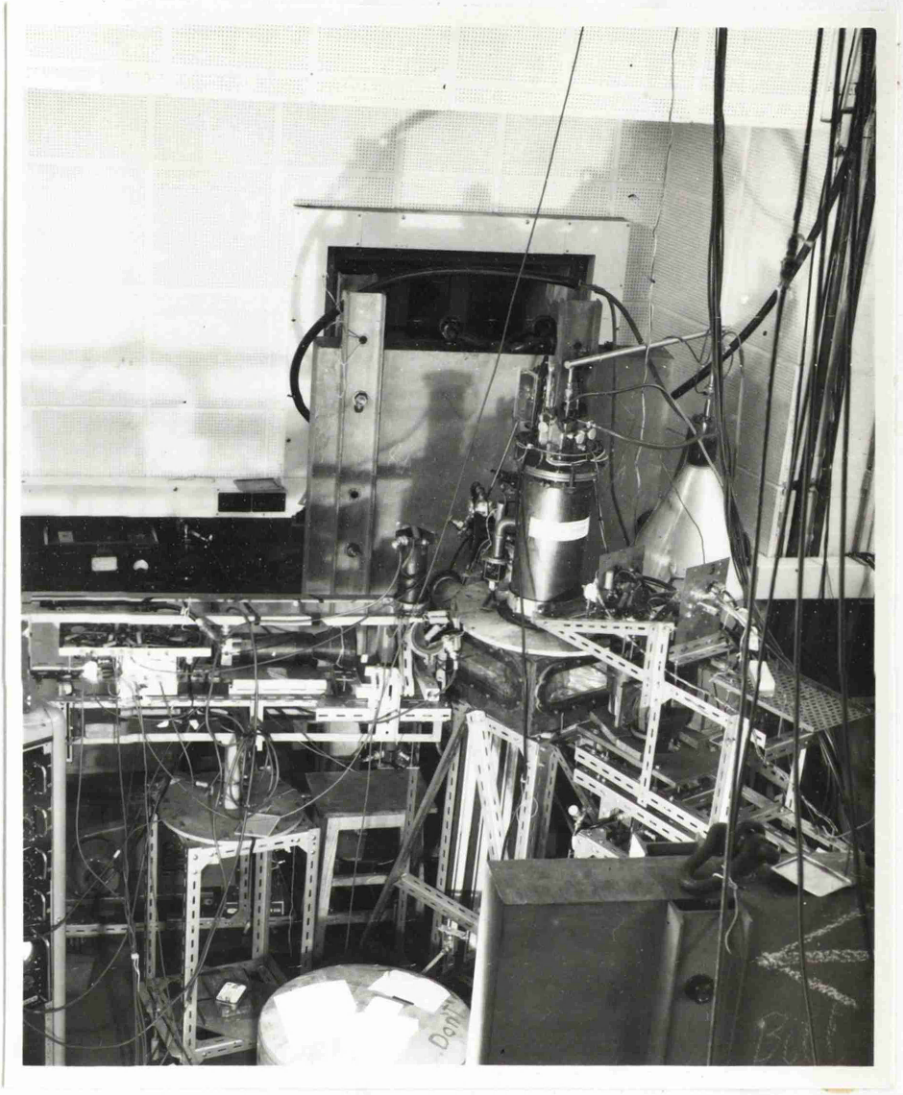

Figure 4.7. General view of apparatus in the beam room showing the target and the two counter telescopes.

to the incident beam. The telescope aperture was defined by a 2 inch diameter hole in a half inch thick lead block placed between counters 1 and 2. The central plane of this block was 16.5 ± .2" from the centre of the target and defined a solid angle of .0115 ± .0003 steradians at that point. The angular acceptance of the proton telescope was ±3.5 degrees. Lead blocks 1 inch thick were placed either side of the proton telescope to shield it from charged particles produced by the beam in the target window and in the air near the counters. Pulses from counters 1 and 2 were displayed on an oscilloscope whenever a pion was detected. The oscilloscope traces were photographed.

The angular distribution of the protons detected in coincidence with the negative pions was measured. Protons were detected at 4 angles, 22, 30, 38, and 46 degrees measured from the incident beam direction. The uncertainty in the position of the proton telescope was ±1 degree in each case.

The experimental run lasted 33 days in which time a total flux of 5×10^{12} equivalent quanta passed through the target. The empty target background was measured at the beginning and end of the experimental run. The

proton telescope 81 MeV endpoint calibration was obtained at the beginning and end of the run using protons produced at 65 degrees in a perspex target, and once during the run using protons produced in the deuterium target. The proton telescope was calibrated at the beginning and end of each day's run using thorium C^{11} 2.62 MeV, and sodium 22 1.28 MeV gamma rays, and 160 KeV internal conversion electrons from indium 11^4. At least one hour was allowed after switching on for the electronics to become stable before calibration.

The performance of the pion detection system was checked several times each day by photographing the cathode ray tube spot display (see figure 3.9). The 100 channel kicksorter display (figure 3.10) was used as a continuous monitor of the pion detection system. The operation of the single channel kicksorter and the oscilloscope trigger system was monitored by checking that the oscilloscope was triggered whenever an event was recorded in the pion group on the 100 channel kicksorter display. The E.H.T. voltages and the various trigger levels were checked each day before data was recorded. The operation of the amplifier-integrator system which was used to record the total

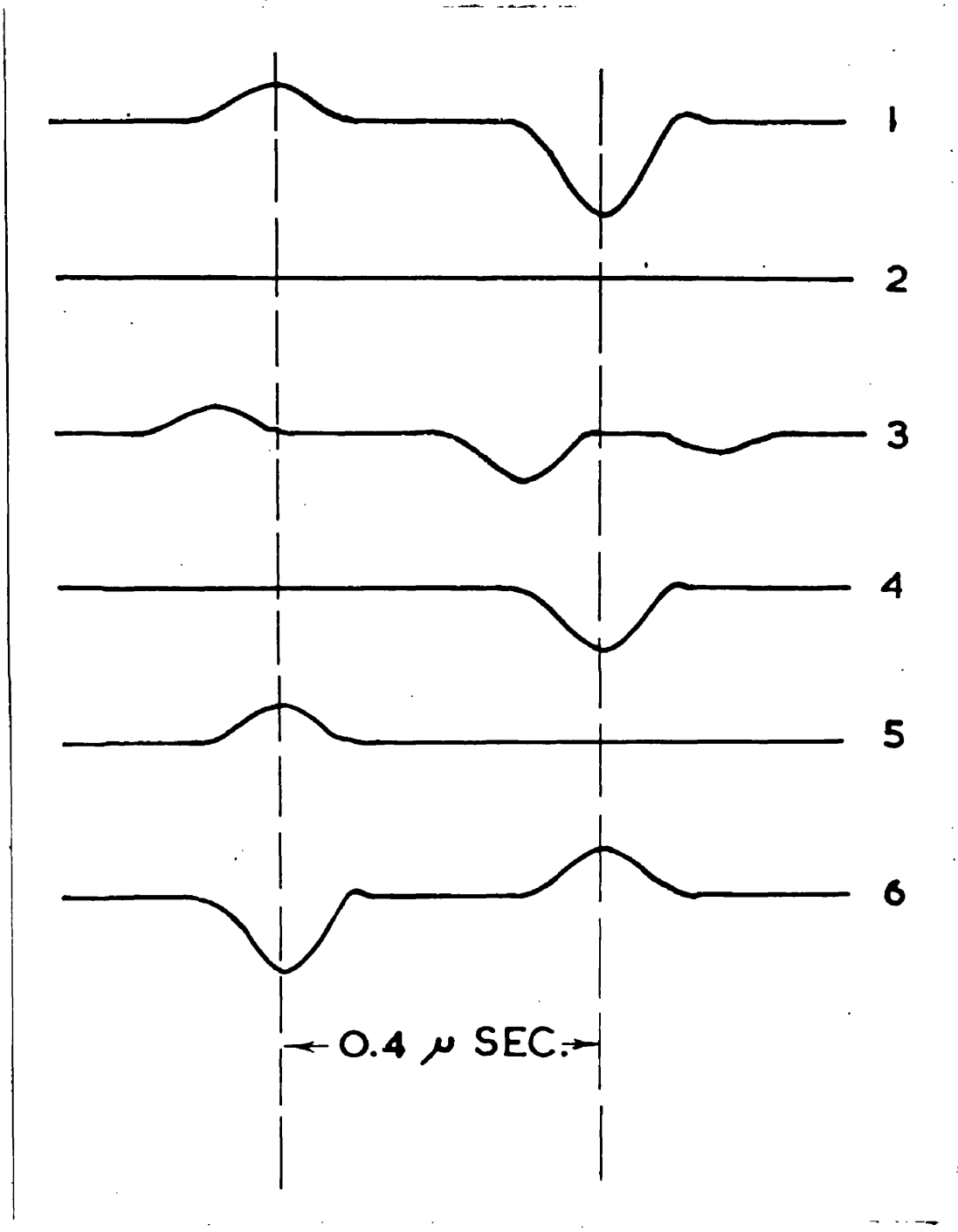

Figure 4.8. Typical oscilloscope traces. The dashed lines indicate the delay between counters 1 and 2.

charge collected by the beam monitor was checked several times each day. The various checks gave a good indication of the operation of the detection system and allowed faults to be found quickly.

Data recorded when the operation of the detection system or the beam monitor were suspect were rejected. The remaining film was analysed to select coincident protons. The position and separation of pulses from counters 1 and 2 were used to select coincident particles. The traces shown in figure 4.8 were selected to illustrate the various types of traces that were found. Positive deflections are produced by counter 1, negative ones by counter 2. The first trace is due to a coincident particle entering the telescope. The majority of the traces were like 2 in which no particles were detected in either counter. In 3 the trace produced by a random particle entering the telescope is shown. The last pulse is not associated with a pulse from counter 1 and may be attributed to a photon or to a charged particle that missed counter 1. Four illustrates the trace expected when a coincident neutron produces a knock on proton in counter 2. Since the pion telescope does not distinguish between negative and positive pions, there is

a high probability of traces like 4 occurring. The counter geometry prevents particles produced in the target from entering counter 2 directly without traversing counter 1. The background runs indicated that traces of this type were due to particles from the target. All traces like 4 were attributed to neutrons produced in reaction (1.3). Coincident charged particles which traverse counter 1 only produce traces like 5. The probability of random background pulses producing traces like 1 and 6 is expected to be equal. Since no traces like 6 were found it has been assumed that all traces like (1) were due to coincident particles.

The height of pulses from counters 1 and 2 were measured for all coincident traces. The pulse height from counter 1 was plotted against that from 2 as shown in figure 4.9. The specific ionization and energy selection of the proton telescope was used to eliminate events not due to protons. In all 17,000 traces were scanned and 453 coincidence protons were identified at all angles. In figure 4.9 the coincidence events observed with the proton telescope at 30 degrees are plotted. The expected response to pions protons and deuterons is also shown. The bottom edge of the proton

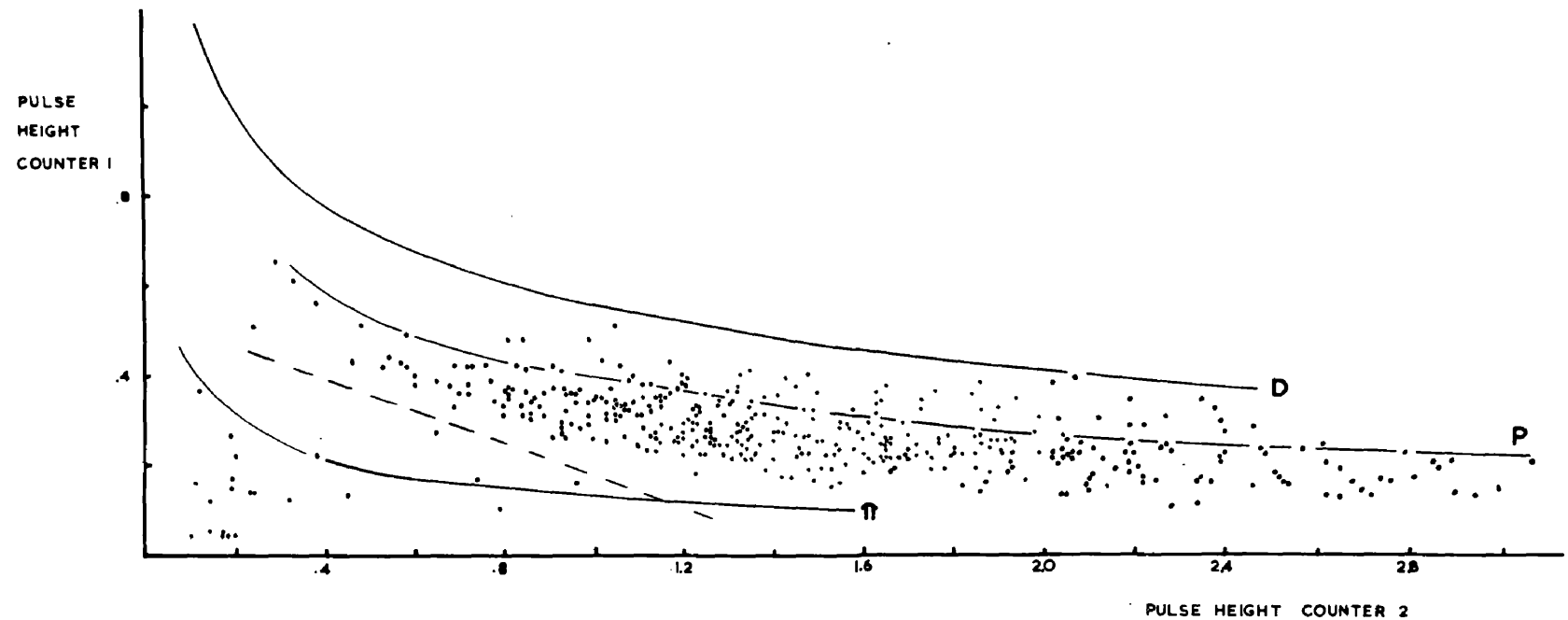

Figure 4.9. Plot of pulse height in counter 1 against pulse height in counter 2. All pulses that occurred in coincidence with oscilloscope triggers when the proton telescope was at 30 degrees are shown.

band is more sharply defined than the upper edge. This is a consequence of the Landau distribution of energy loss in the thin scintillator. All spots above the dashed line were attributed to protons.

The calibration of the proton telescope changed by about 8% during the run. Within the uncertainty of the calibration the pulse height from both counters 1 and 2 decreased uniformly throughout the run. The pulse height resolution did not change. The decrease in pulse height was most likely due to change in gain of the distributed amplifier in the oscilloscope. The gain in this type of amplifier is very dependent upon valve characteristics. A direct check that the change in gain occurred in the oscilloscope could not be made since the initial sensitivity was not known to better than 10 percent. The morning and evening calibrations done each day never differed by more than 6 percent, which was within the uncertainty of the individual calibrations. To allow for the change in calibration the measured pulse heights were normalized using the average source calibration each day before they were plotted in figure 4.9. After the normalization the proton end point calibrations done at the beginning and end of the run agreed to within

0.5 percent, and differed from the average source calibration by 6 precent. The average of the source and endpoint calibrations was adopted. Expressed in deflection measured in the film reader it was $.0483 \begin{smallmatrix} + .0035 \\ - .003 \end{smallmatrix}$ inches/1 MeV.

As an additional check on the energy calibration of the proton telescope, the pulse height produced by fast electrons traversing counter 2 was measured. A .005 inch copper sheet was placed in the bremsstrahlung beam. The oscilloscope was triggered by 1 + 3 coincidences and the pulses from counters 1 and 2 were displayed on the oscilloscope trace. The discriminator was set using a thorium source to select particles loosing more than 2 MeV in counter 2. A $\frac{1}{2}$ inch thick perspex absorber was placed between counters 2 and 3 so that only electrons leaving counter 2 with energy $>$ 2 MeV were selected. The oscilloscope traces were photographed and the heights of pulses from counters 1 and 2 were measured. A histogram of the pulse height distribution for counter 2 is shown in figure 4.10. The most probable pulse height estimated from the relative numbers in the two most probable intervals is shown by the arrow. Following the suggestion of Cranshaw (1952) it

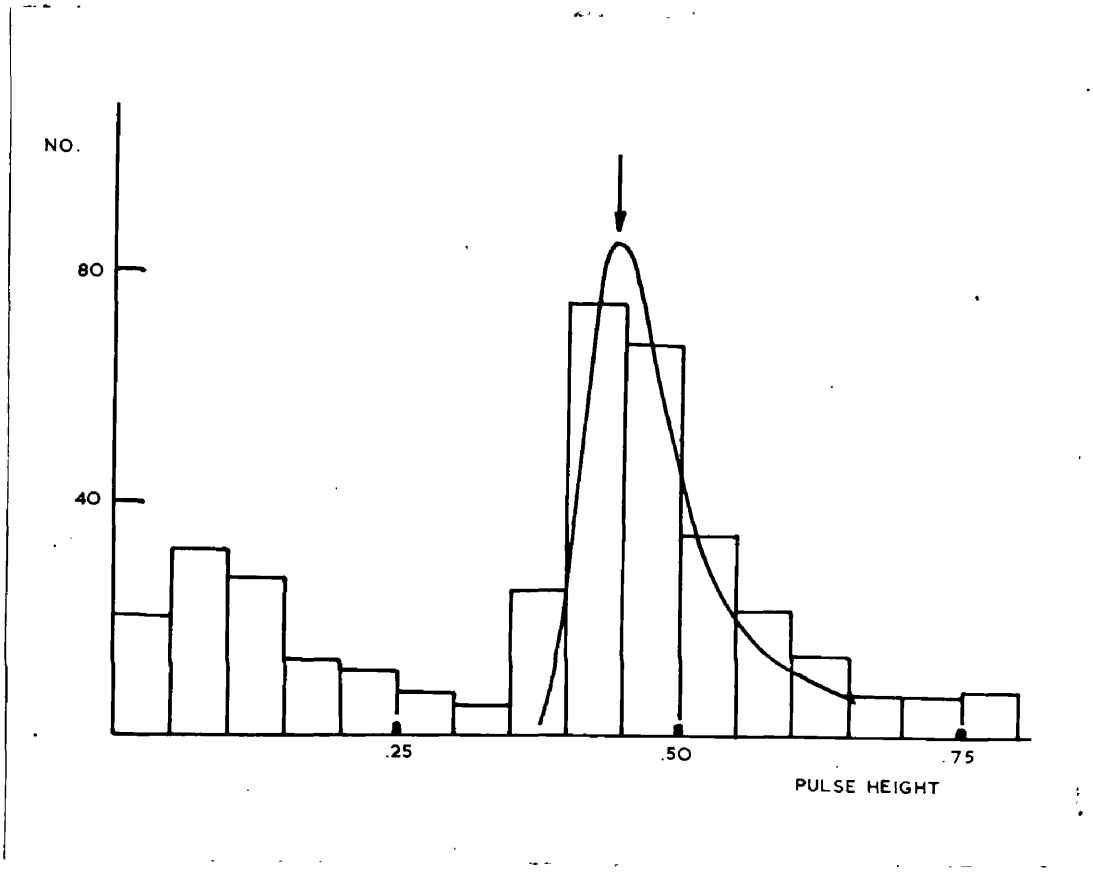

Figure 4.10. Histogram of pulse height produced in counter 2 by relativistic electrons traversing the proton telescope. The arrow indicates the most probable pulse height. The curve is the Landau distribution including counter resolution.

was assumed that published values of specific ionization refer to the most probable energy loss. The most probable energy loss for the electrons in counter 2, 9.5 MeV, was obtained using 1.8 MeV cm^2/gm as the specific ionization for minimum ionizing particles. The curve in figure 4.10 is the Landau distribution of energy loss with counter resolution (assumed 10 percent full width at half height) folded in. The Landau distribution was obtained using the prescription of Rossi (1952). The pulse height distribution implies the energy calibration is $.0462 \begin{smallmatrix} + .007 \\ - .003 \end{smallmatrix}$ inches/MeV in good agreement with the adopted calibration.

The energy measured in the counter telescopes must be corrected for energy lost by the particles escaping from the target to obtain the particle energy at creation. As the production occurs uniformly throughout the target volume a single energy for particles entering the telescope will correspond to a range of energy at creation. Thus 15 and 20 MeV protons produced at the near and far sides of the target will have the same energy entering the counter telescope. At higher energy the spread is less being 2.5 and 1.6 MeV for 40 and 70 MeV protons respectively. The creation energy of both

protons and pions have been related to measured particle energy by assuming that production occurred at the median plain of the target.

In the background runs a total of 6.49×10^{11} equivalent quanta passed through the empty target. No coincident recoil protons were observed.

The continuous spot distribution in figure 4.9 was divided into bins corresponding to 10 MeV intervals for protons produced at the median plane of the target. The energy intervals are given in column 1 of table 4.1. The number of protons in each interval was obtained by counting the spots in the proton band and is given in column 2. The R.M.S. deviations are given in the third column.

The experimentally observed angular distribution is presented in table 4.2. The number of protons observed at each angle is given in column 2 and the corresponding total flux at each angle in column 3. The errors are R.M.S. deviations only. The error due to relative monitoring of the photon flux were 5% and are small compared with the R.M.S. deviations. The angular resolution is indicated in column 1.

Figure 4.11 shows the energy spectrum for recoil

Table 4.1

Energy Spectrum of Recoil Protons from Negative Pion Photoproduction in Deuterium

Proton Energy Interval	No. of Protons	R.M.S. Deviation
17 - 27	15	3.9
27 - 37	82	9.0
37 - 47	133	11.6
47 - 57	84	9.2
57 - 67	54	7.4
67 - 77	23	4.8
> 77	5	

Table 4.2

Angular Distribution of Recoil Protons from Negative Pion Production in Deuterium.

Angle degrees ±3.5	No. of Protons Detected	Total Photon Flux 10^{11} Q	No. of Protons per 10^{11} Q
22	23	3.59	6.4 ± 1.3
30	396	26.7	14.8 ± .74
38	32	3.44	9.3 ± 1.6
46	2	1.73	1.2 ± .85

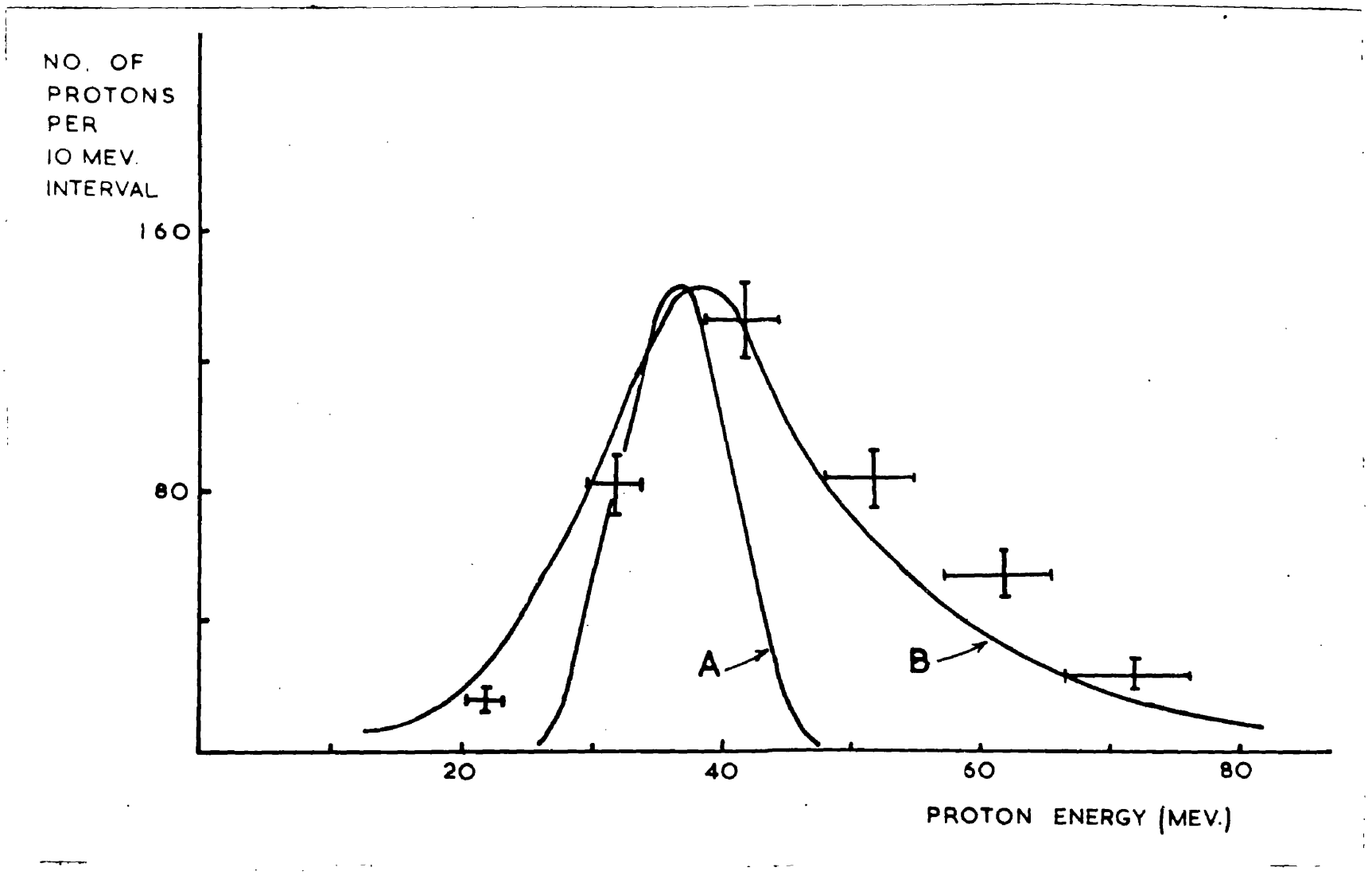

Figure 4.11. Energy spectrum of recoil protons detected at 30 ± 3.5 degrees in coincidence with 46.3 to 60.4 MeV negative pions produced at 90 degrees in the reaction $\gamma + d \rightarrow p + p + \pi$

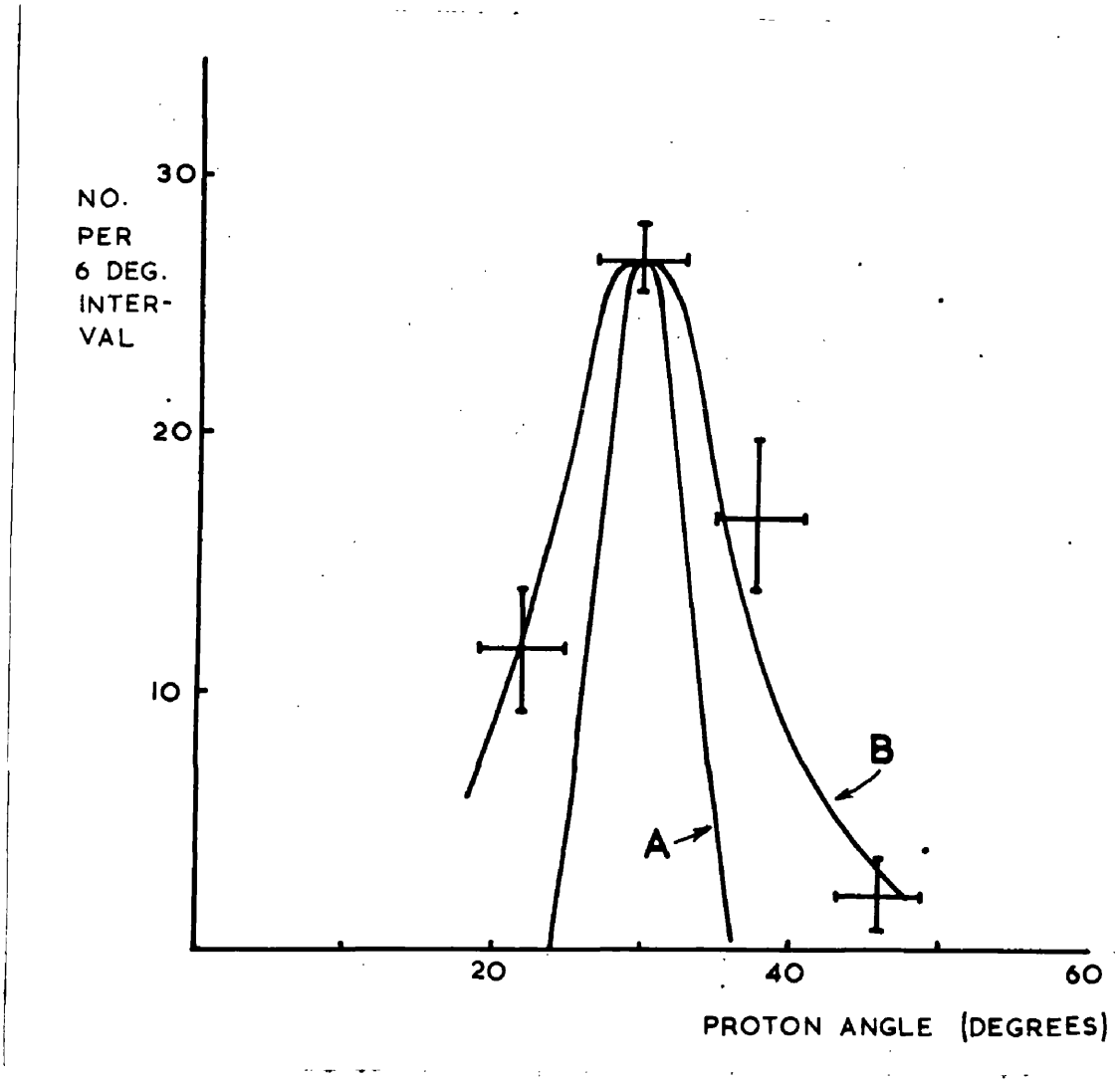

Figure 4.12. Angular distribution of recoil protons detected in coincidence with 46.3 to 60.4 MeV negative pions produced at 90 degrees in the reaction $\gamma + d \rightarrow p + p + \pi^-$.

protons measured at 30 ± 3.5 degrees in coincidence with 46.3 to 60.4 MeV negative pions detected at 90 ± 3.7 degrees. The experimental points are taken from table 4.1. The vertical bars indicate R.M.S. deviations. The horizontal bars indicate the uncertainty due to the energy calibration which was + 7.2, - 6.2 percent. Curve A is the energy spectrum calculated for negative pion production at a free neutron at rest. Curve B is the energy spectrum obtained in the spectator model calculations. Curve B was normalized to the area under a histogram drawn through the experimental points.

The angular distribution of recoil protons detected in coincidence with the negative pions is shown in figure 4.12. The experimental points were obtained from table 4.2. The vertical bars are R.M.S. deviations. The horizontal bars represent the angular resolution, ±3.5 degrees, of the proton telescope. The curves A and B are the angular distributions calculated for negative pion production at a free neutron at rest, and for the spectator model description of pion production in deuterium. The curves were normalized to the experimental point at 30 degrees.

CHAPTER V

Calculation of Energy and Angular Distributions.

The experimental angular and energy distribution for recoil protons detected in coincidence with negative pions from deuterium are compared with the distributions calculated when the process is described by the spectator model. The agreement between the experimental and calculated distributions furnishes the test for validity of the spectator model. The simpler reaction $\gamma + n \rightarrow p + \pi^-$ (1.2) is also considered, although it is not expected to give a good description of the proton energy and angular distributions. The comparison of the distributions calculated in the two approximations illustrates the effect of nucleon momentum on the observed distributions.

The energy and momentum conservation conditions for negative pion photoproduction at a free nucleon are

$$\begin{aligned} V &= \mu + P \\ V_o + M_N &= \mu_o + T_p + M_p \end{aligned} \qquad (5.1)$$

where V and V_o are the photon momentum and energy,

μ and μ_o are the pion momentum and energy,

and P and T_p are the proton momentum and kinetic energy.

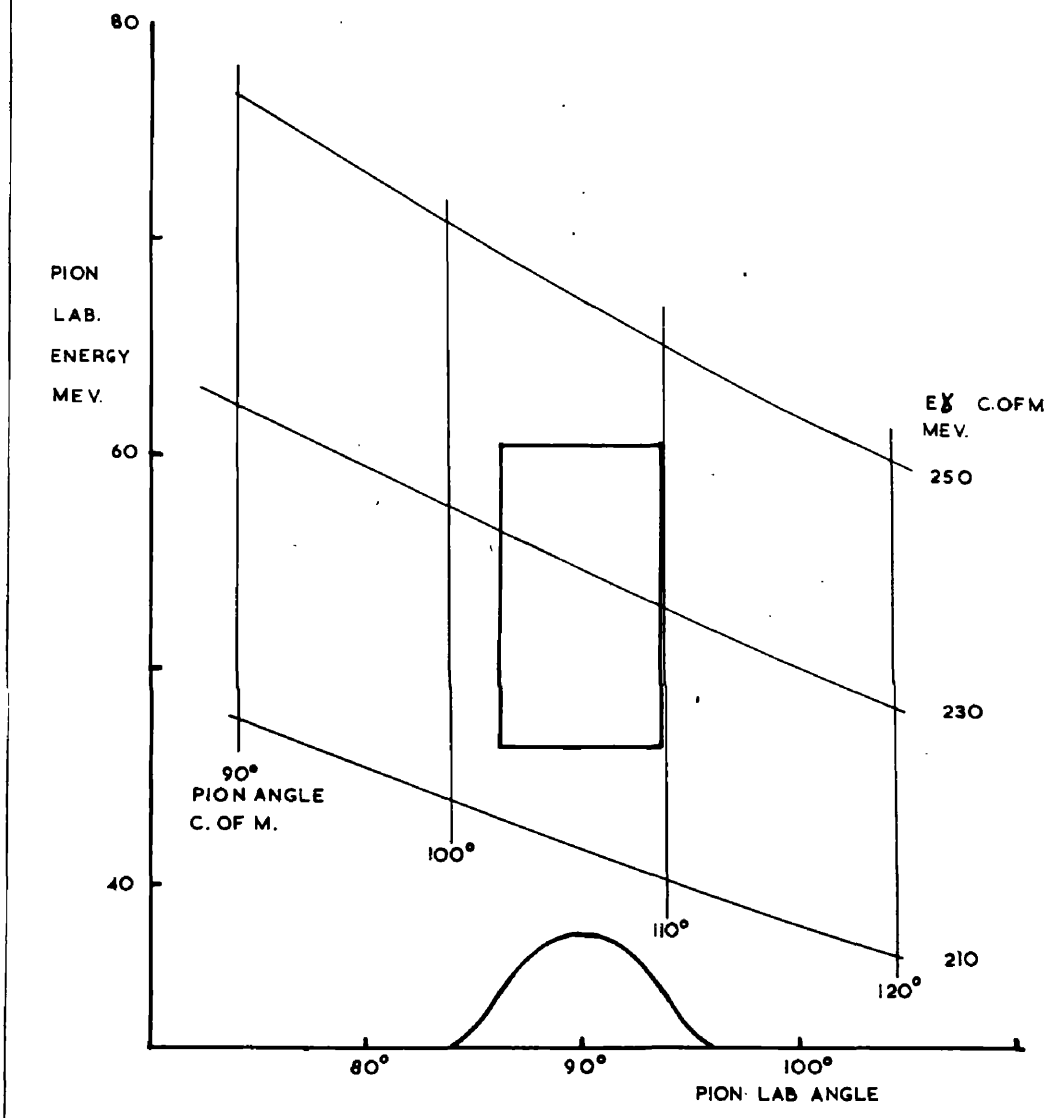

Figure 5.1. Diagram of pion kinematics for negative pion production at a free neutron. The angular resolution of the pion telescope is shown.

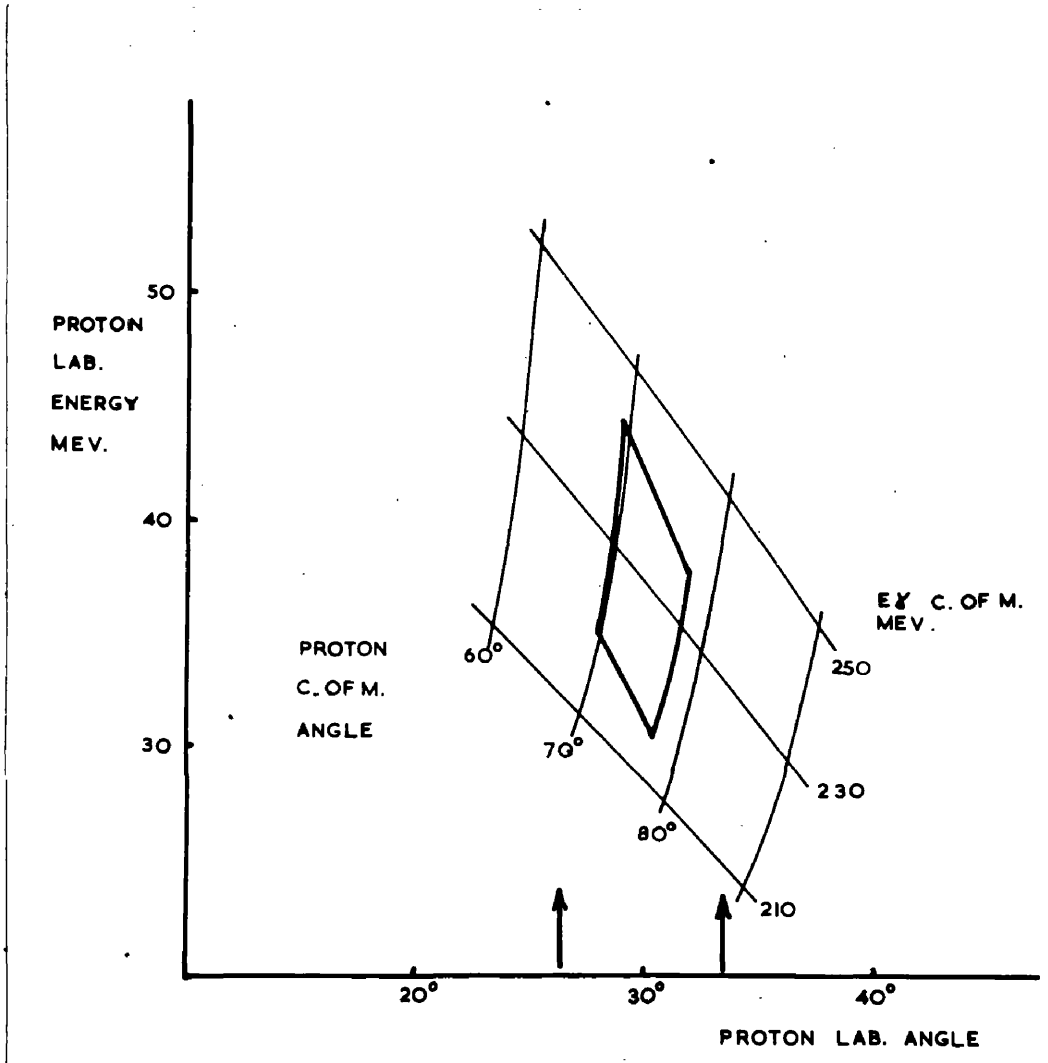

Figure 5.2. Diagram of proton kinematics for negative pion production at a free neutron. The angular acceptance of the proton telescope is indicated by the arrows.

M_n and M_p are the neutron and proton rest masses.

Equations (5.1) are a special case of the general two-body energy and momentum conservation conditions that have been used to compute tables of kinematic relations for many reactions. Reaction (1.2) can not be observeddirectly and kinematical tables for this reaction have not been published. A desk calculator was used to compute the kinematical relations for reaction (1.2) for the small energy and angular range of interest here. The solutions given by Malmberg and Koester (1953) were used to solve for T_p, θ_p, T_π and θ_p for various values of V_o and θ_p^* and θ_π^*, where θ_p and θ_π are the proton and pion production angles measured from the incident photon direction and T_π is the pion kinetic energy. The asterisk indicates quantities expressed in the centre of mass system. The conventional kinematical diagrams are shown in figures 5.1 and 5.2. Pion (proton) laboratory angle and energy are plotted on the X and Y axes respectively. Lines of constant photon energy and pion (proton) centre of mass angle are drawn on these diagrams. The two diagrams and the relation between pion and proton centre of mass angles, $\theta_\pi^* = 180 - \theta_p^*$, may be used to obtain laboratory angle

and energy for the pion and proton for any particular centre of mass angle and incident photon energy.

A graphical method using figures 5.1 and 5.2 has been used to calculate the angular and energy distributions expected for recoil protons observed in coincidence with 46.3 to 60.4 MeV pions produced at 90 degrees. The angular resolution of the pion telescope is shown in figure 5.1. The effect of a finite target and the counter aperture have been considered. The angular acceptance of the pion telescope, 7.5 degrees, is the full width at half height given by the angular resolution curve. The pion energy and angular range accepted by the telescope is indicated by the rectangle in figure 5.1. The corresponding energy and angular range for the recoil protons is represented by the "diamond shaped" area in figure 5.2. If the cross section for pion production is assumed to be constant over the range of pion energy and angle accepted by the pion telescope, then to a good approximation the relative probability of a recoil proton being observed at a particular angle is given by the length of a line of constant Θ_p which lies inside the "diamond shaped" area. The effect of finite target volume is considered by replacing the target by a number

of sources and adding the contribution from the various sources at each angle. The angular resolution of the proton telescope was folded in to obtain the expected experimentally observed angular distribution. Curve A in figure 4.12 is the angular distribution expected for recoil protons detected in coincidence with negative pions produced at 90 degrees and 46.3 to 60.4 MeV at a free neutron at rest.

The energy distribution of recoil protons was obtained in a similar way. The length of a line of constant T_p lying inside the "diamond shaped" area in figure 5.2 was used to obtain the relative probability of a recoil proton being produced at a particular energy. The energy resolution of the proton telescope was taken to be 10 MeV wide, the width of the bins used to obtain the experimental energy distribution. The effect of the energy resolution was included in calculating the energy spectrum by taking the probability of detecting a pion at an energy T_p to be proportional to the area under the energy distribution between $T_p - 5$ and $T_p + 5$ MeV. The observed energy distribution calculated for recoil protons from pion photoproduction at a free neutron is curve A in figure 4.11. Since the angular acceptance of the

proton telescope was wider than the distribution of recoil protons shown in figure 5.2 no restriction on proton angle was required in calculating the observed energy distribution.

Spectator Model Calculation

The energy and momentum conservation conditions for negative pion photoproduction in deuterium are

$$\begin{aligned} V + D &= \mu + P + S \\ V_o + M_D &= 2M_p + T_p + T_s + \mu_o \end{aligned} \qquad (5.2)$$

where S and T_s are the momentum and kinetic energy of the spectator proton, and D and M_D are the momentum and mass of the deuteron. Although there are only two particles in the initial state, there are three in the final state and measurement of the angle and energy of one final state particle does not allow a solution of 5.2. The spectator model assumption is that the pion is produced at the neutron and the proton momentum is the same in the initial and final states. Since the deuteron is at rest

$$D = N + S = 0 \qquad (5.3)$$

where N is the neutron momentum. S may be eliminated

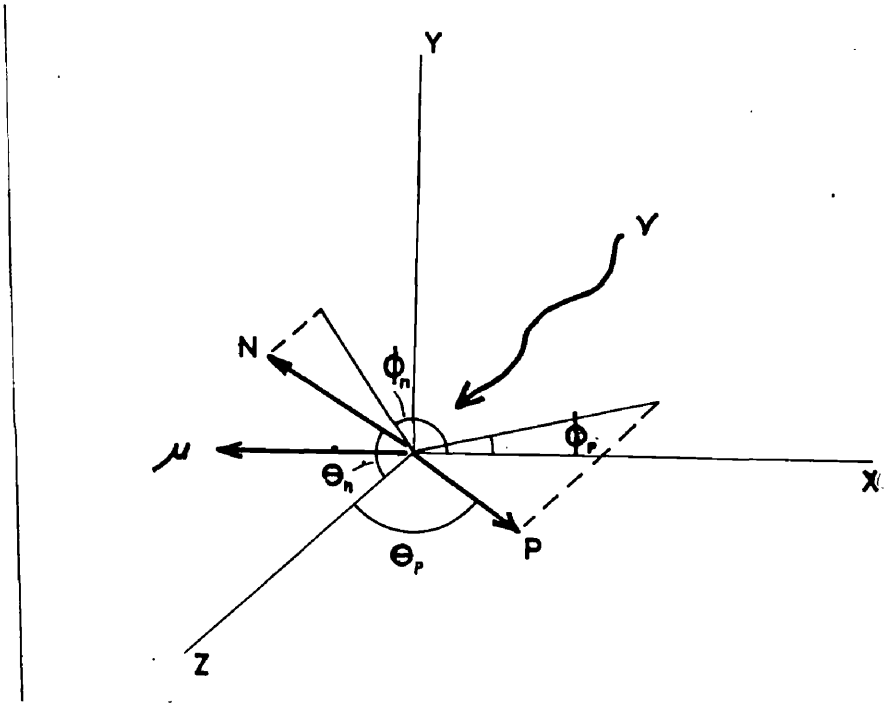

Figure 5.3. Geometry of spectator model description of negative pion photoproduction in deuterium.

from (5.2) and the spectator proton energy, $T_s = N^2/2M_p$ in the non relativistic limit. The binding energy of the deuteron B, is included since $M_D = M_p + M_n - B$. Pion production in deuterium has now been reduced to a two body reaction in which neither of the particles in the initial state are at rest. The geometry of the spectator model reaction is illustrated in figure 5.3. The photon is incident along the Z-axis. The pion momentum is shown directed along the negative X-axis corresponding to the detection of the pion at 90 degrees. The initial neutron and recoil proton momenta are shown.

Equations (5.2) have been solved in the spectator model for proton energy T_p angles θ_p and ϕ_p and for the laboratory and centre of mass photon energy. The solutions are.

$$T_p = A - \left\{ A^2 - [M_p - A]^2 - [|N| \sin\theta_n \sin\phi_n]^2 - [(\mu_o^2 - M_\pi^2)^{1/2} + |N| \sin\theta_n \cos\phi_n]^2 \right\}^{1/2} \qquad (5.3)$$

$$\theta_p = \cos^{-1} \frac{(M_p - A) + T_p}{(2 M_p T_p)^{1/2}} \qquad (5.4)$$

$$\sin\phi_p = \frac{|N| \sin\theta_n \sin\phi_n}{(2 M_p T_p)^{1/2} \sin\theta_p} \qquad (5.5)$$

$$V_o = M_p - M_n + B + T_s + \mu_o + T_p \qquad (5.6)$$

$$V_o^* = \frac{V_o}{\left[1 - \frac{|N|^2 + 2|N|V_o\cos\theta_n + V_o^2}{(V_o + M_n)^2}\right]^{1/2}} \times \left\{1 - \frac{V_o + |N|\cos\theta_n}{V_o + M_n}\right\} \qquad (5.7)$$

where $A = M_n - B - T_s - \mu_o - |N|\cos\theta_n$,

V_o^* is the centre of mass photon energy, and $C = 1$. The various angles are defined in figure 5.3. The non relativistic relation between proton energy and momentum has been used.

The numerical computation of T_p etc. requires that the pion energy and the initial neutron momentum be known. The pion energy was defined by the pion telescope. The probability distribution for nucleon momenta in the deuteron was obtained from the Hulthén wave function. It is

$$P(|N|) = \frac{K N^2}{\left[(N^2+\alpha^2)(N^2+\beta^2)\right]^2} \qquad (5.8)$$

where $\alpha = (MB)^{\frac{1}{2}} = 45.7$ MeV and $\beta = 260 \pm 2$ MeV (White et al., 1960. The nucleon momentum distribution is isotropic

in space. The numerical computation was done for the range of nucleon momenta appropriate to the deuteron. The Glasgow University Deuce computer was used and T_p, θ_p, sin ϕ_p, V_o and V_o^* were computed for

10 values of N from 10 to 190 MeV,

7 values of ϕ_n from 0 to 180 degrees,

5 values of θ_n from 30 to 150 degrees,

3 values of E_π from 188.2 to 197.6 MeV,

a total of 1050 combinations in all. The reaction is symmetrical about the X - Z plane in figure 5.3.

The pion centre of mass angle θ_π^* in the photon neutron centre of mass system corresponding to pion emission at 90 degrees in the laboratory system is

$$\theta_\pi^* = \tan^{-1} \frac{\left[\cos^2\theta \cos^2\phi_n + \sin^2\phi_n\right]^{1/2}}{-\gamma\left[\sin\theta \cos\theta_n + v_{cm}(\mu_o/\mu)\right]} \qquad (5.9)$$

where $V_{cm} = (N^2 + 2|N|V_o \cos\theta_n + V_o^2)^{\frac{1}{2}}/(V_o + M_n)$ is the velocity of the centre of mass in the laboratory system.

$$\gamma = 1 / \sqrt{1 - V_{cm}^2}$$

$$\cos\theta = (V_o + |N| \cos\theta_n)/(N^2 + 2|N|V_o \cos\theta_n + V_o^2)^{\frac{1}{2}}$$

and $\sin\theta = |N| \sin\theta_n / (N^2 + 2|N| V_o \cos\theta_n + V_o^2)^{\frac{1}{2}}$

θ_π^* was calculated for each combination of θ_n and ϕ_n for a few values of $|N|$ and $\mu_o = 193$ MeV and graphs of θ_π^* vs $|N|$ drawn.

The probability of a pion being produced by a photon of energy V_o, at a neutron with momentum N is proportional to the weighting function

$$W = \rho(|N|)\ \rho(\phi_n)\ \rho(\theta_n)\ \rho(V_o)\ d\sigma/d\Omega(V_o^*\ \theta_\pi^*) \quad (5.10)$$

where $\rho(|N|)$ is the area under the nucleon momentum probability distribution (5.8) between N - 10 and N + 10 MeV.

$\rho(\phi_n) = 1$ and $\rho(\theta_n) = \sin\theta_n$ for an isotropic distribution.

$\rho(V_o)$ was obtained from the Schiff thin target spectrum with $E_{max} = 307$ MeV,
and $d\sigma/d\Omega(V_o^*\ \theta_\pi^*)$ is the differential cross section for negative pion production at a free neutron expressed as a function of centre of mass photon energy and the pion production angle.

The appropriate weight W was assigned to each calculated recoil proton energy and angle. The energy

spectrum was obtained from the assigned weights. The probability of a recoil proton being produced in an energy interval ΔE_p about E_p is given by the sum of the weights W assigned to protons in the interval. In calculating the proton energy spectrum to be compared with the experimentally observed spectrum the requirement that the recoil proton enter the proton telescope was imposed by considering the calculated θ_p and sin ϕ_p. The effect of the finite target was included by considering that protons were produced at a number of sources. The limits on θ_p and sin ϕ_p depended on the proton telescope aperture and the source position in the target. The relative probability of detecting a proton at energy E_p was then proportional to $\sum W$ where the sum was taken from E_p - 5 to E_p + 5 MeV, corresponding to the width of the energy bins used to obtain the experimental spectrum. Curve B in figure 5.2 shows the energy spectrum calculated in the spectator model for recoil protons detected at 30 $\pm$ 3.5 degrees in coincidence with 46.3 to 60.4 MeV pions produced at 90 degrees.

The angular distribution of the recoil protons was calculated in a similar way. Only protons for which sin ϕ_p indicated that the proton entered the proton

telescope were included. The telescope angular resolution was included by summing $\sum W$ from $\theta_p - 3$ to $\theta_p + 3$ degrees. The calculation was done for the centre of the target only. The angular distribution calculated in the spectator model for the recoil proton detected in coincidence with a negative pion at 90 degrees isshown in figure 5.1 curve B.

The differential cross section for pion photoproduction was obtained from Moravcsik's paper (1957). Graphs were drawn of positive pion production cross sections as a function of centre of mass photon energy V_o^* for different centre of mass pion angles θ_π^*. The -/+ ratio was assumed constant over the range of V_o^* and θ_π^* involved and was not used in calculating W. Apart from the -/+ ratio the use of cross sections for pion production at a nucleon at rest is not strictly correct since the transformation of the cross section from the centre of mass to the laboratory system depends on nucleon momentum N.

The efficiency of the detection system may be checked by calculating the cross section for negative pion production. The number of recoil protons n, is related to the pion photoproduction cross section by

$$n = \left[\frac{d\sigma}{d\Omega dE} \quad \frac{\Delta V_0}{V_0} \quad Q \quad \Delta\Omega \quad N \right] \times F \qquad (5.11)$$

where Q is the total flux expressed in equivalent quanta

$\Delta\Omega$ is the solid angle subtended by the pion telescope at the centre of the target,

and N is the total number of nuclei in the beam per cm^2. The photon energy and interval V_o and ΔV_o are determined by the kinematics for negative pion photoproduction at a free neutron at rest. The quantity in brackets is the usual expression for the number of pions detected. F is the fraction of the recoil protons expected to enter the proton telescope. The spectator model calculation gives F = .097.

The number of recoil protons detected was corrected for counting losses due to multiple scattering and absorption of pions in the counter telescope and for pion decay in flight. The multiple scattering correction was calculated using the graphs of Sternheimer (1954). The data of Shapiro (1951) and Byfield et al. (1952) for negative pion absorption in carbon including elastic and inelastic scattering was used. It was assumed that all pion decays in flight resulted in the μ meson being

scattered out of the pion telescope. The corrections were,

multiple scattering	+ 3 percent
absorption	+ 13 percent
decay in flight	+ 8 percent.

The cross section for negative pion photoproduction calculated from (5.11) is then 15.8×10^{-30} cm.^{2}/steradian MeV ±12 percent.

The error assigned to the cross section was obtained from the errors listed below

beam monitor	10 percent
R.M.S. deviation	5 percent
definition of photon energy interval	4.5 percent
determination of E_{max}	2 percent
pion telescope solid angle	1.5 percent

The error in F depends on the impulse approximation calculations and was not included. The large error assigned to the beam monitor was largely due to instability in the amplifier integrator system used.

The cross section for negative pion production in

deuterium may be calculated using the experimentally measured positive pion cross section from hydrogen and the -/+ ratio from deuterium. The value obtained by interpolation of the experimental points given in Moravcsik's paper (1957) was 17.5×10^{-30} cm.^{2}/steradian MeV $\pm$10 percent. The cross section obtained from the experiment is $\sim$10 percent lower. This may be due to the competing photodisintegration process.

CHAPTER VI

Discussion and Conclusions.

The agreement between the experimentally observed angular distribution for the recoil proton from negative pion photoproduction in deuterium and the distribution calculated in the spectator model is good. Figure 4.12 indicates that the width of the angular distribution is several times that expected from negative pion production at a free neutron at rest. The additional width of the spectator model angular distribution is due to the neutron momentum. The angular distribution, like that obtained by Keck and Littauer (1952) supports the spectator model description of negative pion photoproduction in deuterium.

The energy spectrum observed for the recoil proton from negative pion photoproduction in deuterium differs from the spectrum calculated using the spectator model approximation. The disagreement between individual experimental points in figure 4.11 and the curve B is not large but the fact that all the experimental points are shifted towards higher energy is significant. The "shift" is approximately 8 percent with respect to curve B for all points, and is slightly larger than the estimated uncertainty in the energy calibration. The

shape of the observed spectrum is well represented by the spectator model calculation. In particular the excess of protons above the most probable energy agrees with the experimental points.

It is tempting to speculate that the"shift" is due to an error in the energy calibration of the proton telescope. The energy calibration has been done using high energy protons, and thorium C^{11} and sodium 22 gamma ray sources. The calibrations agreed to within ±3 percent. The independent check of the calibration using relativistic electrons agreed with the adopted calibration well within the accuracy of the measurement. There is no evidence that the error in the energy calibration is larger than indicated in figure 4.11. It was concluded that the "shift" can not be entirely due to errors in the energy calibration.

The possibility of including random events or particles which were not protons has been considered. The single channel kicksorter was set to include pulse heights that extended well above and below the pion group to ensure that no pions were missed. The oscilloscope was triggered on large electron pulses and the probability of detecting electron pairs was considerable. The

electrons were well separated from protons by the dE/dx and E measurement of the proton telescope. The spots occurring close to the origin in figure 4.9 were attributed to electron pairs.

The separation between the pion and proton groups in the kicksorter display was large and few protons were expected to trigger the oscilloscope. Consideration of the kinematics indicates that protons from pion production are not expected at 90 degrees. The detection of a coincident negative pion in the proton telescope was very improbable.

The probability of detecting a recoil deuteron from elastic neutral pion production in deuterium was small. The correlation between a π^o decay photon and the recoil deuteron is weak and the efficiency for the pion telescope detecting such photons is small. The two particles, pions and deuterons, most likely to be confused with protons in the proton telescope are thus very unlikely to occur in coincidence with an oscilloscope trigger.

The total absence of inverted coincidence events (trace 6 figure 4.8) is good evidence that the probability of a random particle being included in the energy

spectrum is small.

Coincident recoil neutrons from positive pion photoproduction in deuterium were excluded by the lack of a dE/dx pulse. A total of 52 events of this type were found. Most of the pulses produced by counter 2 for these events corresponded to proton energies between 20 and 35 MeV. An appreciable distrotion of the observed recoil proton spectrum would have occurred if the dE/dx and E proton identification had not been used.

Multiple scattering of the protons in the deuterium target was a small effect and was not strongly energy dependent. Scattering in the thin front scintillator in the proton telescope may be neglected. The counter geometry indicated that the number of protons striking the edges of the lead collimator equalled 6 percent of the number passing cleanly through it. An inelastic proton scatter in the edges of the collimator or penetration of the edges would produce a distortion in the proton spectrum. Since only a few spots occur in figure 4.9 that are not clearly electrons or protons it was assumed that effects due to the collimator edges were small. The counting losses calculated for the pion telescope were nearly independent of pion energy in the

energy interval defined by the telescope.

The energy resolution of the detection system due to counter resolution and particle energy loss in the target, was typically ± 3 MeV. It was narrower than the 10 MeV intervals used to obtain the experimental spectrum. The width of the intervals was mainly dictated by the need to have significant statistical accuracy for the experimental points.

The consideration of the experimental technique outlined above did not reveal any effect likely to produce a significant distortion in the energy spectrum.

The calculation of the energy spectrum in the spectator model approximation necessarily involved a number of approximations. The pion -/+ ratio was assumed constant. The data included in Moravcsik's paper (1957) indicate that it may be expected to vary by about 10 percent in the energy and angular region that was expected to make the main contribution to the proton energy spectrum. The relation between the centre of mass and the laboratory cross section for pion production was assumed to be independent of the neutron momentum N. The error introduced by this approximation is difficult to estimate. It was considered that the

general accuracy of the spectator model calculations did not warrant detailed consideration of the -/+ ratio or the cross section transformation. The errors introduced by the other assumptions made in the spectator model calculation are expected to be smaller than those discussed above. It was concluded that the Curve B in figure 4.11 gives a good representation of the recoil proton energy spectrum predicted by the spectator model.

A small discrepancy between the recoil energy spectrum predicted by the spectator model and the observed spectrum exists. Although it is unlikely to be entirely due to experimental errors or errors in calculating the recoil proton energy spectrum, this possibility can not be completely ruled out. The spectator model neglects the interaction of the particles in the final state. The impulse approximation which includes the final state interaction has been shown to describe accurately pion photoproduction in deuterium near threshold (Adamovic et al., 1959). It is expected to be valid at higher energy also. The impulse approximation calculations of Thie (1952) for the recoil proton energy spectrum (curve C figure 1.10) indicate that the impulse approximation predicts an energy distribution shifted

towards higher energy with respect to the spectator model calculations. The final state interaction is considered to be the most probable cause of the discrepancy observed between the spectator model spectrum and experiment.

Although the energy and angular acceptance differed slightly, the results of the present experiment may be compared with those of Keck and Littauer (1952). The energy spectra of the recoil proton obtained in the two experiments differ. In particular the peak of the energy spectrum obtained by Keck and Littauer was shifted towards higher energy by 10 to 12 MeV compared with the spectator model predictions. In the present experiment the peak is shifted towards higher energy by 3 to 4 MeV. Keck and Littauer did not obtain an excess of protons above the most probable energy which was obtained in the present experiment and is predicted by the spectator model calculation. The experimental technique used in the present investigation was superior to that of Keck and Littauer in that a liquid deuterium target was used and the identification of particles included in the energy spectrum was more complete. It is considered that the large discrepancy observed by Keck and Littauer

was due to an experimental effect. This view is supported by the difference between the measured cross sections. In the present experiment a value of $15.8 \pm 1.9 \times 10^{-30}$ cm.^{2}/(steradian MeV) was obtained in good agreement with the cross section predicted by recent experimental values of the -/+ ratio and positive pion production cross section. Keck and Littauer quote $10.8 \pm 1.0 \times 10^{-30}$ cm.^{2}/(steradian MeV) for the same cross section. Unless the difference is due to errors in beam monitoring the two values indicate that a substantial number of events were not detected in the earlier experiment.

It may be concluded from the present work that the spectator model provides a reasonable description of negative pion photoproduction in deuterium for photon energies about 230 MeV. There is some evidence that the interaction between particles in the final state has a small effect at this energy. A large discrepancy between the experimental energy spectrum for the recoil proton and that predicted by the spectator model is ruled out. The present findings agree with those of White et al. (1960) that the spectator model description of pion photoproduction in deuterium is justified at energies

well above threshold.

The differential cross section for negative pion photoproduction in deuterium at 90 ± 3.7 degrees and 53 ± 7 MeV is 15.8 ± 1.9 x 10^{-30} $cm.^2$/(steradian MeV). This is ~10 percent below the value calculated from the -/+ ratio in deuterium and the positive pion photoproduction cross section in hydrogen. Although the difference can be accounted for by the Wilson (1956) model for photodisintegration of the deuteron the errors are too large for the difference to be significant.

PUBLICATIONS.

The Response of Plastic Scintillators to Protons,
H.C. Evans and E.H. Bellamy, 1960, Proc. Phys. Soc.
74, 483.

A Level Controller for Liquid Nitrogen,
D. Miller and H.C. Evans, 1960, J. Sci. Instrum.
38, 162.

REFERENCES

Adamovic, M.I., 1959, Soviet Physics (J.E.T.P.) 35, (8), 29.

Adamovic, M.I., Gorzhevskaya, E.G., Larionova, V.G., Popova, V.M., Kharlamov, S.P., and Yagudina, F.R., 1960, Soviet Physics (J.E.T.P.) 38, (11), 779.

Adamovic, M.I., Kuzmichiva, G.V., Larionova, V.G., and Khatlamov, S.P., 1959, Soviet Physics (J.E.T.P.) 35, (8), 21.

Ammiraju, P., Lederman, L.M., 1956, Nuovo Cim. 4, 283.

Atkinson, J.R., McFarlane, W., Reid, J.M., and Swinbank, P., 1957, Nucl. Instr. 1, 152.

Atkinson, J.H. Jr., and Willis, B.H., 1957, High Energy Particle Data, Vol 11, URCL. 2426 (U.S. Atomic Energy Commission).

Baldin, A.M., 1958, Nuovo Cim. 8, 569.

Bellamy, E.H., 1960, Prog. Nucl. Phys. 8, Pergamon Press, London.

Bellamy, E.H., Hogg, W.R., and Miller, D., 1960, Nucl. Instr. 7, 293.

Beneventano, M., Bernardini, G., Carlson-Lee, D., Stoppini, G., and Tau, L., 1956, Nuovo Cim. 4, 323.

Beneventano, M., Bernardini, G., Stoppini, G., and Tau, L., 1958, Nuovo Cim. 10, 1109.

Beneventano, M., Carlson-Lee, D., Stoppini, G., Bernardini, G., and Goldwasser, E.L., 1954. Nuovo Cim. 12, 156.

Birks, J.B., 1953, Scintillation Counters (London: Pergamon Press).

Borelli, F., and Grimeland, B., 1955, Nuovo Cim. 2, 236.

Byfield, H., Kessler, J., and Lederman, L.M., 1952, Phys. Rev. 86, 17.

Cassels, J.M., Fidecaro, G., Wetherell, A.M., and Wormald, J.R., 1957, Proc. Phys. Soc. A70, 405.

Chew, G.F., 1950, Phys. Rev. 80, 196.

Chew, G.F., Goldberger, M.L., Low, F.E., and Nambu, Y., 1957, Phys. Rev. 106, 1337, 1345.

Chew, G.F., and Lewis, H.W., 1951, Phys. Rev. 84, 779.

Chew, G.F., and Wick, G.C., 1952, Phys. Rev. 85, 636.

Cini, M., Gatto, R., Goldwasser, E.L., and Ruderman, M., 1958, Nuovo Cim. 10, 243.

Corson, D.R., DeWire, J.W., McDaniel, B.D., and Wilson, R.R. 1953, Cornell University publication.

Cranshaw, T.E., 1952, Prog. Nucl. Phys. 2, Pergamon Press, London.

Evans, H.C. and Bellamy, E.H., 1959, Proc. Phys. Soc.74, 483.

Gooding, T.J., and Pugh, H.G., 1960, Nuc. Phys. 18, 46.

Hagerman, D.C., Crow, K.M., and Friedman, R.M., 1957, Phys. Rev. 106, 818.

Hogg, W.R., and Bellamy, E.H., 1958, Proc. Phys. Soc. 72, 895.

Keck, J.C., 1955, Phys. Rev. 85, 410.

Keck, J., Littauer, R., 1952, Phys. Rev. 88, 139.

Kharlamov, S.P., Adamovic, M.I., and Larionova, V.G., 1959, Soviet Physics (J.E.T.P.) 36, (9), 668.

Knapp, E., Imhof, W., Kenney, R.W., and Perez-Mendez, V., 1957, Phys. Rev. 107, 323.

Knapp, E.A., Kenney, R.W., and Perez-Mendez, V., 1959, Phys. Rev. 114, 605.

Land, R.H., 1959, Phys. Rev. 113, 1141.

Landau, L., 1944, J. Phys. U.S.S.R. 8, 4, 201.

Lattes, C.M.G., Occialini, G.P.S., and Powell, C.F., 1947, Nature 160, 453, 486.

Lax, M., and Feshbach, H., 1952, Phys. Rev. 88, 509.

Littauer, R.M., and Walker, D., 1952, Phys. Rev. 86, 838.

MacDonald, N., 1960, Nuovo Cim. 15, 301.

McFarlane, W., Darden, S.E., and Oldroyd, D.L., 1955, Nature 176, 666.

McMillan, E.M., Peterson, J.M., 1949, Science 109, 438.

Malmberg, J.H., and Koester, L.J. Jr., 1953, Tables of Nuclear Reaction Kinematics at Relativistic Energies, Physics Dept., Univ. of Illinois.

Malmberg, J.H., and Robinson, C.S., 1958, Phys. Rev. 109, 158.

Moravcsik, M.J., 1956, Phys. Rev. 104, 1451.

Moravcsik, M.J., 1957, Phys. Rev. 105, 267.

Moravcsik, M.J., 1958, Nuovo Cim. 7, 442.

Rich, M., Madey, R., 1954, Range Energy Tables, URCL. 2301 (U.S. Atomic Energy Commission).

Rossi, B., 1952, High-Energy Particles, Prentice-Hall, Inc., New York.

Rutherglen, J.C., and Walker, J.K., 1960, Nucl. Inst. 8, 239.

Rutherglen, J.C., Walker J., Miller, D., and Patterson, J.M., 1960, Rochester Conference Report, pg.23.

Sands, M., Walker, R.L., and Teasdale, J.G., 1954, Phys. Rev. 95, 592.

Schiff, L.I., 1946, Phys. Rev. 70, 87.

Shapiro, A.M., 1951, Phys. Rev. 84, 1063.

Sternheimer, R.M., 1954, Rev. Sci. Inst. 25, 1070.

Swanson, W.P., Gates, D.C., Jenkins, T.L., and Kenney, R.W., 1960, Phys. Rev. Letters, 5, 336.

Thie, J.A., 1952, Phys. Rev. 88, 420.

Tollestrup, A.V., Keck, J.C., and Worlock, R.M., 1955, Phys. Rev. 99, 220.

Uretsky, J.L., Kenney, R.W., Knapp, E.A., and Perez-Mendez, V., 1958, Phys. Rev. Letters, 1, 12.

Walker, J., 1960, Ph.D. Thesis, Glasgow University.

Walker, R.L., Teasdale, J.G., Peterson, V.Z., and Vette, J.I., 1955, Phys. Rev. 99, 210.

White, R.S., Jacobson, M.J., and Schultz, A.G., 1952, Phys. Rev. 88, 836.

White, D.H., Schectman, R.M., and Chasan, B.M., 1960, Phys. Rev. 120, 614.

Wilson, R.R., 1956, Phys. Rev. 104, 218.

Wilson, R.R., 1957, Nucl. Instr. 1, 101.

Wolfe, B., Silverman, A., and De Wire, J.W., 1955, Rev. Sci. Instr. 26, 504.

Yukawa, H., 1935, Proc. Phys. - Math. Soc. Japan 17, 48.

Summary of Ph.D. Thesis

Photoproduction of Negative Pions in Deuterium

by H.C. Evans

Deuterium provides the most suitable target for studying the basic process of negative pion photoproduction at a free neutron. For photon energies well above threshold the spectator model has been used to relate photoproduction in deuterium to photoproduction at a free neutron. Until recently no experimental test of the spectator model that clearly supported its validity for negative pion photoproduction in deuterium had been reported. The spectator model has been investigated using the 307 MeV bremsstrahlung beam of the Glasgow electron synchrotron. The simultaneous detection of pions and protons produced in a thin liquid deuterium target was accomplished using scintillation counter telescopes. The pions were detected at 90 ± 3.7 degrees in the energy range 46.3 to 60.4 MeV. The angular distribution of recoil protons, and the energy spectrum of recoil protons detected at 30 ± 3.5 degrees were measured.

The measured angular distribution was well described by the angular distribution calculated in the spectator

model. The measured energy spectrum has a broad maximum at 42 MeV. The shape of ~~the~~ this spectrum is also well described by the spectator model calculations, although the measured spectrum appears to be shifted towards higher energy by 3 to 4 MeV. It may be concluded that the spectator model provides a reasonable description of negative pion photoproduction in deuterium for photon energies about 230 MeV. The differential cross section for negative pion photoproduction in deuterium at 90 ± 3.7 degrees and 53 ± 7 MeV is 15.8 ± 1.9 x 10^{-30} cm^2/steradian MeV.